Dehydroalkylation of Benzene with Mixtures of Ethane and Propane over Zeolite Catalysts

Von der Fakultät Chemie der Universität Stuttgart

zur Erlangung der Würde eines

Doktors der Naturwissenschaften (Dr. rer. nat.)

genehmigte Abhandlung

vorgelegt von

Dennis Wan Hussin

aus Ostfildern

Hauptberichter:	PD Dr. Yvonne Traa
Mitberichter:	Prof. Dr.-Ing Elias Klemm

Tag der mündlichen Prüfung: 06. Juli 2017

Institut für Technische Chemie

der Universität Stuttgart

2018

Für Taska

Danksagungen

Mein besonderer Dank gilt Frau PD Dr. Yvonne Traa für die Überlassung dieses faszinierenden und vielschichtigen Themas sowie für die sehr gute und engagierte Betreuung meiner Arbeit.

Danken möchte ich auch den Herren Prof. Dr.-Ing. Elias Klemm und Prof. Dr.-Ing. Jens Weitkamp für die sehr guten Rahmenbedingungen am Institut für Technische Chemie.

Herrn Prof. Dr.-Ing. Elias Klemm danke ich sehr herzlich für die freundliche Übernahme des Koreferats.

Ebenso danken möchte ich allen Mitwirkenden am EU-Projekt NEXT-GTL, deren Zusammenarbeit und hilfreiche Vorschläge zur Bearbeitung meines Themas beigetragen haben. Hierbei danke ich in besonderem Maße Daniel Geiß, dessen Vorleistungen ich übernehmen durfte.

Ganz besonders möchte ich allen meinen Kollegen am Institut für Technische Chemie danken. Durch die sehr gute Zusammenarbeit unter allen Doktoranden ergaben sich viele fruchtbare und interessante, sowie erheiternde Diskussionen.

Ferner danke ich Michael Paolillo, der im Rahmen des RISE-Programms als Praktikant zu dieser Arbeit beigetragen hat.

Dank gebührt ebenfalls Heike Fingerle, Barbara Gehring, Herrn Prof. Dr. Michael Hunger, Matthias Scheibe, Michael Dyballa, Christian Lieder und Thomas Montsch für die Durchführung diverser Analysen und Charakterisierungen.

Ein großer Dank gilt meinen Eltern, die mich während meines Studiums immer unterstützt haben. Meinen Freunden und besonders meiner Ehefrau möchte ich für die Unterstützung und die Geduld während meines Studiums und vor allem während der Anfertigung dieser Arbeit danken.

Die vorliegende Arbeit entstand in der Zeit von Juni 2011 bis April 2017 am Institut für Technische Chemie der Universität Stuttgart. Im Rahmen dieser Arbeit entstanden folgende Publikationen:

[1] D. Wan Hussin, Y. Traa, *Energy & Fuels*, **2014**, 28, 3352-3356, DOI: 10.1021/ef500333b.

[2] D. Wan Hussin, Y. Traa in "Small-Scale Gas to Liquid Fuel Synthesis", chapter 13 "Production of High-Octane Fuel Components by Dehydroalkylation of Benzene with Mixtures of Ethane and Propane", ISBN 1466599383.

[3] Y. Traa and D. Wan Hussin: "Production of High-Octane Fuel Components by Alkylation of Benzene with Mixtures of Ethane and Propane", 21st World Petroleum Congress Pre-print Proceedings, World Petroleum Council, 2014, Forum 13.

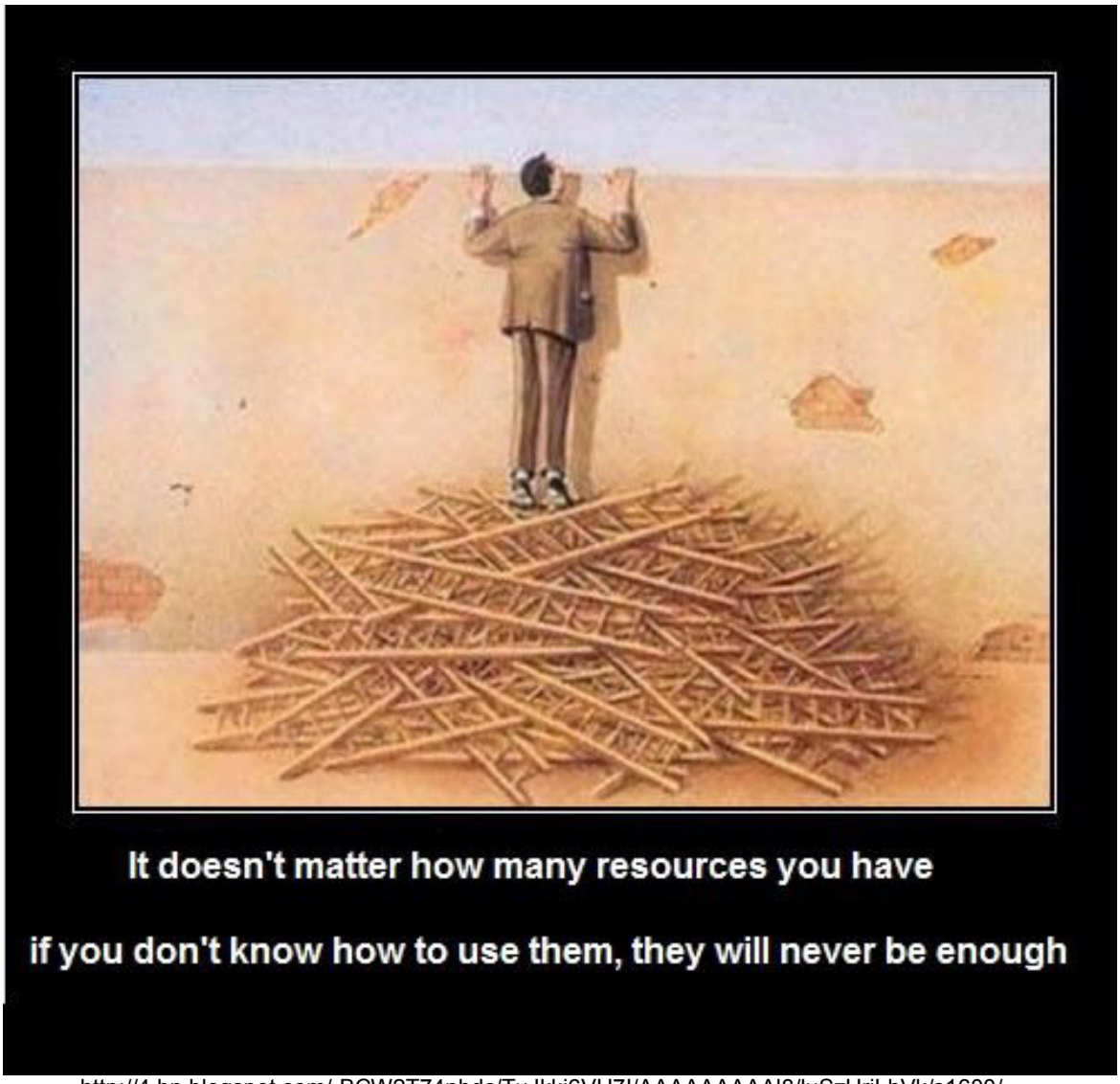

http://4.bp.blogspot.com/-BCW2T74nbdc/TuJkki6VH7I/AAAAAAAAAI8/luSzHrjLhVk/s1600/391934_2349670665563_1363983719_32150712_1046939243_n.jpg (21.10.2014)

Table of Contents

Symbols IX

Abbreviations and Acronyms X

Nomenclature of Catalysts XIII

1 Zusammenfassung 1

2 Summary 6

3 Introduction 10

4 Literature Review 12

4.1 Natural Gas as a Resource 12

4.1.1 Genesis and Occurrence of Natural Gas 12

4.1.2 Modes of Natural Gas Transportation 15

4.1.3 Gas to Liquid (GTL) 19

4.2 Zeolites 23

4.2.1 Zeolite ZSM-5 25

4.2.2 Zeolite Beta 27

4.2.3 Zeolite MCM-22 29

4.3 Activation of Alkanes 32

4.3.1 Aromatization of Light Alkanes to Benzene 33

4.3.2 Disproportionation of Propane 35

4.4 Alkylation of Aromatics 37

4.4.1 Catalyst Deactivation during Benzene Alkylation 43

4.5 Automotive fuels 45

4.6 Octane Number 48

5 Motivation and Objectives 50

6 Experimental Section 51

6.1 Chemicals 51
6.2 Preparation of the Catalysts 52
6.2.1 Synthesis of Zeolite ZSM-5 52
6.2.2 Synthesis of Zeolite Beta 53
6.2.3 Synthesis of Zeolite MCM-22 54
6.2.4 Calcination 54
6.2.5 Ion Exchange 54
6.2.6 Pelletizing of the Catalyst 55
6.3 Catalyst Characterization 56
6.3.1 Magic Angle Spinning Nuclear Magnetic Resonance Spectroscopy 56
6.3.2 Scanning Electron Microscopy (SEM) 56
6.3.3 Thermogravimetric Analysis (TGA) 57
6.3.4 X-Ray Powder Diffractometry (XRD) 57
6.3.5 Inductively Coupled Plasma Optical Emission Spectrometry (ICP-OES) 57
6.3.6 Elemental Analysis (CHN) 58
6.3.7 Gas Chromatography coupled with Mass Spectrometry (GC/MS) 59
6.4 Catalytic Experiments 60
6.4.1 Alkylation in the Fixed-Bed Reactor 61
6.4.2 Alkylation in the Membrane Reactor 61
6.5 Evaluation of the Catalytic Experiments 63
6.5.1 GC Analysis 63
6.5.2 Calculations 64
7 Results and Discussion 66
7.1 Results of Catalyst Characterization 66
7.2 Preliminary Experiments 67
7.2.1 Influence of the Reactants 68
7.2.2 Influence of the n_{Si}/n_{Al} Ratio 71
7.2.3 Influence of the Noble Metal 72

7.3 Influence of the Reactor Type 77
7.3.1 Pre-coking of the Catalyst 79
7.3.2 Effects of the Membrane Reactor and H_2 Scavengers for Hydrogen Removal 82
7.3.3 Calculation of the H_2 Permeation Rate through the Membrane 85
7.4 Time on Stream Behavior and Regeneration of the Catalyst 90
7.5 Dehydroalkylation at Different Temperatures and Influence on Product Distribution .. 95
7.6 Investigations of the *n*-/*iso*-Ratio of Propylbenzene during Dehydroalkylation 99
7.7 Dehydroalkylation over different Pore Systems 104
7.7.1 Benzene Dehydroalkylation over MCM-22 104
7.7.2 Benzene Dehydroalkylation over Zeolite Beta 107
7.7.3 Comparison of Catalysts with different Pore Systems 109
8 References 112
8.1 Table of Figures 123
8.2 Table Summary 126
9 Appendices 128

Symbols

Symbol	Unit	Dimension
A	m^2	Area
E	J, MMBtu	Energy
I	A	Current
m	g, kg, t	Mass
n	mol	Molar Amount of Substance
p	Pa, bar	Pressure
Q_i	$mol \cdot s^{-1}$	Permeation Flow Rate of Component i
Q_{H2}	$mol \cdot s^{-1}$	Permeation Flow Rate of H_2
S_{Tot}	$m^2 \cdot g^{-1}$	Total Surface Area
T	K, °C	Temperature
t	s, min, h,d	Time
U	V	Voltage
V	l, m^3	Volume
z	m	Thickness
λ	m	Wavelength
ρ_i	$mol \cdot m^{-1} \cdot s^{-1} \cdot Pa^{-1}$	Permeability of Component i
ρ_{H2}	$mol \cdot m^{-1} \cdot s^{-1} \cdot Pa^{-1/2}$	Permeability of H_2

Abbreviations and Acronyms

Abbreviation	Meaning
ATR	Auto Thermal Reforming
bbl	Blue Barrel (~159 dm^3)
bcm	Billion Cubic Meters
BEA	Zeolite with the Structure type Beta
BTX	Benzene, Toluene, Xylene
Bz	Benzene
CFR	Cooperative Fuel Research
CIS	Commonwealth of Independent States
CNG	Compressed Natural Gas
DME	Dimethyl Ether
EB	Ethylbenzene
EFA	Extra Framework Aluminum
EN	European Norm
Et	Ethane
EU	European Union
FCC	Fluid Catalytic Cracking
FID	Flame Ionization Detector
GTC	Gas to Commodity
GTL	Gas to Liquids

Abbreviation	Meaning
GTS	Gas to Solid
GTW	Gas to Wire
FT	Fischer-Tropsch
HTFT	High-Temperature-Fischer-Tropsch
IPB	*iso*-Propylbenzene
IUPAC	International Union of Pure and Applied Chemistry
IZA	International Zeolite Associatioon
LNG	Liquefied Natural Gas
LTA	Linde Type A
LTFT	Low-Temperature-Fischer-Tropsch
MAS	Magic Angle Spinning
MCM	Mobil Composition of Matter
mcm	million cubic meters
MFI	Mobil Five
MON	Motor Octane Number
MR	Membered Ring
MTG	Methanol to Gasoline
MWW	Mobil Twenty-two
NG	Natural Gas
NGH	Natural Gas Hydrate
NMR	Nuclear Magnetic Resonance
NPB	*n*-Propylbenzene

Abbreviation	Meaning
OMR	Oxygen Membrane Reforming
POX	Partial Oxidation
Pr	Propane
SEM	Scanning Electron Microscope
SMR	Steam Methane Reforming
RON	Research Octane Number
TCD	Thermal Conductivity Detector
tcm	Trillion Cubic Meters
TGA	Thermogravimetric Analysis
toe	Tons of Oil Equivalent
TOS	Time on Stream
TPABr	Tetrapropylammonium bromide
USA	United States of America
USD	US Dollar
WHSV	Weight Hourly Space Velocity
XRD	X-Ray Powder Diffractometry
ZSM	Zeolite Socony Mobil

Nomenclature of Catalysts

The nomenclature of the catalysts consists of the type of zeolite, while the nature of the cations to stabilize the negative charge from the aluminum in the lattice is stated by prefixes. In case of different cations in one catalyst the amount wt.-% related to the dry catalyst is added to the prefix. The n_{Si} / n_{Al} ratio is given in parentheses as suffix. For example the catalyst 1.9Pt-H-ZSM-5(35) is a zeolite ZSM-5 with an n_{Si} / n_{Al} ratio of 35, which contains 1.9 wt.-% Pt as cations, the rest of the cations being protons. A H-ZSM-5(35) catalyst would only contain protons as cations, and would be only acidic not bifunctional.

1 Zusammenfassung

Die Welt ist abhängig von fossilen Brennstoffen als Energiequelle. Erdgas ist als Ressource sauberer und in größerem Maß verfügbar als Kohle oder Öl. Die meisten fossilen Brennstoffe, die wir verbrauchen, werden zur Wärmeerzeugung oder als Treibstoff verbrannt. Während sich die Ausbeutung großer Erdgasfelder wirtschaftlich lohnt, ist die Erschließung vieler kleinerer Erdgasvorkommen wirtschaftlich nicht sinnvoll. Das Erdgas über Ölvorkommen wird meist einfach abgefackelt um das darunter liegende Öl sofort zu fördern. Des Weiteren sind Kohle und Öl viel leichter zu transportieren als Erdgas. Die Europäische Union hat daher ein Projekt zur Nutzbarmachung von kleineren, abgelegenen Erdgasvorkommen initiiert. Das Ziel dieses NEXT-GTL Projekts war eine Methode zu entwickeln, Erdgas direkt an seiner Quelle in eine flüssige, einfach zu transportierende Form zu bringen mittels einer möglichst kleinen chemisch-technischen Anlage. Hierzu gab es mehrere Ansätze innerhalb des NEXT-GTL Projekts. Die vorliegende Arbeit beschäftigt sich mit dem Ansatz, den Hauptbestandteil des Erdgases Methan zu Benzol zu aromatisieren und anschließend das gebildete Benzol mit den häufigen Nebenbestandteilen Ethan und Propan zu Alkylaromaten zu alkylieren. Die Aromatisierung wurde von anderen Projektpartnern bearbeitet.

In der vorliegenden Arbeit wurde die Dehydroalkylierung von Benzol mit Gemischen aus Ethan und Propan untersucht. Als Katalysator wurde hauptsächlich Zeolith ZSM-5, sowie die Zeolithe Beta und MCM-22 verwendet. Das Hauptaugenmerk lag auf der Maximierung der Oktanzahl der flüssigen Produktphase $RON_{(l)}$ zur Nutzung als Treibstoffkomponente. Die $RON_{(l)}$ des Gemischs wurde aus den Mischungsoktanzahlen der jeweiligen Komponenten berechnet. Bei der Dehydroalkylierung von Benzol mit Gemischen aus Ethan und Propan entsteht ein weites Spektrum an Produkten, bestehend aus den primären Alkylierungsprodukten Ethylbenzol (EB), *iso*-Propylbenzol (IPB) und *n*-Propylbenzol (NPB), den sekundären Alkylierungsprodukten Toluol, *o*-,*m*-,*p*-Xylole , welche durch Folgereaktionen aus Primärprodukten gebildet werden, sowie Alkanen als Nebenprodukte (Methan, C_4 - C_5). Die $RON_{(l)}$ wird hauptsächlich von dem Benzolumsatz bestimmt, da alle alkylaromatischen Produkte eine höhere Mischungsoktanzahl besitzen als Benzol. Unter den Nebenprodukten kann Methan quasi als verlorener Kohlenstoff angesehen werde, sofern

dieser nicht in einem integrierten Prozess rückgeführt wird. Pentane sind flüssige Nebenprodukte, die die $RON_{(l)}$ aufgrund ihrer Mischungsoktanzahlen, die entweder niedriger oder gleich dem Wert von reinem Benzol sind, meist senken. Butane können als Kraftstoffzusätze im Winterbenzin genutzt werden und sind zudem leichter vom Reaktionsgemisch abtrennbar. Die Dehydroalkylierung von Benzol mit Ethan verläuft sehr selektiv und ergibt fast ausschließlich EB. Die Vielzahl an Produkten wird durch Propan als Edukt verursacht, das viel reaktiver als Ethan ist, da es ein sekundäres Carbeniumion bilden kann. Die auftretende Bildung von Butanen rührt von der Disproportionierung von Propan her. Methan ist ein weiteres, häufiges Nebenprodukt, welches durch Hydrogenolysereaktionen gebildet wird. Bei der Reaktion eines Gemisches aus Ethan und Propan ohne Benzol an einem bifunktionellen Katalysator ist trotzdem eine Bildung von aromatischen Verbindungen zu beobachten.

Die Dehydroalkylierung verläuft über eine Dehydrierungsstufe vom Alkan (Ethan/Propan) zum jeweiligen Alken, wonach in einem zweiten Schritt das gebildete Alken Benzol alkyliert. Die Dehydrierung ist der geschwindigkeitsbestimmende Schritt. Deshalb ist die Olefinkonzentration während der Dehydroalkylierung niedrig. Dies verhindert eine Polyalkylierung des Benzols, obwohl ein Überschuss an Alkan vorliegt. Um die Geschwindigkeit der Dehydrierung zu erhöhen wurde ein Membranreaktor verwendet, der dem Reaktionsgemisch selektiv gebildeten Wasserstoff entzieht und so das Reaktionsgleichgewicht zugunsten der Produkte verschiebt. Die erzielten Ergebnisse im Membranreaktor waren leicht besser als im Vergleich zum Festbettreaktor. Der positive Einfluss der Membran konnte jedoch nachgewiesen werden.

Um den Katalysator zu optimieren wurde das n_{Si}/n_{Al}-Verhältnis im Bereich von 20 - 90 variiert. Als optimales n_{Si}/n_{Al}-Verhältnis ergab sich beim Zeolith ZSM-5 35. Als Edelmetall wurde Pd oder Pt durch Ionenaustausch in den jeweiligen Zeolithkatalysator eingebracht. Pt ist katalytisch aktiver als Pd bei der Dehydroalkylierung, sowohl bei der Dehydrierung als auch bei der Hydrogenolyse. Es wurde festgestellt, dass an einem Katalysator mit Pd als Edelmetall und einem n_{Si}/n_{Al}-Verhältnis von ~20 keinerlei Methan gebildet wird. Es wurde dennoch vorzugweise Pt verwendet, weil damit höhere Benzolumsätze und somit eine höhere $RON_{(l)}$ als mit Pd erzielt werden konnte. Mit Pt als Edelmetall ergab sich während der Dehydroalkylierung eine hohe anfängliche Selektivität zu Methan und Sekundärprodukten. Mit fortschreitender Laufzeit (TOS) verschiebt sich die Selektivität zugunsten der Primärprodukte. Dies wird durch die verschiedenen aktiven Zentren des Pt verursacht. Einige

dieser Zentren sind besonders aktiv in der Katalyse von Hydrogenolysereaktionen, die für die Folgereaktionen der Primärprodukte zu Sekundärprodukten und Methan verantwortlich sind. Diese „Hydrogenolysezentren“ deaktivieren schneller als die Metallzentren, die für die Dehydrierung verantwortlich sind. Die Deaktivierung wird höchstwahrscheinlich durch Verkokung des Katalysators verursacht. Zu Beginn der Reaktion wird ein Benzolumsatz von 41 %, was einer $RON_{(l)}$ von 110 entspricht, an einem 1.9Pt-H-ZSM-5(35) Katalysator bei einer Reaktionstemperatur von 350 °C erzielt. Dieser Benzolumsatz nimmt mit zunehmender TOS ab auf bis zu 16 % und $RON_{(l)}$ = 103 nach ~3 Tagen Laufzeit, während die Nebenproduktselektivität sich von vorwiegend Methan zu vorwiegend höhere Alkane (C_4-C_5) hin ändert. Die Dehydroalkylierung erreicht nach ~24 Stunden Laufzeit einen quasistationären Zustand. Die beschriebene Deaktivierung wurde bei Reaktionstemperaturen von 350 °C und höher beobachtet. Ein Versuch die Aktivität des Katalysators zu Beginn der Reaktion durch eine Hydrierung des gebildeten Koks wiederherzustellen blieb erfolglos. Obwohl der Benzolumsatz während der Reaktion abnimmt, nimmt die Menge an gebildeten Primärprodukten, durch die Selektivitätsverschiebung weg von den Sekundärprodukten, zu.

Der Einfluss der Reaktionstemperatur auf die Dehydroalkylierung wurde im Bereich von 300 - 400 °C untersucht. Bei 400 °C ist der höchste anfängliche Benzolumsatz zu beobachten, der zu einer $RON_{(l)}$ von 113 führt. Dieser hohe anfängliche Benzolumsatz von 48 % nimmt über den Verlauf eines Tages auf 20 % ab, was dem Wert bei einer Temperatur von 350 °C entspricht. Bei hohen Reaktionstemperaturen wird zu Beginn der Reaktion große Mengen an Sekundär- und Nebenprodukten, v. a. Methan, gebildet. Bei höheren Laufzeiten im Bereich von 350 - 400 °C verschiebt sich die Produktverteilung zugunsten der Primärprodukte, Butane und Pentane. Bei 300 °C liegt der anfängliche Benzolumsatz deutlich unter denen der verwendeten höheren Temperaturen, zeigt dafür jedoch keine Abnahme und hält einen stabilen Wert von 13 %, bei $RON_{(l)}$ = 102.6, für 2 Tage. Es werden dabei hauptsächlich Primärprodukte gebildet. Die einzig anderen beobachteten Produkte sind Butane, Methan und geringe Mengen an Toluol.

Bei dem Vergleich von drei verschiedenen Zeolithkatalysatoren zeigte sich als der für die Dehydroalkylierung geeignetste der Zeolith ZSM-5. Der Zeolith MCM-22 erzielt die gleiche $RON_{(l)}$ wie der Zeolith ZSM-5, bildet aber weit mehr Methan anstelle von Butanen als gasförmige Nebenprodukte. Zeolith Beta zeigt nur geringe Aktivität bei der Umsetzung von Benzol, was in einer niedrigen $RON_{(l)}$ resultiert. Es werden jedoch bei langen Laufzeiten ausschließlich Primärprodukte, sowie Methan als einziges Nebenprodukt beobachtet. Die

Mengen an akkumuliertem Koks auf den jeweiligen Zeolithtypen hängen von der Größe der Poren ab. In Zeolithen mit großen Poren kann sich mehr Koks ablagern als in denen mit kleinen Poren.

Nachdem ein Projektpartner des NEXT-GTL Projekts besonderes Interesse an der Selektivität zu IPB geäußert hatte, wurde das NPB/IPB-Verhältnis näher untersucht. Es konnte gezeigt werde, dass die Reaktionstemperatur keinen Einfluss auf das NPB/IPB-Verhältnis hat. Die NPB/IPB-Verhältnis zu Reaktionsbeginn unterscheiden sich noch, aber mit zunehmender Laufzeit ergibt sich über das gesamte verwendete Temperaturspektrum ein NPB/IPB-Verhältnis von ~1.5. Allerdings lässt sich das NPB/IPB-Verhältnis durch den Zeolithtyp beeinflussen. Als bester Katalysator zeigte sich 2.1Pt-H-Beta(24), wobei ein 2.5facher Überschuss an IPB gegenüber NPB (NPB/IPB-Verhältnis = 0.4) bei einem Benzolumsatz von 10 % erreicht wurde. Die Katalysatoren der Zeolithe ZSM-5 und MCM-22 bildeten durchweg mehr NPB als IPB. Die direkte Benzolalkylierung mit Propen ist viel selektiver und benötigt keinen bifunktionellen Katalysator. Somit ist diese zur Produktion von IPB besser geeignet.

Der beste verwendete Katalysator zur Dehydroalkylierung war 1.9Pt-H-ZSM-5(35). Die höchste $RON_{(l)}$ von 113 der vorliegenden Arbeit wurde an diesem Katalysator bei 400 °C zu Beginn der Reaktion erhalten. Nach einer Laufzeit von 9 Tagen bei einer Temperatur von 350 °C wurde an diesem Katalysator ein Benzolumsatz von 15 % und eine $RON_{(l)}$ von 103 beobachtet. Die Produkte der flüssigen Phase bestanden nahezu ausschließlich aus Primärprodukten (20 % NPB, 15 % IPB, 9 % EB), während die gasförmigen Nebenprodukte vorwiegend aus Butanen mit 42 % bestanden.

Für die Produktion von Kraftstoffkomponenten, bei der das Hauptaugenmerk allein auf der $RON_{(l)}$ liegt und die genaue Zusammensetzung der Alkylaromaten nicht von Belang ist, ist die Dehydroalkylierung mit Gemischen aus Ethan und Propan ein geeignetes Mittel. Eine Erhöhung der $RON_{(l)}$ von 99 auf 103 konnte erreicht werden. Jedoch benötigt das Produktgemisch eine weitere Aufarbeitung um als Fahrzeugkraftstoff zu dienen. Vor allem nicht umgesetztes Benzol muss innerhalb des Prozesses zurückgeführt, oder anderweitig verwendet werden. Der Einfluss des Membranreaktors auf das Reaktionsgleichgewicht brachte bei der Dehydroalkylierung nur einen geringen Vorteil. Die verwendeten Reaktionsbedingungen waren für den Betrieb des Membranreaktors nicht optimal. Ein höherer Druck als der verwendete Bereich von 0.5 - 0.65 MPa, um höhere Eduktkonzentrationen auf der Reaktionsseite der Membran zu erreichen, könnte dazu führen,

dass der Effekt der Membran besser ausgenutzt würde. Leider ist dies bei der Verwendung von Propan als Edukt nicht möglich, da Propan über einen zu geringen Dampfdruck verfügt. Für die Verwendung von Ethan ohne Propan ist der Membranreaktor besser geeignet.

2 Summary

The world relies on fossil fuels as a source of energy. Natural gas is a resource far more abundant than oil, and much cleaner than coal. Most of the fossil fuel we consume is burned for heating or transportation fuel. While it is profitable to exploit large natural gas fields, many smaller natural gas deposits are economically not worthwhile to exploit. Natural gas over oil deposits is regularly flared in order to reach the oil beneath immediately. Also oil and coal are easier to transport than natural gas. Therefore, the European Union started a project to utilize natural gas from small, remote gas fields. The aim of this NEXT-GTL project was to devise a novel method to convert natural gas directly at its well, requiring only a small-scale plant, into an easy transportable liquid form. Several approaches were attempted in the frame of the NEXT-GTL project. This work focuses on the path of aromatizing the main natural gas component methane to benzene, and subsequently alkylating the produced benzene with the common minor components of natural gas ethane and propane to produce alkylaromatic compounds. The aromatization of methane to benzene was investigated by other project partners of the NEXT-GTL project.

In this thesis the dehydroalkylation of benzene with mixtures of ethane and propane over a bifunctional zeolite catalyst was studied. As catalysts mainly zeolite ZSM-5 was used. Other used catalysts were based on zeolite Beta and zeolite MCM-22. The main focus lay on the maximization of the research octane number of the received liquid phase $RON_{(l)}$ for use as fuel component. The $RON_{(l)}$ of the mixture was calculated with the blending RONs of the respective components. The dehydroalkylation of benzene with a mixture of ethane and propane produces a widely varied product distribution consisting of the primary alkylation products ethylbenzene (EB), *iso*-propylbenzene (IPB), and *n*-propylbenzene (NPB), the secondary alkylation products toluene, *o*-,*m*-,*p*-xylenes, which derive from further reactions of primary products, and alkane side products (methane, C_4-C_5). The $RON_{(l)}$ mainly depends on the amount of converted benzene, since all alkylaromatics have a higher blending RON than benzene does. Among the side products, methane is effectively wasted carbon unless recycled to an integrated process. Pentanes are liquid, but do not contribute to or even lower the $RON_{(l)}$, since the blending RONs of pentanes are equal to or lower than that of unreacted benzene. Butanes can be used as fuel components in winter gasoline among other uses, and can more easily be separated. The dehydroalkylation of benzene with ethane is selective and

produces EB almost exclusively. The diversity of products is caused by propane as reactant, which is far the more active than ethane, due to the ability to form a secondary carbenium ion. The production of butanes, which are regularly observed, is attributed to the disproportionation of propane. Another major side product is methane, which is produced from hydrogenolysis reactions. When reacting a mixture of ethane and propane over a bifunctional catalyst the formation of aromatic compounds can be observed.

The dehydroalkylation proceeds via a dehydrogenation step of the alkane (ethane/propane) to the respective alkene. Subsequently, the alkene alkylates benzene. The dehydrogenation is the rate limiting step, therefore, the alkene concentration during dehydroalkylation is low. This fact avoids polyalkylation, although an excess of alkane is used. To improve the dehydrogenation rate by removing the hydrogen from the reaction stream and thus shift the equilibrium towards the product side, a membrane reactor was utilized. The results from the membrane reactor are slightly superior to those from a fixed-bed reactor. However, the effect of the membrane could be proven.

To find an optimal catalyst the n_{Si}/n_{Al} ratio was varied in the range of 20 – 90. The optimal n_{Si}/n_{Al} ratio of the used ZSM-5 catalyst is 35. As noble metal Pd and Pt were used. Pt is more active than Pd during dehydroalkylation, for dehydrogenation and hydrogenolysis reactions. It was found that when using Pd as noble metal *and* an n_{Si}/n_{Al} ratio of ~20 the catalyst does not produce unwanted methane during dehydroalkylation. Pt was used preferentially due to the higher benzene conversion and thus higher $RON_{(l)}$ obtained with Pt than Pd. With Pt as noble metal the selectivity to methane and secondary alkylation products was initially high during the dehydroalkylation. However, with increased time on stream (TOS) the selectivity shifted towards primary alkylation products. This was attributed to the different nature of Pt sites. Some sites are very active in catalyzing hydrogenolysis reactions, which are responsible for the further reaction of primary products to secondary products and the formation of methane. These “hydrogenolysis” sites seem to deactivate faster than those sites active in dehydrogenation. This deactivation is most likely caused by coking. Initially a benzene conversion of 41 %, which corresponds to a $RON_{(l)}$ of 110, is achieved over 1.9Pt-H-ZSM-5(35) at a reaction temperature of 350 °C. This benzene conversion decreases over increased TOS to 16 % and $RON_{(l)}$ = 103 after ~3 days, while the selectivity to side products shift from mainly methane to mainly higher alkanes (C_4 - C_5). The dehydroalkylation reaches a steady state after ~24 h on stream. This deactivation is observed at temperatures of 350 °C and higher. An attempt to restore the initial activity of the catalyst by hydrogenating the formed

coke on the catalyst proved ineffective. Although, the benzene conversion decreases over time, the amount of primary products increases due to the shift in selectivity away from secondary products.

The influence of the reaction temperature on the dehydroalkylation was investigated in the range of 300 – 400 °C. At 400 °C the initial benzene conversion is the highest obtained in this thesis resulting in the highest produced $RON_{(l)}$ of 113. This initially high conversion of 48 % decreases over one day on stream to 20 %, which is on par with results obtained at 350 °C. Higher temperatures initially produce large amounts of secondary alkylation products and side products, most of all methane. At longer times on stream the selectivity shifts towards primary products, butanes and pentanes in the temperature range of 350 - 400 °C. For 300 °C the results are different. The initial conversion and $RON_{(l)}$ are considerably lower than at the higher temperatures used, but maintains a stable value of 13 % and $RON_{(l)}$ 102.6 over two days on stream. Mainly primary products are produced, the only other products being butanes, methane and little toluene.

The comparison of three different zeolites as catalysts showed, that for the dehydroalkylation zeolite ZSM-5 is the catalyst of choice. Zeolite MCM-22 produces the same $RON_{(l)}$ as zeolite ZSM-5 does, but produces a far greater amount of methane instead of butanes as gaseous side products. Zeolite Beta shows low activity for benzene conversion and thus low $RON_{(l)}$. However, only primary products and methane as the only other product are observed at long times on stream. The amount of coke accumulated on the respective zeolites proved to be dependent on the available space inside the pores. Those catalysts with large pores could support more coke than those with small ones.

Since one cooperating partner from the NEXT-GTL project uttered particular interest in the selectivity to IPB, the NPB/IPB ratio was investigated. It was found, that the reaction temperature does not influence the NPB/IPB ratio. The initial ratios differ, but at longer times on stream in the entire employed temperature range of zeolite ZSM-5 produces an NPB/IPB ratio of ~1.5. The NPB/IPB ratio can, however, be influenced by the use of a different parent zeolite as catalyst. The best results were obtained over 2.1Pt-H-Beta(24), which produces a 2.5-fold excess of IPB over NPB (NPB/IPB ratio = 0.4) with a benzene conversion of 10 %. Catalysts with zeolite ZSM-5 and zeolite MCM-22 as parent zeolite consistently produce more NPB than IPB. The direct alkylation of benzene with propene is much more selective, and requires no bifunctional catalyst, and thus is better suited for the production of IPB.

The best catalyst for the dehydroalkylation was found to be 1.9Pt-H-ZSM-5(35). The highest $RON_{(l)}$ of 113 was achieved over this catalyst at a temperature of 400 °C at the start of the reaction. At 350 °C and long times on stream of 9 days a stable benzene conversion of 15 % and a $RON_{(l)}$ of 103 were observed over this catalyst. The liquid products were almost exclusively primary products (20 % NPB, 15 % IPB, 9 % EB), while the gaseous side products consisted mainly of butanes with 42 %.

For the production of fuel components, where the focus lies solely with the $RON_{(l)}$ and the composition of the alkylaromatics is of no importance, the dehydroalkylation of benzene with mixtures of ethane and propane is feasible. An increase of the $RON_{(l)}$ from 99 to 103 was achieved. However, the product composition requires further separation and refining in order to be used as fuel for vehicles. Mainly unreacted benzene needs to be recycled to the process or used otherwise. The effect of the membrane reactor on the equilibrium proved to be only of little benefit to the dehydroalkylation of benzene with mixtures of ethane and propane. The applied operating conditions were not optimal for the use of a membrane reactor. Higher operating pressures than the used 0.57 - 0.65 MPa to achieve higher reactant concentrations on the reaction side of the membrane could help to fully exploit the potential of this reactor type. This is unfortunately not possible when using propane as reactant, due to its comparatively low vapor pressure. For the dehydroalkylation with only ethane a greater membrane effect can be expected.

3 Introduction

The worldwide need for fossil fuels continues to rise. Yet, it is economical to flare natural gas in order to reach below lying crude oil. Natural gas is far more abundant than oil, and the reserves continue to rise. New technologies, such as hydraulic fracturing prominently employed in the United States of America or the utilization of natural gas hydrates from the bottom of the ocean researched by Japan, together with the existing large amounts of reserves make natural gas a reliable resource in the foreseeable future. Although natural gas is abundant enough, the worldwide distribution does not match the demand. The transport of natural gas from the gas field to its destination would be easier and cheaper, if the transporting good would be liquid and not gaseous. Natural gas consists mainly of methane, other hydrocarbons can be ethane and propane. Other components can include CO_2 and H_2S which makes the natural gas corrosive and more elaborate to handle, as well as nitrogen and helium, which is quite a valuable side product from natural gas. Currently, the liquefaction of natural gas is conducted commercially by cooling to condensation at -161 °C and transportation via ship, or the Fischer-Tropsch synthesis to fuels and higher hydrocarbons.

The aim of the NEXT-GTL project by the European Union was to find an economically feasible method of utilizing natural gas on a small scale and convert it to a liquid form. The process from gas to liquids (GTL) can be achieved in multiple ways. This work is based on the participation in the NEXT-GTL project, and continues the work of D. Geiß, who started the participation of the University of Stuttgart in the project together with Y. Traa. The pursued approach, on which this work focuses, is to aromatize the methane fraction of the natural gas to already liquid benzene, and further alkylate the produced benzene to alkylaromatics with the ethane/propane fraction for use as fuel components. These alkylaromatics are well suited for use as fuel components, since they improve the research octane number (RON) of an otherwise inferior fuel by their addition, since they have very high blending RONs, and therefore greatly improve the quality of the blended fuel.

In order to alkylate benzene with ethane/propane a dehydroalkylation has to be conducted. This work focuses on the use of a mixture of ethane and propane. In the scope of the NEXT-GTL project the use of a feed stream not requiring extensive purification was aspired. Also the alkylation with only one alkane is already well studied. For the dehydroalkylation a

bifunctional zeolite catalyst is used in this work. Zeolite catalysts are well known, reliable catalysts in the petrochemical industry, that see wide use in many applications. Zeolites are alumosilicates that possess distinctive micropores, which have a size in the order of simple organic molecules and can therefore influence chemical reactions, since reactants have to enter these pores in order to reach a catalytically active site.

For the dehydroalkylation, the catalyst must be active in the dehydrogenation of the alkane to the respective alkene, and the subsequent alkylation of the aromatic. The dehydrogenation activity can be bestowed on the catalyst by incorporating noble metals such as Pd or Pt. The highly endothermic dehydrogenation of ethane or propane outweighs the respective exothermic alkylation of benzene. Therefore, the dehydroalkylation is overall endothermic and requires heating. The equilibrium shifts to the alkylated products with higher temperatures. Another way to influence the equilibrium of the dehydroalkylation in the scope of the NEXT-GTL project employed in this work is the use of a hydrogen-selective membrane reactor. The dehydroalkylation produces H_2, therefore the equilibrium is shifted toward the products when H_2 is selectively removed from the reaction. The overall aim of this work is to maximize the RON of the liquid phase.

This work will give a deeper insight into the dehydroalkylation, and its ability to produce fuel components from a product stream originating from natural gas. The influence of the reactants as mixture and individually will be discussed. The influence of the noble metal used in the catalyst and its aluminum content on the dehydroalkylation will be investigated. The performance of the catalysts in fixed-bed and membrane reactor setup, and during short and long times on stream will be compared. Finally, the application of the dehydroalkylation for the production of fuel components as well as other applications will be examined.

4 Literature Review

4.1 Natural Gas as a Resource

4.1.1 Genesis and Occurrence of Natural Gas

Natural gas (NG) is formed by anaerobic degradation of organic matter together with the formation of oil or coal (Fig. 1). The first step in this process is the diagenesis forming initial kerogen [4]. Some of the organic polymers are already then transformed into methane, producing biogenic natural gas, which is mostly "wet" (see below). The second step is the catagenesis during which oil is formed in depths of 2000 - 4000 m at a pressure of hundreds of MPa and temperatures of 65 - 120 °C. During this process thermogenic natural gas is formed while the organic matter is transformed into oil. At even greater depths (>4000 m), oil is further converted to methane. During this metagenesis, "dry" (see below) natural gas is prominently formed. Another source of natural gas formation is the process of coalification, where also particularly dry natural gas is formed. The composition of natural gas together with its notable impurities is listed in Table 1. The term "wet" for natural gas originates from the fact that when compressed the natural gas containing not only methane but also ethane, propane and higher hydrocarbons in notable amounts will partly condense. Likewise, natural gas consisting nearly entirely of methane is called "dry" or "lean". NG comprising higher amounts of CO_2 and/or H_2S is called "sour" or "acidic" natural gas.

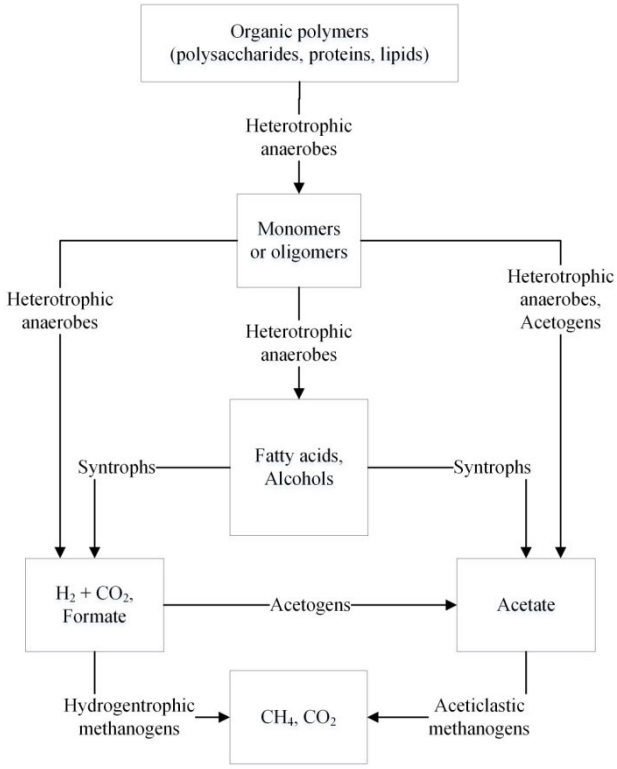

Fig. 1: Anaerobic food chain for the conversion of organic matter to methane, modified from [4].

Table 1: Composition of natural gas [5].

Compound	Molar fraction
Hydrocarbons	
Methane	75 - 99 %
Ethane	1 - 15 %
Propane	1 - 10 %
i-Butane	0 - 1 %
n-Butane	0 - 2 %
i-Pentane	0 - 1 %
n-Pentane	0 - 1 %
Hexanes	0 - 1 %
Heptanes and higher	0 - 0.1 %
Nonhydrocarbons	
Nitrogen	0 - 15 %
Carbon dioxide	0 - 30 %
Hydrogen sulfide	0 - 30 %
Helium	0 - 5 %

Natural gas is mainly used as combustible gas for the production of heat. Therefore, it is not surprising that it is traded at stock exchanges by measures of energy (MMBtu). The calorific value of NG is ~ 40 MJ · m^{-3} [6].

The first utilization of NG by mankind as fuel is attributed to the production of salt from boiling brine in China 500 B.C., where natural gas was transferred from its well through "pipelines" fashioned from bamboo [7]. Industrially, NG is used since the 19th century mainly for heating and illumination.

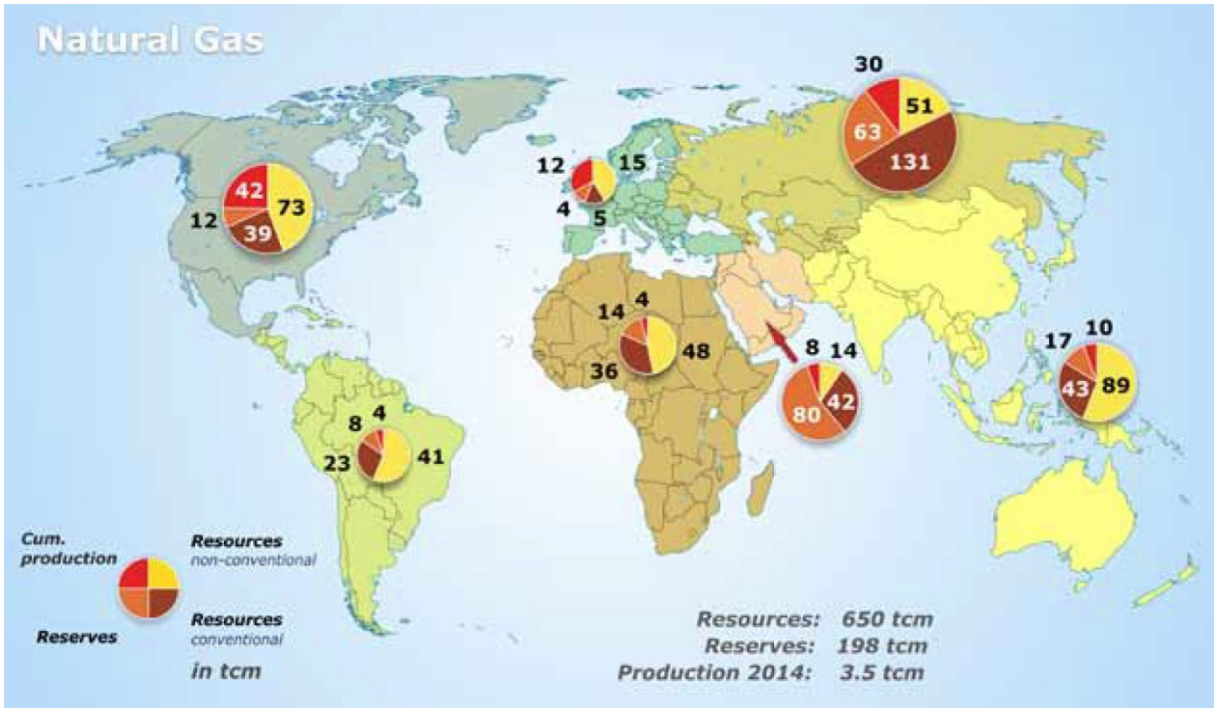

Fig. 2: Global distribution of natural gas potential, data status 2014 [6].

The global distribution of natural gas together with some information on how much of the NG has already been exploited (cumulative production), how much proven reserves exist by the end of 2014 and how much resources are possibly exploitable can be seen in Fig. 2. The global production of NG in 2014 amounted to 3.5 trillion cubic meters (tcm).

The world´s natural gas reserves, whose existence is proven and technologically and economically exploitable at current market prices, are located mainly in the Commonwealth of Independent States (CIS, former Soviet Republics) and the Middle East. The term "reserves" is not to be confused with "resources", which relates to proven amounts of NG, which currently cannot be exploited for technical and/or economic reasons, as well as to unproven but geologically suspected amounts of NG that may be exploitable in the future. The sum of reserves and resources (conventional and non-conventional) is the "remaining potential", which together with the cumulated production totals to the "estimated ultimate potential". The CIS and the Middle Eastern states are therefore naturally among the world´s top producers of natural gas [6]. In recent years, the United States of America (USA) have replaced Russia as the world´s greatest producer of natural gas. This is mainly due to the exploitation of shale gas by means of hydraulic fracturing, which is heavily disputed for its environmental impact on water [8] and air [9]. Europe plays only a minor role in the world´s production of NG, with the only notable producing countries being Norway and the Netherlands.

Among the world´s top consumers of natural gas is first by far the USA, followed by Europe, Russia, China, Iran, and Japan. The global distribution of natural gas reserves and producers unfortunately does not match the distribution of consumers. Therefore, the NG has to be transported from producer to consumer. The transportation of natural gas will be discussed in detail in the next chapter. One exception is the USA. Here the production and consumption are (relatively) nearby. It is expected, that the USA will continue to increase the production of NG further and, despite being the greatest consumer, become a net exporter of NG within the next few years (ca. 2018) [10]. Europe, and Germany in particular, will remain dependant on natural gas imports. Germany covers only mere 13 % of its NG consumption by own production, receiving the remainder from the CIS, Norway and the Netherlands via pipeline [6].

On a global scale natural gas resources are sufficiently large to last many decades, even if an increase in consumption (which is very likely) is accounted for. It is therefore viewed as a promising transition fuel on the way to more sustainable, renewable energies [6,8-11].

4.1.2 Modes of Natural Gas Transportation

As shown in the previous chapter, the regional distribution of natural gas reserves and its production does not match the distribution of its demand. Therefore, the NG must be transported from the production site to its consumer. In principle, there are several different modes of transporting natural gas or the energy stored in it [12], such as:

1. pumping gas through a pipeline (onshore/offshore)
2. by ship as liquefied natural gas (LNG) with subsequent regasification
3. compression of the NG up to p > 20 MPa (CNG, Compressed Natural Gas)
4. converting the NG chemically into liquid products (GTL, Gas to Liquids)
5. conversion of NG into or direct mining of hydrate (GTS, Gas to Solid)
6. direct combustion in power plant to produce electricity (GTW, Gas to Wire)
7. use of natural gas to produce goods and transport of these (GTC, Gas to Commodity)

Strictly speaking, only the first tree methods represent the transportation of natural gas. Yet, the other methods, where the NG is converted in some way prior to transport, can also be considered as transport of the energy or value stored within the natural gas.

The use of natural gas to produce commodities (GTC) which require large quantities of energy, such as aluminum, iron/steel, glass, bricks, cement, etc., is only practical when certain conditions are met. The natural gas well should be in close proximity to an industrial center, otherwise said industry would have to be built explicitly at the site of NG production. Also the other required raw materials should be found nearby, or else they would have to be transported, which can - depending on the materials - easily exceed the costs of NG transportation [12].

Since a good portion of the natural gas is used to produce electricity (GTW), it is possible to build a power plant directly at a well of natural gas and transport the energy as electricity by cable. For longer distances, however, the energy loss from long distance transmission lines becomes too high to be an alternative to the transport of the NG by other methods such as pipelines [12].

Pipelines are the most common mode of natural gas transportation. Pipelines are divided into onshore and offshore pipelines. Onshore pipelines for transport over long distances are operated at pressures up to 8.4 MPa, while every 150 - 200 km a compressor station is needed

to keep the pressure between 6 and 8.4 MPa [13]. Regional distribution of NG is accomplished by a network of pipelines with pressures of ~ 1.6 MPa, and finally for supply of individual households pressures of less than 1 bar are employed. These low-pressure lines are often fashioned from plastic materials. Offshore pipelines, on the other hand, operate at pressures up to 20 MPa and can cover distances of up to 1400 km in depths of 600 m without a compressor station. Offshore pipelines are more expensive than onshore pipelines and the specific costs of transportation are much higher for natural gas than for other fossil fuels, due to its lower energy density (see Fig. 3) [14]. High-pressure pipelines are therefore built onshore wherever possible. However, the longer the required transport distance, the more economically reasonable becomes the shipping via LNG carrier. Equality of specific transport costs with LNG ships are reached at 2000 km for offshore pipelines and 4000 km for onshore pipelines [15], or in between for combinations thereof. Exact determination depends on the capacity to be transported and the corresponding costs of LNG ships for size, construction and maintenance, as well as pipeline design (diameter, on-/offshore construction, etc.).

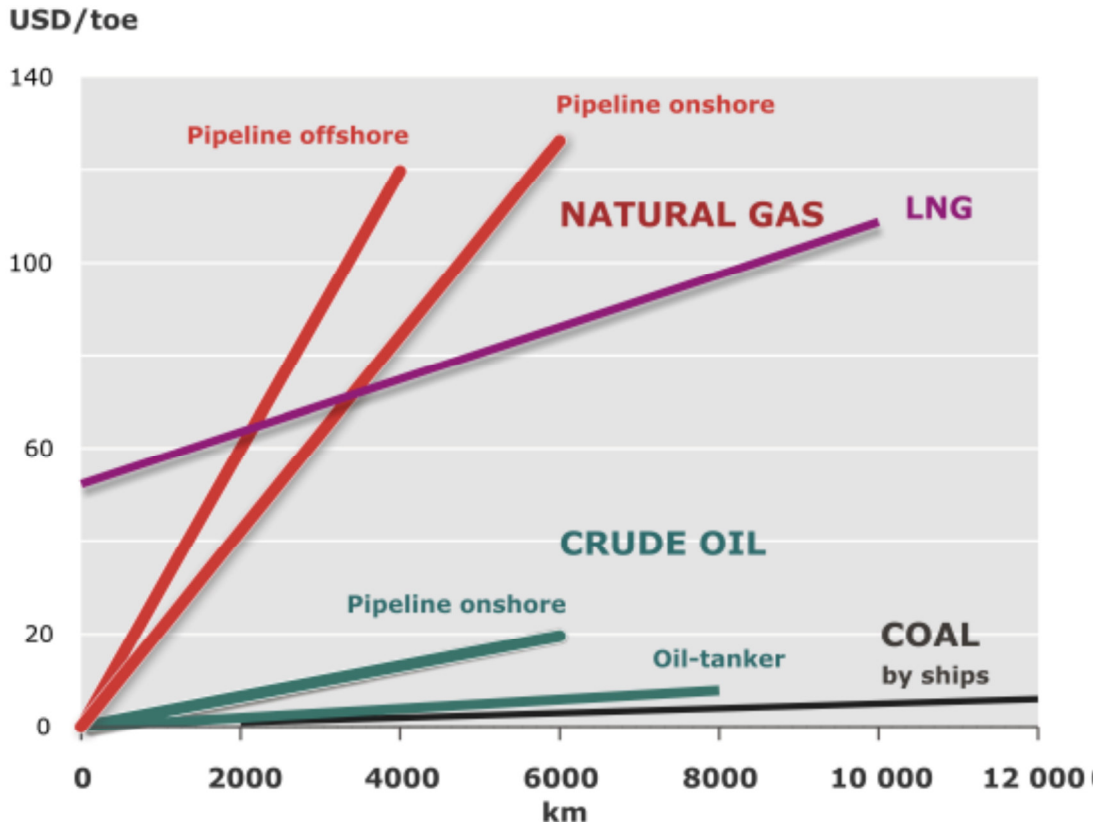

Fig. 3: Comparison of the transportation costs for different fossil fuels [14].

The transport of NG as liquefied natural gas is advantageous at long distances, especially overseas. The natural gas needs to be cooled to -162 °C in order to condense. The volume is reduced by a factor of 600, which increases the energy density of the transported material

accordingly. The condensed NG can be loaded into specialized ships (LNG carriers) transported to the port of destination for regasification and distribution through the local pipeline network [13]. These processes are energy intensive and require special facilities. Therefore, LNG trade is reasonable only on a large scale. The more natural gas is to be transported and the longer the covered distance is, the more worthwhile LNG shipment gets. As shown in Fig. 4, it is therefore expected for the LNG trade to further increase, since the traded amounts increase, as do the transport distances. Investment costs are high, and long-term planning is required for the huge facilities required for liquefaction/regasification and storage. Modern LNG carriers require good insulation and additionally are equipped with on board re-liquefaction units to prevent the boil off of the liquid gas. Their cargo capacity is up to 266000 m³ [16] LNG, this corresponds to ~ 160 mcm (million cubic meters).

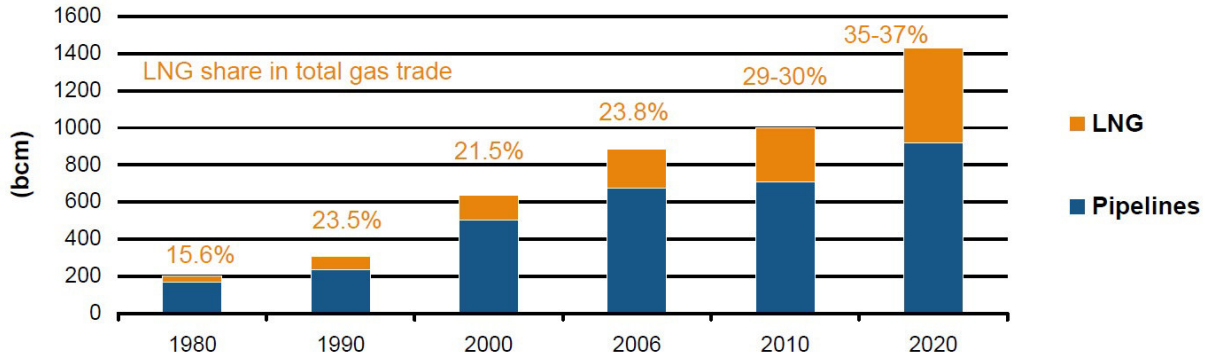

Fig. 4: Traded natural gas volume (worldwide) in billion cubic meters (bcm), used by permission of the World Energy Council, London, www.worldenergy.org [17].

Europe is in a relatively comfortable position considering its dependency on foreign gas reserves. A well developed infrastructure of pipelines covers Europe and connects to the Middle East, the CIS and even North Africa, while also featuring LNG receiving terminals in the Mediterranean Sea, the North Sea and along the Atlantic coastline. In contrast, Japan – the world´s greatest importer of NG [6] – heavily relies on LNG transportation (see Fig. 5) [18]. To reduce its dependency on NG imports, Japan has undertaken experiments to exploit non-conventional resources of methane hydrate deposits at the bottom of the ocean [19].

Utilizing reservoirs of natural gas hydrates (NGH) is not only interesting for Japan, since NGH resources are found on many shorelines all over the world [20]. NGH can also be produced from the NG recovered from other sources and then transported as a solid (GTS) [12]. To produce NGH, water is mixed with NG at pressures from 8 - 10 MPa at temperatures of 2 - 10 °C. If refrigerated at T = -15 °C, the NGH slurry decomposes very slowly and can be transported by ship to its destination at atmospheric pressure. This would spare the need for

expensive LNG carriers, since NGH ships need only be insulated. At its destination, the NGH could be regasificated, while releasing 170 m³ of NG per cubic meter of hydrate [21]. There are theories, that the GTS technology based on the production of NGH could become a practical method for transporting natural gas [22]. The storage density of 170 m^3 per m^3 for NGH is lower than for CNG or LNG as shown in Table 2. Yet, although the space requirement of NGH requires larger ships, the storage conditions on board are much easier which reduces the specific costs again.

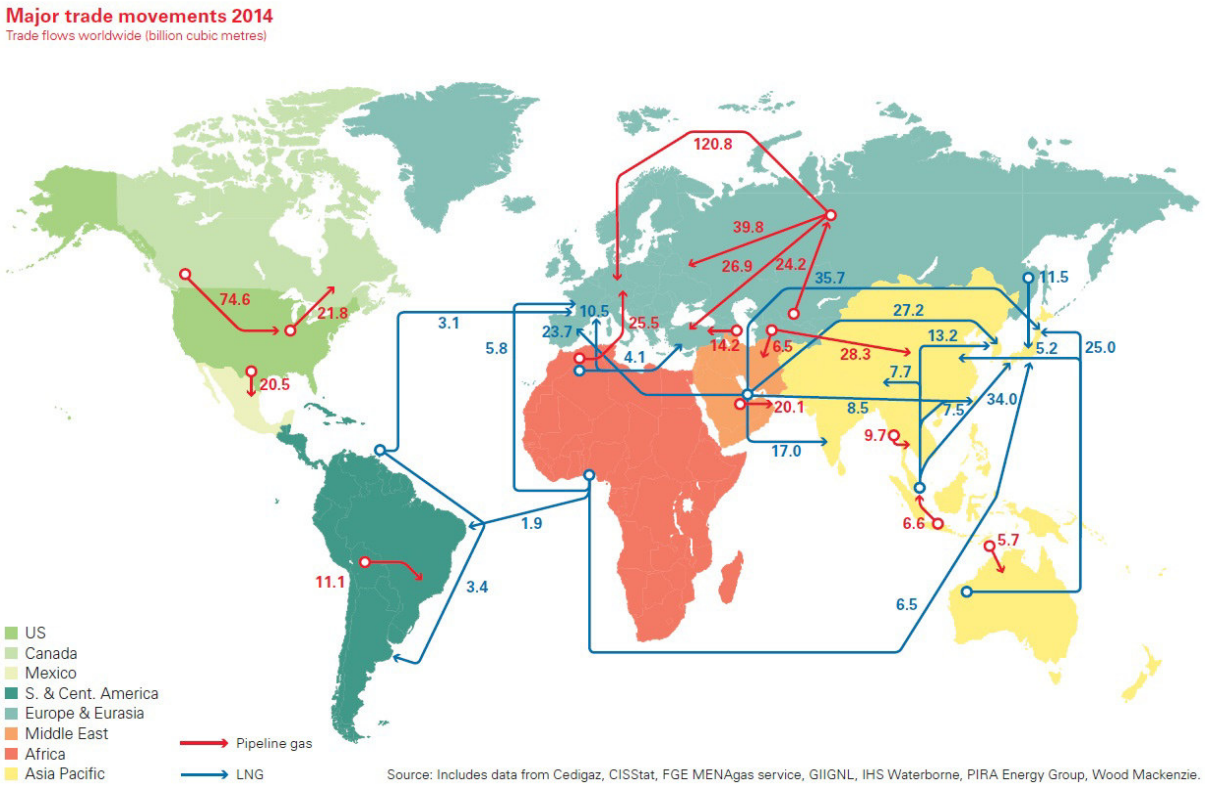

Fig. 5: Global trade of natural gas in 2014 [18].

The transport of NG as compressed natural gas (CNG) is not used for long-distance overseas trade, but is in some countries a common alternative for conventional fuel in vehicular transport [12]. Iran, China, Pakistan, Argentina, India and Brazil each host fleets of 1.5 – 3.5 million vehicles powered by CNG [23]. Germany, for comparison, has ~ 100,000 CNG powered vehicles. On a global scale, the transport of NG as CNG does not compete with LNG. This is mainly because the storage density is still 3 times lower (see Table 2), and compressing and decompressing the natural gas at port to 20 MPa along with the heat generation or cooling is not much more practical on a large scale than the processing of LNG [12].

Another method for the utilization of natural gas is the transport as a liquid, which was produced prior to transport from NG as reactant (GTL). This method will be discussed in detail in the following chapter.

Table 2: Comparison of transport conditions for ship-bound NG transport [12].

Transport method	**Storage density** $[V_{NG,\ as\ gas}/V_{NG,\ stored}]$	**Temperature [°C]**	**Pressure [MPa]**
LNG	> 600	-162	atmospheric
CNG	200	ambient	>20
NGH	170	-15	atmospheric

4.1.3 Gas to Liquid (GTL)

The chemical conversion of natural gas to products - which are liquid at ambient conditions - simply for transportation is economically unreasonable [13]. Yet, the natural gas can be converted to liquid products of higher value, making the GTL process economically viable, if the added value is sufficiently high compared to transporting and selling the NG directly.

The direct selective conversion of NG to liquid products is being investigated. Yet, developing a partial oxidation directly to e.g. methanol with H_2O_2 [24] or other higher alcohols with CF_3CO_2H [25], while avoiding total oxidation, proves difficult. These reactants would have to be substituted by less costly and environmentally friendlier reactants, in order to compete economically with existing GTL technologies. Currently, all GTL processes follow an indirect path via the production of synthesis gas or "syngas" with O_2 followed by either conversion to methanol, with an optional further conversion to gasoline (MTG), or Fischer-Tropsch (FT) synthesis [26]. A list of the occurring reactions can be seen in Table 3 [27]. The principle of the FT synthesis was developed in the mid 1920s by Franz Fischer and Hans Tropsch [28] and is shown in Fig. 6. Natural gas is well suited as feedstock for FT synthesis since synthesis gas with an n_{H2}/n_{CO} ratio of 2 is produced from it [29].

The generation of syngas involves steps such as steam methane reforming (SMR), which produces a syngas mixture with a n_{H2}/n_{CO} ratio of 3, while syngas produced from the partial

Table 3: Reactions during Fischer-Tropsch synthesis [27].

Reaction			**Energy**
Fischer-Tropsch	n (CO + 2 H_2)	→ -$(CH_2)_n$- + n H_2O	ΔH = -167 kJ · mol^{-1}
Synthesis of paraffins	n CO + (2n+1) H_2	→ C_nH_{2n+2} + n H_2O	
Synthesis of olefins	n CO + 2n H_2	→ C_nH_{2n} + n H_2O	
Synthesis of oxygenates	n CO + 2n H_2	→ $C_nH_{2n+1}OH$ + (n-1) H_2O	
Methanation reaction	CO + 3 H_2	→ CH_4 + H_2O	ΔH = -206 kJ · mol^{-1}
Water gas shift reaction	CO + H_2O	→ CO_2 + H_2	ΔH = -41 kJ · mol^{-1}
Boudouard reaction	2 CO	→ C + CO_2	ΔH = -172 kJ · mol^{-1}
Coke formation	CO + H_2	→ C + H_2O	ΔH = -133 kJ · mol^{-1}

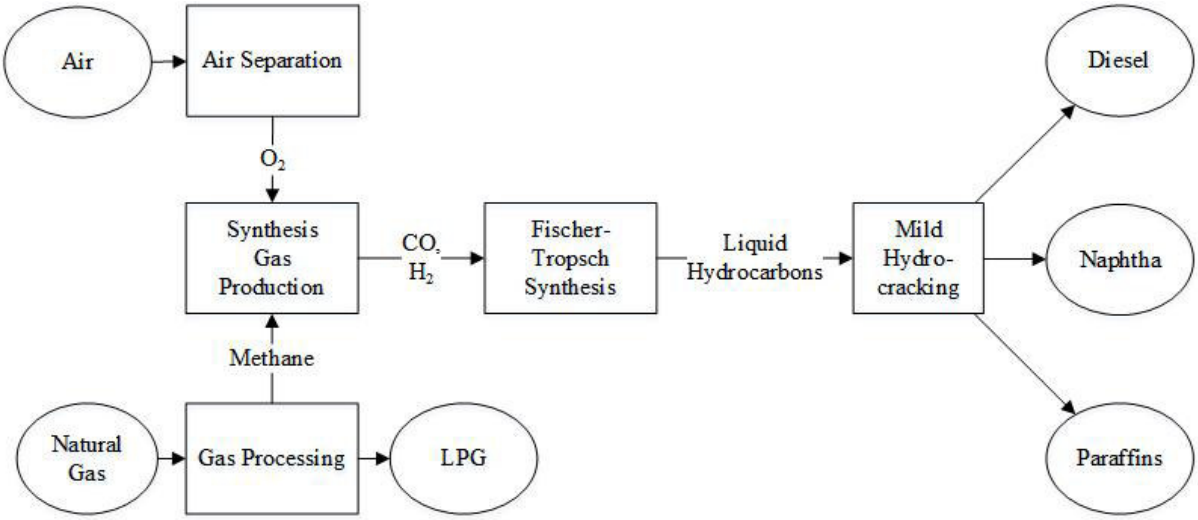

Fig. 6: Schematic of the Fischer-Tropsch process.

oxidation (POX) of methane typically has a H_2/CO ratio of 1.6 [30]. Since FT synthesis ideally requires a n_{H2}/n_{CO} ratio of 2, a combination of SMR and POX is usually applied. An alternative to SMR/POX is autothermal reforming (ATR), which is also widely accepted and commercially applied [31]. Here the syngas is produced from a feed consisting of NG, steam and O_2. The advantage of ATR is, that the n_{H2}/n_{CO} ratio can be controlled by variation of the temperature [30].

During Fischer-Tropsch synthesis, the product distribution highly depends on operating conditions. The FT reaction being exothermic requires very good heat exchange properties to avoid reactor heating at hot spots. This would lead to an increase in selectivity to unwanted methane, increased coke formation and sintering of the catalyst, effectively reducing its activity [29].

The low-temperature Fischer Tropsch synthesis (LTFT) is conducted at temperatures of 190 – 250 °C in slurry-bed or multitubular reactors. Due to its higher activity, Co is used in the employed catalysts instead of the much cheaper iron. The main products are long-chain unbranched alkanes such as waxes, but also diesel. The produced diesel is of high quality, since its cetane number benefits from the linearity of the compounds and the low aromatic content. When the desired product is gasoline, shorter hydrocarbons and terminal olefins, thermodynamics call for the high-temperature Fischer Tropsch synthesis (HTFT). The syngas is typically converted in two-phase fluidized-bed reactors at around 340 °C. The formation of waxes must be avoided, otherwise the catalyst particles clump together, rendering the fluidized bed unusable. At higher temperatures the less active but more readily available Fe can be used as catalyst [29].

Alternative technologies to reduce the high investment costs of FT plants are sought-after, such as employing air instead of O_2 for syngas generation [29], since the air separation unit makes up for almost a quarter of the investment costs [30]. In practice, the air blown ATR proved commercially not beneficial. The amount of N_2 carried along downstream necessitates far larger plant equipment due to the lower partial pressures of the components. This increase in costs exceeds the savings from the air separation unit. However, reducing the costs of O_2 generation could be achieved by permeation through membranes selective to oxygen. This process is called oxygen membrane reforming (OMR) [32]. A list of existing GTL plants is given in Table 4.

Table 4: Existing GTL plants [33].

Location	**Operator**	**Start-up**	**Capacity**	**Owner**
Sasolburg, South Africa	Sasol	1955[a]	5600 bbl/d	Sasol
Mossel Bay, South Africa	Petro SA	1992	36000 bbl/d	Petro SA
Bintulu, Malaysia	Shell	1993	14700 bbl/d	Shell
Ras Laffan, Qatar	Oryx GTL	2006	34000 bbl/d	Qatar Petroleum & Sasol
Ras Laffan, Qatar	Shell	2011	140000 bbl/d	Qatar Petroleum & Shell
Escavros, Nigeria	Chevron	2014	34000 bbl/d	NNPC & Chevron

[a] switched from coal to natural gas in 2004

In search of a novel and direct route from natural gas to liquid products competitive to FT synthesis the EU sponsored the “Next-GTL” project within the 7th Framework Programme. The overall concept of the project was to enable the utilization of natural gas in remote locations, so called “stranded gas”, with conversion to easy-to-transport liquid fuels on site, to

circumvent the need for large-scale plants such as FT synthesis or LNG transport, since these technologies are particularly undesirable for remote or small natural gas fields. The project was divided into three general approaches, see Fig. 7.

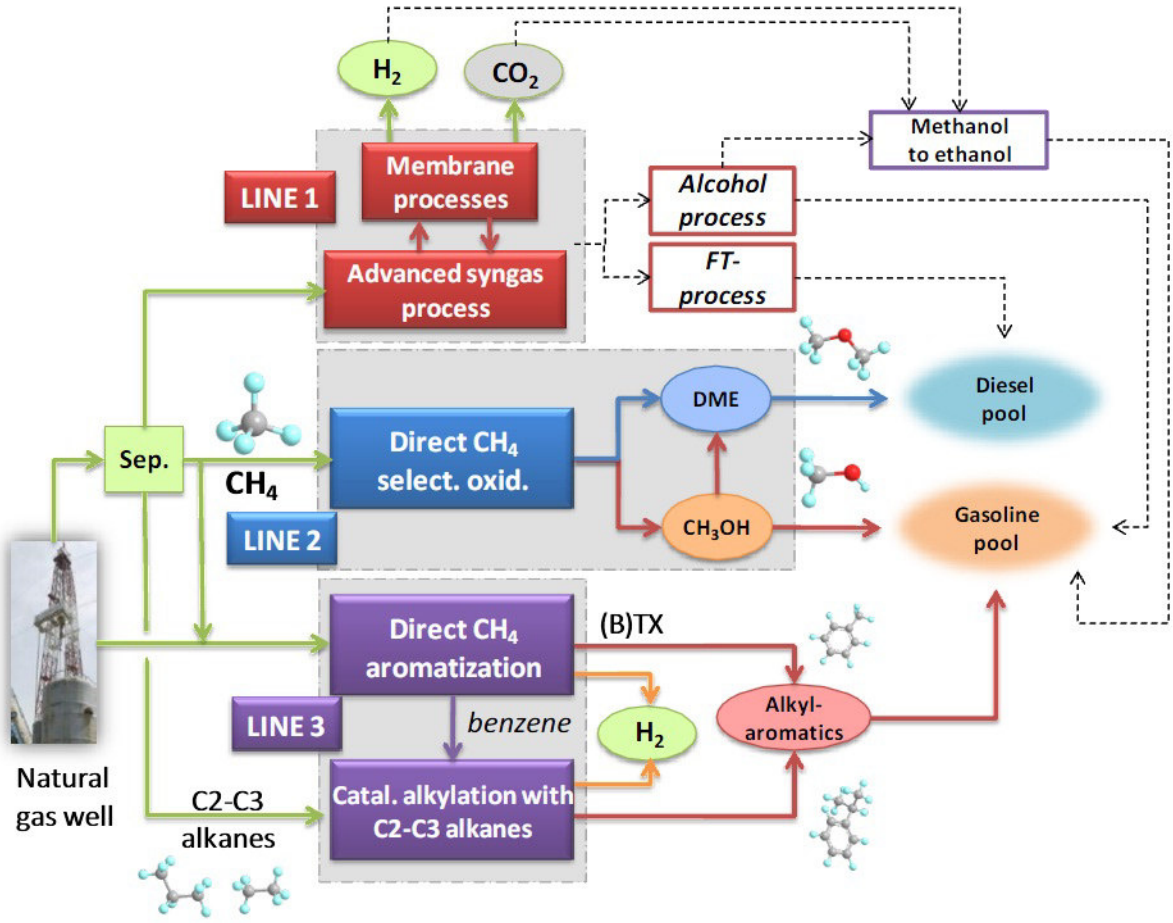

Fig. 7: Conceptual scheme of the Next-GTL project [34].

The first approach was to be an improvement over the existing FT synthesis, employing selective membrane reactors for gas separation, creating an "advanced syngas process", since the bulk of the investment costs occur upstream of the actual FT plant [32]. The second approach concerned the direct oxidation of methane selectively to oxygenates such as DME or methanol. The third approach envisaged the methane in NG to be aromatized to benzene, and some small amounts of toluene and xylenes in the process, while the higher alkanes from the NG should be used to further alkylate the benzene to alkylaromatics.

This work focuses on the approach from line 3 in Fig. 7, particularly with the catalytic alkylation of over zeolite catalysts. To provide some background information related to the zeolites used during the experiments the following chapter discusses the characteristics of the parent zeolites.

4.2 Zeolites

Zeolites are either naturally occurring minerals or synthesized alumosilicates. The name "zeolite" was first described by A. F. Cronstedt [35] in 1756 and is derived from a combination of the Greek words "zein" (to boil) and "lithos" (rock). Cronstedt used this descriptive name because of the ability of the mineral to "boil" when heated due to the water evaporating as steam from the pores of the material [36]. Zeolites can be described as inorganic macromolecules with a defined structure. The basic building units consist of SiO_4 and AlO_4 tetrahedrons, which are connected over an O-atom at each corner. Therefore, the elemental formula (Eq. 1) consists of SiO_2 and AlO_2^- units, where each charge of an AlO_2^- unit must be compensated for with a cation.

Eq. 1: $$A_{y/m}^{m+}[(SiO_2)_x \cdot (AlO_2^-)_y] \cdot zH_2O$$

A is a cation with the charge m, (x+y) the number of tetrahedrons and z the number of water molecules per crystallographic unit cell. The ratio of x/y determines the n_{Si}/n_{Al} ratio, which is of great importance for zeolites [37]. The empirical Loewenstein's rule [38] states that no two Al-atoms can be bridged by an O-atom, therefore any two adjacent tetrahedrons must at least have one Si-atom at the center. This means the n_{Si}/n_{Al} ratio must be at least 1 or higher. Usually the n_{Si}/n_{Al} ratio is required to range within certain limits, in between which a particular type of zeolite structure is stable. The tetrahedrons form a three-dimensional framework which possesses voids and cavities interconnected to each other and the crystals surface by channels with a certain diameter. These systems are classified by the International Zeolite Association (IZA) into structure types, which are denominated by 3-letter-codes. To date, there are 232 different structure types acknowledged by the IZA [39].

The zeolites are further distinguished by the size of the pores' openings, which generally are in the range of microporous materials with porediameters smaller than 2 nm. The number of tetrahedron central atoms, or T-atoms, is used to describe the width of a pore opening, e.g. eight-membered ring zeolite, ten-membered ring zeolite and twelve-membered ring zeolite. Since the dimension of these ring openings are in the range of simple organic molecules the pore system can have an influence on chemical reactions, if the reaction takes place at the inner surface of the crystal. Therefore, the different structure types have different chemical

and physical properties, because the reactant's size and shape influences how rapidly it can diffuse into the pore system, reach an active site to react and diffuse to the surface again. This dependency of the selectivity on the dimensions of the pore size is called shape selectivity.

The subcommittee on zeolites of the International Mineralogical Association gave the following definition for zeolites [40] that has been acknowledged by the IUPAC [41]:

"A zeolite mineral is a crystalline substance with a structure characterized by a framework of linked tetrahedra, each consisting of four O atoms surrounding a cation. This framework contains open cavities in the form of channels and cages. These are usually occupied by H_2O molecules and extra-framework cations that are commonly exchangeable. The channels are large enough to allow the passage of guest species. In the hydrated phases, dehydration occurs at temperatures mostly below about 400°C and is largely reversible. The framework may be interrupted by (OH,F) groups; these occupy a tetrahedron apex that is not shared with adjacent tetrahedra."

After the first description in 1756 by Cronstedt a long time had passed until zeolites came to scientific attention by A. Damour in 1857 who demonstrated, that the loss of water from a zeolite is reversible. One year thereafter H. Eichhorn exchanged the Ca^{2+} ions in chabazite from soil with two Na^{+} ions [42]. This was the basis for the first application of zeolites on a commercial scale in 1905 as water softener by Robert Gans, an application for which zeolites are still in use until the present day [36]. The first use of zeolites as molecular sieve by O. Weigel and E. Steinhoff was the separation of methanol, ethanol and formic acid from acetone, ether and benzene by adsorption on a previously dehydrated chabazite in 1924 [43]. Union Carbide used a "Linde Type A" zeolite – eponym of the LTA structure – to separate O_2 from Ar in 1953 [36]. The fact that high-silica – and thus low-Al – zeolites show a higher affinity for organic molecules and less for water, made them particularly interesting for the oil industry (see also chapter 4.5 Automotive fuels). In the 1960s, zeolites were rapidly introduced into refining and chemical industry as catalysts for catalytic cracking, hydrocracking, isomerization, alkylation, toluene disproportionation and xylene isomerisation. The industrially important process of fluid catalytic cracking (FCC) produces gasoline from heavy petroleum destillates and used zeolite catalysts since 1962, and it has been estimated that the petroleum refining industry would face additional costs of more than $10 billion per year if it would still rely on amorphous silica catalysts [37]. Today, zeolite based commercial catalyst are widely used and on average contain only 36 wt.-% of zeolite, the remainder being mainly binder material, which can be catalytically active itself [44].

Zeolite ZSM-5 has also been used to separate gas mixtures as a membrane supported on clay [45] at elevated temperatures. Zeolitic membranes can not only be used for separation applications but also as active catalysts. Thereby, zeolites can either be active catalysts themselves, or function as an inert coating on an active support such as Pt-TiO_2 [46]. Membranes with the MFI (Mobil Five) structure managed to withstand pressure differences between the two sides of up to 1 MPa at temperatures up to 700 K and have been operated for two years without loss of properties [47].

4.2.1 Zeolite ZSM-5

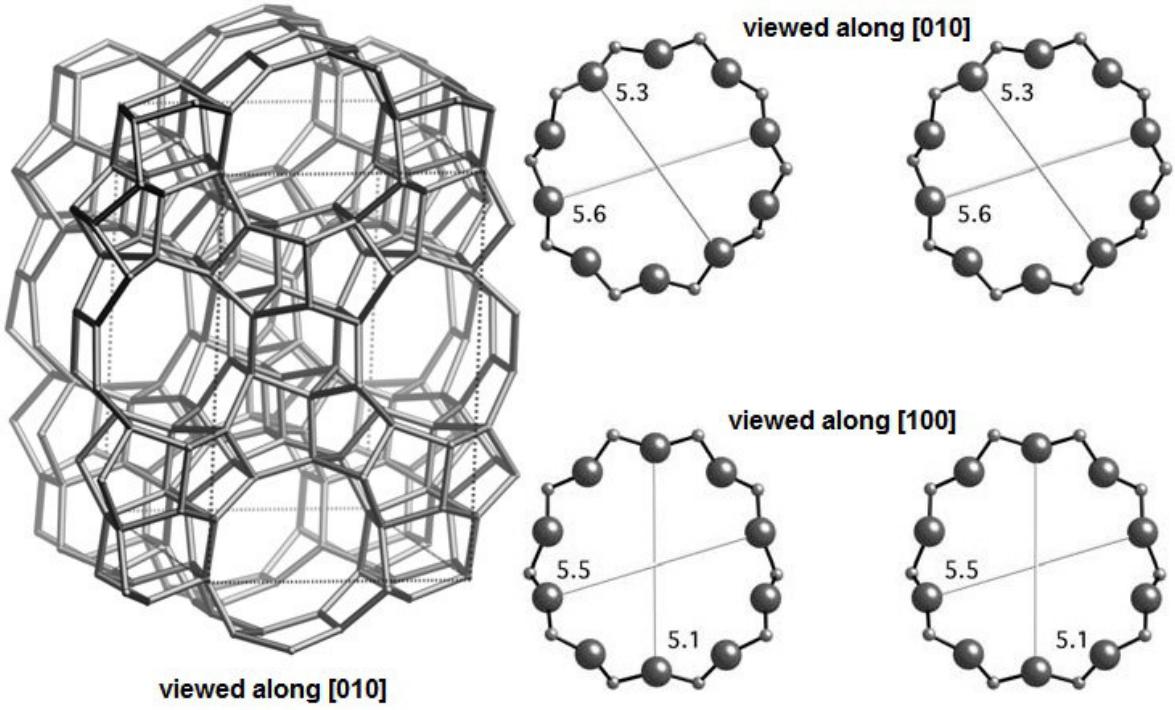

Fig. 8: Schematic of the MFI structure of zeolite ZSM-5, modified from [39].

Zeolite ZSM-5 was first synthesized by Argauer and Landoldt and patented by Mobil Oil Corp. in 1972 [48]. The structure of ZSM-5 is MFI and shown in Fig. 8. The MFI structure consists of a 3-dimensional channel system of 10-membered rings. The channels running along [010] are linear with the dimensions 0.53 x 0.56 nm, and orthogonal to those the channels along [100] run sinusoidal having the dimensions 0.51 x 0.55 nm (see Fig. 8 and Fig. 9). The vertical channels in Fig. 9 are in the [010] direction and the horizontal channels in

[100]. The largest voids are at the intersections within the MFI structure and have a diameter of 0.63 nm [49]. The MFI structure crystallizes orthorhombic in the space group P*nma* and has the following cell parameters: a = 2.0 nm, b = 2.0 nm, c = 1.3 nm [39].

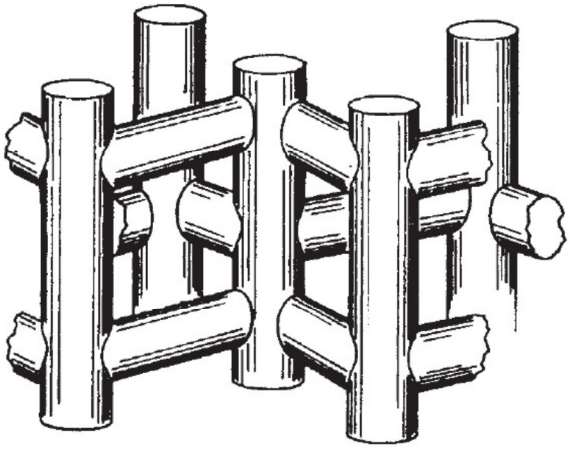

Fig. 9: Illustration of the 3-dimensional channel system of the MFI structure [50].

When zeolite ZSM-5 is synthesized without Al in the framework, it is no longer denominated as ZSM-5, but as silicalite-1 [51]. The MFI structure is unchanged by the lack of Al in an all Si crystal as silicalite-1. Having no Al sites, silicalite-1 possesses neither Lewis acid sites nor Brønsted acid sites. Silicalite-1 is therefore highly hydrophobic, but small organic molecules can enter the pore system and adsorb. This can be of interest for applications such as water purification, but is particularly useful for shape selectivity enhancement [52]: When an existing ZSM-5 crystal is coated with an overgrowth of silicalite-1, a catalyst is formed with no active sites on the outer surface, but active sites inside the pore system, therefore unselective surface reactions can be excluded and highly shape-selective results can be obtained. Since both crystals have MFI structure, silicalite-1 can be grown on ZSM-5 and their pore systems connect to each other. The dimensions of the MFI structure enable molecules such as benzene, toluene and ethylbenzene to freely and rapidly diffuse through the pore system of ZSM-5 or silicalite-1. In contrast, molecules such as *o*- and *m*-xylene are reported to diffuse only slowly [53].

4.2.2 Zeolite Beta

Zeolite Beta was first described in 1967 by Wadlinger, Kerr and Rosinski [54]. It is colloquially denoted by the structure type *BEA. The asterisk denotes that the structure is disordered. Zeolite Beta actually comprises two structures with own 3-letter-codes, the *BEA and BEC structures. The *BEA structure is in fact a disordered intergrowth of two structures, namely polymorph A and polymorph B. Together with a third structure polymorph C with the BEC structure, zeolite beta is formed. All three have a 3-dimensional pore system with 12-membered ring channels. They are distinguished by their different orders of stacking [55].

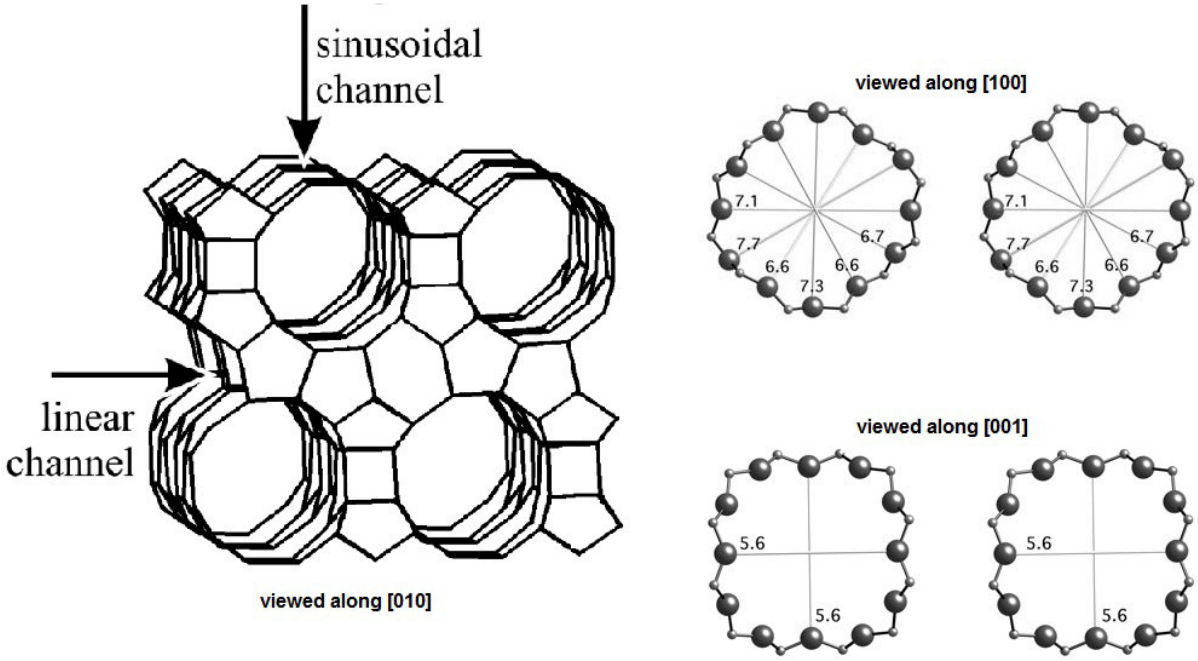

*Fig. 10: Schematic of the *BEA structure of zeolite Beta, modified from [39], marked with arrows to indicate the directions of the two other channel systems [56].*

The polymorph A of the *BEA structure consists of two enantiomorphic structures crystallizing in the space groups $P4_122$ and $P4_322$ [57]. The polymorph A structure is shown in Fig. 10. The 3-dimensional pore system is connected via linear channels with dimensions of 0.67 x 0.66 nm in two dimensions, and in the third dimension via sinusoidal channels with a diameter of 0.56 x 0.56 nm [39]. The stacking order of polymorph A is ABAB… as shown in Fig. 11. The largest included sphere at an intersection in the *BEA structure has a diameter of 0.66 nm [49].

Polymorph B of the *BEA structure also has layers with straight 12-membered ring channels as polymorph A, which are interconnected via inclined channels along the third dimension. This angle derives from the stacking order of layers as shown in Fig. 11 [55].

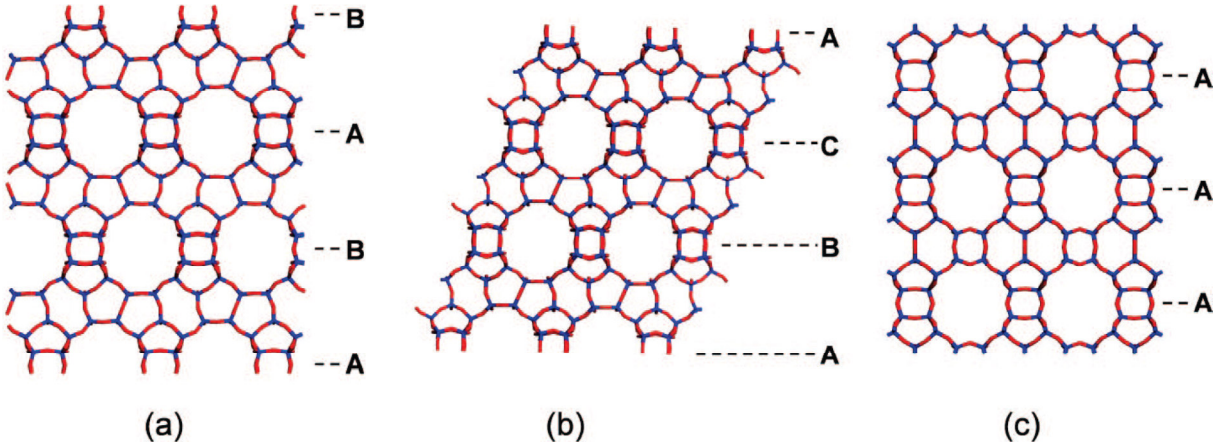

Fig. 11: Schematic of the structures of polymorph A (a), polymorph B (b) and polymorph C (c) of zeolite Beta viewed along [010], with their respective stacking orders ABAB…(a), ABCABC…(b) and AA…(c) [55].

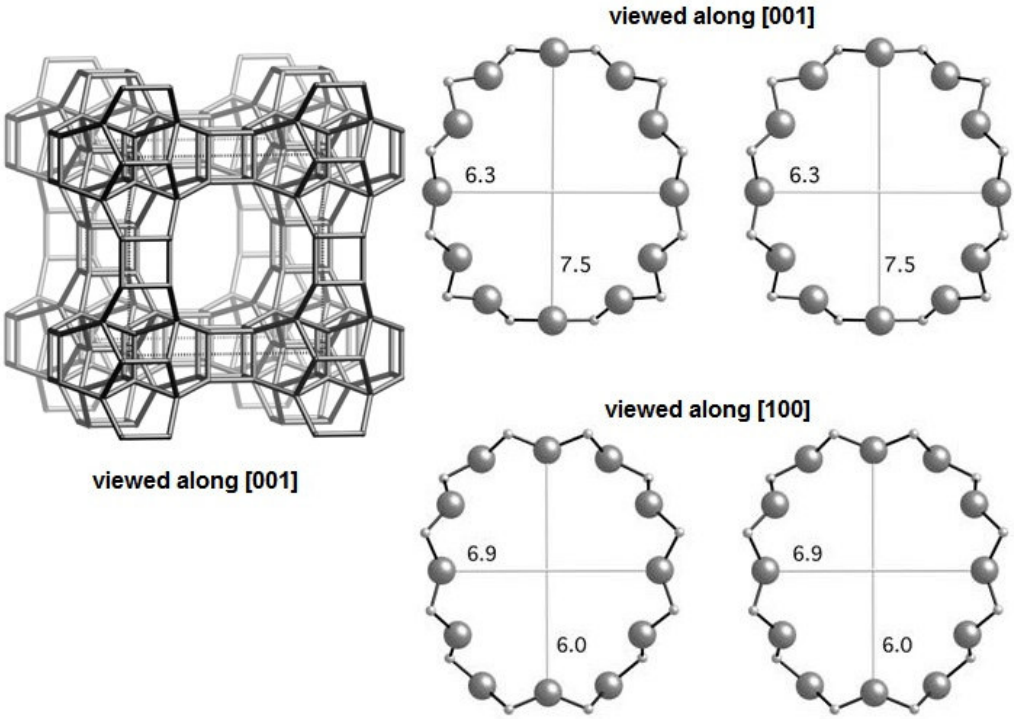

Fig. 12: Schematic of the BEC structure of polymorph C in zeolite Beta, modified from [39].

The third structure in zeolite Beta is polymorph C, which possesses its own 3-letter code BEC and its structure is shown in Fig. 12. The channels within the layers have a diameter of

0.60 x 0.69 nm, while those between layers have dimensions of 0.63 x 0.75 nm [39]. The channels along the three spatial axes are perpendicular to each other. The largest included sphere at an intersection in the BEC structure has a diameter of 0.69 nm [49].

Together the *BEA (comprising polymorphs A & B) and the BEC (polymorph C) structures form zeolite Beta. For comparison, the crystallographic data on the three polymorphs of zeolite beta are compiled in Table 5. The pore systems of the three polymorphs are connected to each other, this means zeolite Beta as a whole has a 3-dimensional pore system throughout its crystals. Therefore, it is possible for reactant molecules of appropriate size to diffuse through borders of different polymorph phases and access the entire crystals' active sites. At these distortions within zeolite Beta, potentially sites possessing Lewis acidity occur, due to T-atoms not incorporated into the crystal's lattice. This facilitates zeolite Beta's unique properties having Brønsted sites on the outer surface and inside the pore system, while having Lewis sites only within the pore system [58].

Table 5: Crystallographic data for the structures of zeolite Beta.

	Polymorph A [39]	**Polymorph B [55]**	**Polymorph C [39]**
Cell Parameters			
a [nm]	1.24	1.79	1.28
b [nm]	1.24	1.79	1.28
c [nm]	2.65	1.43	1.30
α [°]	90	90	90
β [°]	90	114.8	90
γ [°]	90	90	90
Space Group	$P4_122$ & $P4_322$	*C*2/*c*	$P4_2/mmc$
Stacking Order	ABAB…	ABCABC…	AA…

4.2.3 Zeolite MCM-22

The zeolite MCM-22 (Mobil composite of matter) was first described by Rubin and her group [59] and patented by Mobil Oil Corp. [60]. It has the structure type MWW (Mobil twenty-two). The MWW structure crystallizes in the space group P6/*mmm* with the cell parameters $a = b = 1.41$ nm, $c = 2.49$ nm, $\alpha = \beta = 90°$, $\gamma = 120°$ [59]. It consists of two pore systems, which are not interconnected to each other. The first consists of a two-dimensional system of channels with 10-membered rings, in the layer normal to [001]. This system is

located within a crystal layer of MWW and the channels have dimensions of 0.51 x 0.41 nm. The second pore system consists of large cavities of 12-MR as shown in Fig. 13. These large cavities are only accessible through six 10-MR windows, though. These have the dimensions 0.55 x 0.40 nm. The large cavities are located between two crystal layers, one such layer is shown in Fig. 14. When stacking two such layers on top of each other the "cups" form one of the large cavities from Fig. 13. The largest included sphere in such a cavity has a diameter of 0.96 nm [49]. Also it can be seen, that two such cavities connect in the [001] direction via a double 6-MR, which is too small for the diffusion of reactants from one layer to another. Therefore this pore system is also considered two-dimensional. At the crystals' surface, the half cavities take on the form of cups or bowls with 12-MR at the rim.

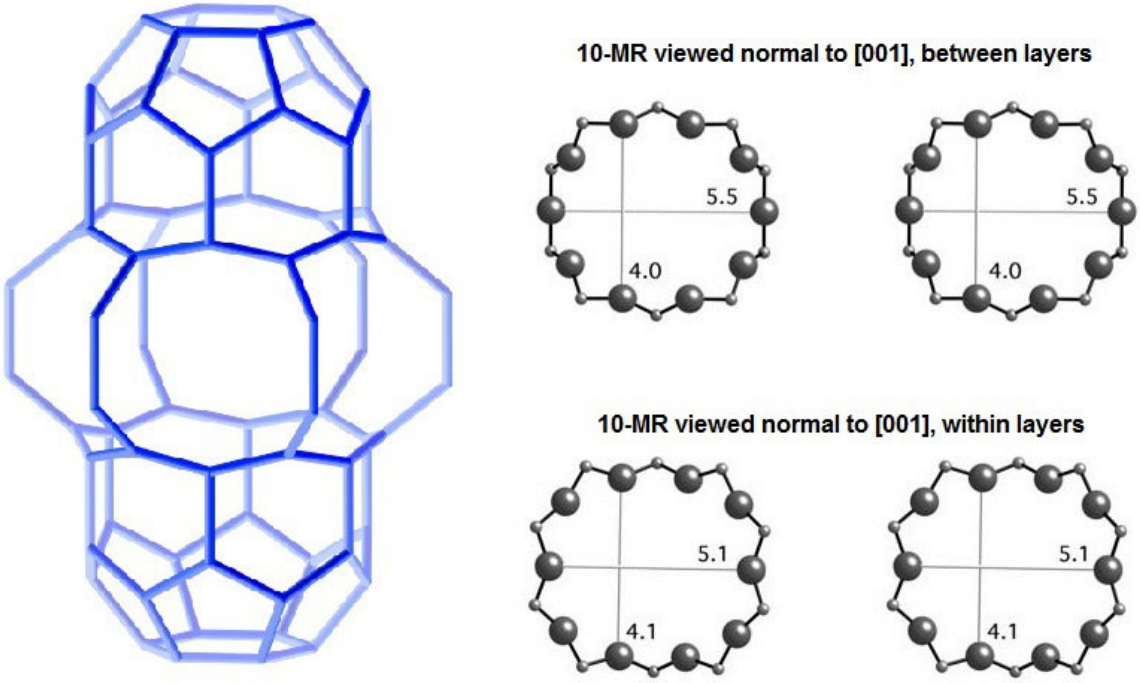

Fig. 13: Schematic of the large cavity in the MWW structure, together with dimensions of the two channel systems, modified from [39].

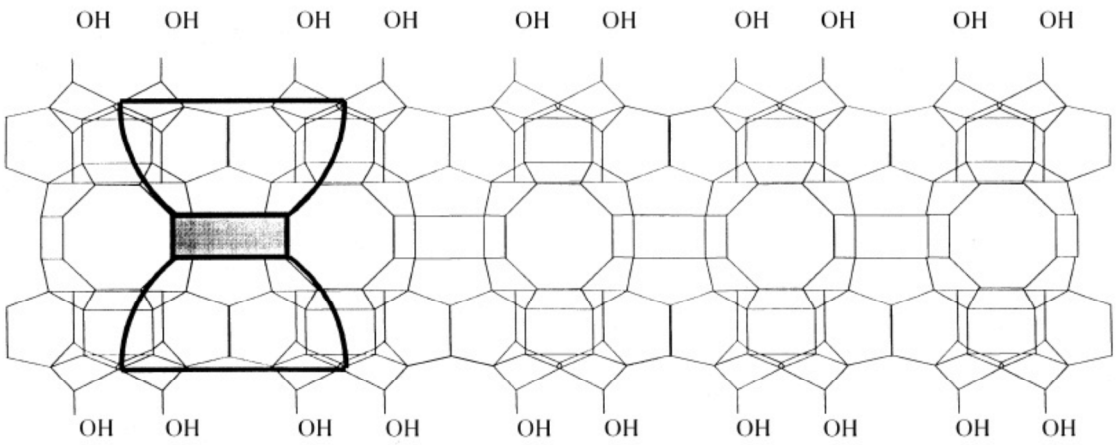

Fig. 14: Schematic of a crystal layer in the MWW structure [61].

4.3 Activation of Alkanes

Alkanes have two major advantages as feedstock in the petrochemical industry: They are a hydrocarbon source which is abundant and cheap. Both properties are vital aspects when considering the use as feedstock. However, they also have a great disadvantage, namely low reactivity (hence the name; lat.: *parum affinis*, little affinity) [62]. The valorization of alkanes is therefore closely associated with catalysis. Possible conversion methods of methane for example include reforming followed by FT-synthesis (as described in chapter 4.1.3 Gas to Liquid (GTL) above), the direct oxidation to methanol, formaldehyde or dimethylether (cf. Fig. 7, Line 2), the oxidative coupling of methane to ethylene or the conversion to aromatics and hydrogen (see next chapter) [63].

To overcome the low reactivity of alkanes, a suitable catalyst must be highly active, since a bond between carbon and hydrogen needs to be broken in order to activate the alkane. The strength of these bonds decreases with higher carbon numbers, therefore it is easier to activate higher alkanes than lower ones [62]. For methane the C-H bond energy is as high as 440 $kJ \cdot mol^{-1}$. For ethane it is 411 $kJ \cdot mol^{-1}$ and for propane 398 $kJ \cdot mol^{-1}$. It can be seen that activating an alkane to a primary carbocation, in the case of methane and ethane, is more difficult than to activate propane, which can form a secondary carbocation. In the case of *i*-butane the activation to a tertiary carbocation amounts to 390 $kJ \cdot mol^{-1}$ [62]. To obtain these carbocations a very active catalyst and harsh reaction conditions are required. The produced cationic species tend to react unselectively at the applied conditions, since they are far more reactive than alkanes. Therefore, the highly active catalyst is also required to be highly selective.

Alkanes can be activated either via oxidative methods or by non-oxidative means. Activation with oxidative methods has the advantage of being thermodynamically favored, since the formation of oxygen-containing species provides a driving force for the reaction. Yet, these methods also include the formation of CO_2 and H_2O, which are unwanted. Non-oxidative activation has in turn the disadvantage of requiring a large amount of energy due to the endothermic nature. The dehydrogenation of propane for example requires 123.4 $kJ \cdot mol^{-1}$ [64], also controlling the selectivity can be challenging under the required reaction conditions. Since the produced propene is more reactive than the original propane, cracking to

methane, ethane and ethene as well as secondary reactions which lead to aromatics, higher hydrocarbons and coke is observed [65]. This intricate network of interdependent reactions calls for a tailored catalyst for non-oxidative alkane activation in order to minimize unwanted side and secondary reactions, that is still highly active since alkanes are quite inert hydrocarbons. A bifunctional ZSM-5 catalyst can vary in alkane activation rates by a factor of 10 for example, by changing its n_{Si}/n_{Al} ratio from 17 to 64 [66]. These results reported by Gounder and Iglesia show also that the ratio between dehydrogenation and cracking can be altered from ~ 1:1 to ~ 2:1. This is important to keep in mind for the alkylation with alkanes, since cracking is an unwanted side reaction there (see chapter 4.4 Alkylation of Aromatics). The dehydrogenation is presumably the step occuring before the actual alkylation reaction. The prevention of cracking proves difficult, since the activation energy of the cracking reaction is lower than that of the dehydrogenation [67]. Another unwanted reaction pathway that has to be considered while activating alkanes over bifunctional catalysts is hydrogenolysis. The presence of hydrogen and a bifunctional catalyst enables e.g. propane to be converted to ethane and methane already at 330 °C [68].

As shown in Fig. 7 from chapter 4.1.3 Gas to Liquid (GTL) the aim of this work is to alkylate benzene with ethane and propane. The benzene is to be obtained by aromatization of methane, therefore, and because other hydrocarbons occurring during the dehydroalkylation can be converted into aromatic compounds the following chapter will cover this subject.

4.3.1 Aromatization of Light Alkanes to Benzene

Table 6: Aromatization temperatures of alkanes.

Alkane	Aromatization Temp.	Ref.
Methane	600-750 °C[a]	[69]
Ethane	575-600 °C[a]	[68]
Propane	450 °C[a]	[68]
Butane	370 °C[b]	[68]
Hexane	360 °C[a]	[68]

[a] to BTX aromatics, [b] to p-xylene

The aromatization of light alkanes, e.g. methane, ethane and propane, to aromatics such as benzene, toluene and xylenes (BTX aromatics) occurs at temperatures, which are listed in Table 6 [68,69]. The aromatization reaction becomes more favored with increasing size of the alkane. Therefore, the required temperature for the aromatization drops

with increasing carbon number of the alkane. This is important to keep in mind, considering the formation of butane and ethane from disproportionation when utilizing propane as alkylating agent, see chapter 4.3.2 Disproportionation of Propane below. A low pressure is also beneficial, since during aromatization H_2 is generated and increased pressure would shift the equilibrium away from the aromatic products.

Due to the above mentioned reasons, the aromatization of methane is the most challenging. The activation of methane cannot be achieved via dehydrogenation to a more reactive alkene intermediate with a bifunctional catalyst, such as Ga/H-MFI as for ethane and propane [68]. Therefore more active catalysts such as Mo/H-ZSM-5 have to be used at temperatures of up to 700 °C [62,69]. It is proposed that methane first dimerizes over Mo sites to C_2, subsequently oligomerizes to C_6 and finally dehydrogenates to benzene over acid sites. Yet, the methane conversion rates are as low as 6 % along with selectivity to benzene of 80 % [70]. These results from Wong *et al.* have been obtained with 5.3Mo/H-MCM-22(16) as catalyst. According to Spivey and Hutchings [71] conversion rates of ~ 10 % can be achieved. Yet, the aromatization reaction is thermodynamically unfavored. The formation of solid carbon and hydrogen is more favorable. Therefore, coke is formed and this leads to deactivation. The coke formation can be reduced by co-feeding CO_2 or steam. This however is known to inhibit the formation of the active Mo_2C species in the aromatization catalyst [69]. By designing the reactor appropriate to the requirements of the thermodynamics, the conversion can be improved. A suggested membrane reactor with a H_2-selective membrane [71] would shift the equilibrium of methane aromatization towards benzene, since H_2 is continuously removed. Yet, the formation of solid carbon is also enforced, which ultimately reduces the catalysts' activity. This does, however, have the advantage of producing large amounts of valuable H_2. An addition of H_2 to the feed can also be used to reduce coking [71], this of course sacrifices valuable H_2 and shifts the equilibrium away from the aromatic products for an increased catalyst lifetime. An alternative is suggested by the use of an O-selective membrane. Here, the oxygen from the air is used as sweep gas. Since the oxidizing agent is not co-fed together with methane the active Mo_2C species on the catalyst remains intact, while reducing the selectivity to coke by a factor of 6 [69]. An application with a constantly regenerated catalyst is suggested to cope with these difficulties [71].

Ethane is aromatized via dehydrogenation, followed by oligomerization to C_4 and C_6 or C_8 and subsequent cyclization to aromatics via dehydrogenation of the naphthene [68]. Among these, alkane dehydrogenation is the rate-limiting step [72]. Once ethylene is initially formed,

the secondary reactions proceed quite fast at the 575 °C required for ethane activation. When co-feeding hydrogen to reduce coking, the same disadvantages as with methane aromatization (see above), as well as hydrogenolysis and the increased formation of unwanted methane occur [68]. The route these reactions take is not clear. One possible reaction path is after the olefin oligomerization up to C_{10}, dienes are formed by dehydrogenation, that undergo cyclization and further dehydrogenation to aromatics [72]. A second path is suggested to be similar in ethene oligomerization, but differs as an olefinic carbenium ion is formed, which after cyclization is dehydrogenated to aromatics. The formation of dienes as in the former pathway is not described [70].

The aromatization of propane is easier than that of methane or ethane, since propane has the ability to form a secondary carbocation instead of a primary. The typical reaction temperature, at which the aromatization is carried out, is in the same range as with ethane, about 550 °C [65,68]. A prominent side reaction of propane over zeolitic catalysts is cracking into ethylene and methane. Therefore the obtained products during aromatization are mainly BTX aromatics (benzene, toluene, ~30 % each) and cracking products (methane + ethane, 23 % together) [73]. Another side reaction of propane that is important especially during dehydroalkylation of benzene together with ethane is its disproportionation, which will be further discussed in the next chapter.

4.3.2 Disproportionation of Propane

Propane does not exclusively undergo aromatization over zeolitic catalysts. According to Ivanova *et al.* [74], propane forms ethane and butane over H-ZSM-5 already at 275 °C and atmospheric pressure. The formation of butane depends on the concentration of propane. At low propane concentrations, a monomolecular reaction is favored, which produces *i*-butane via dehydrogenation of propane, followed by oligomerization and cracking via carbenium ion intermediates. Neither ethane nor *n*-butane is observed. At high concentrations of propane, though, the bimolecular disproportionation is favored, which produces ethane and both butane isomers. This is proposed to occur via two possible mechanisms. Either via the formation of a propenium ion, which cracks into ethane and an adsorbed CH_3 species, which subsequently

forms butane with another molecule of propane, or a concerted mechanism via a proponium ion that reacts with a propane molecule to ethane and butonium [74].

The ethane formed from the disproportionation of propane presents no important difficulties for this work, although ethane is a reactant in the feed stream. Ethane is used in excess as reactant and the amount produced from the disproportionation of propane is comparatively small. The similar amount of produced butane, however, can undergo further side reactions, which are covered in the following chapter.

4.4 Alkylation of Aromatics

The alkylation of aromatics can in principle be conducted by several means. These are the reaction with either alkylhalides, alcohols or olefins. Commercially the reaction is carried out almost exclusively with olefins [75]. The reaction with alkylhalides or alcohols produces stoichiometric amounts of unwanted byproducts, such as H_2O or HCl, which have to be separated. The use of alkenes has the advantage of not producing any byproducts and is H_2 neutral. The dehydroalkylation with alkanes has further the benefit of producing valuable H_2, while consuming the more abundant and cheaper alkane compared to the corresponding olefin. The major drawback of the dehydroalkylation is that when utilizing alkanes as alkylating agent highly active catalysts, as well as more severe reactions conditions are required. The reaction becomes therefore rapidly unselective. That is why the "normal" alkylation of aromatics with olefins can be conducted at less harsh conditions and with higher selectivity to alkylaromatics than the dehydroalkylation with alkanes.

The use of alkanes for the dehydroalkylation of aromatics was first reported in 1973 by Schmerling and Vesely [76] with Friedel-Crafts catalysts and 1975 by Olah *et al.* with the superacid HF-SbF_5 [77]. Although use of alkanes as alkyating agents for aromatics is surely interesting, there is only one commercial application where they are used for this purpose [62], namely the M-forming process by Chen *et al.* [78]. In this process, alkenes are formed *in situ* by cracking of *n*-alkanes, which then further alkylate the aromatics preferably to high octane alkylbenzenes. The application of Friedel-Crafts and superacidic catalysts causes environmental problems and was commercially replaced by the alkylation with olefins [75]. The alkylation of benzene with ethene or propene is commercially conducted at temperatures of 170 - 250 °C for ethene and 200 - 250 °C for propene. These reactions are highly exothermic at -113 kJ · mol^{-1} [75,79]. Acidic zeolite-based catalysts have replaced the formerly used Friedel-Crafts catalyst (first used in 1930 [75]) and hydrofluoric acid (since 1968 [80]) entirely [75].

The alkylation with alkenes over an acidic solid catalyst proceeds via an Eley-Rideal mechanism [81], where benzene molecules react from the gas phase with adsorbed carbenium ions of the respective alkene. Benzene does not compete significantly over the acid sites with e.g. propene, therefore its coverage is low. For ethene as alkylating agent, the expected

primary product is ethylbenzene (EB), for propene it is *i*-propylbenzene (IPB), since this is kinetically favored over the formation of *n*-propylbenzene (NPB). As can be seen in Fig. 15, IPB can be converted into NPB in the presence of benzene via a transalkylation reaction [81,82]. Thermodynamically, the alkylation of alkylbenzenes is favored over the alkylation of benzene, which is reported to occur already at ambient temperature [82]. This leads to unwanted polyalkylation, and has to be avoided. An obvious solution to this problem is to operate with a molar excess of benzene over the alkylating olefin, thus minimizing polyalkylation. This unfortunately comes with the necessity to recover great amounts of unalkylated benzene, which is quite costly. Therefore, it is industrially more convenient to operate at higher temperatures (e.g. 400 °C for EB production) [75], because thermodynamically monoalkylated products are favored. This, however, does not enhance the selectivity to monoalkylated products exclusively, but also the selectivity to by-products from secondary reactions and cracking, which are unwanted. Therefore a balance between these selectivities in terms of reaction temperature is called for, as well as for the application of a shape-selective catalyst, that sterically restricts or hampers the formation of polyalkylated products, while allowing the formation of monoalkylated products [75].

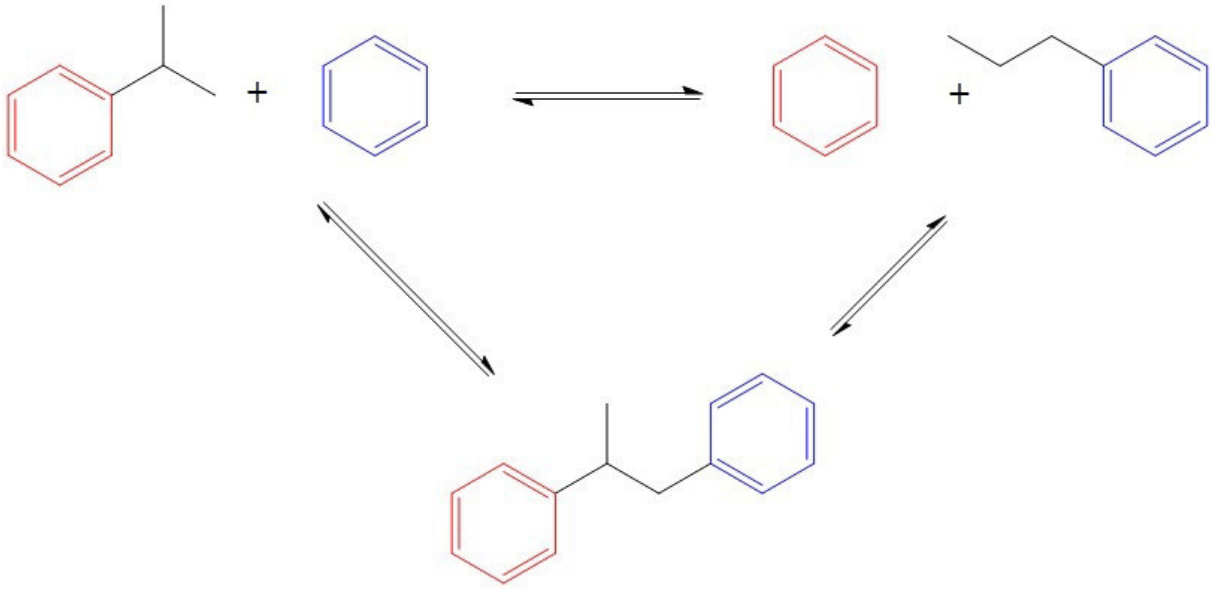

Fig. 15: Isomerization of i-propylbenzene and n-propylbenzene in the presence of benzene, after [82].

When utilizing alkanes instead of alkenes as alkylating agents, the thermodynamics of the reaction changes significantly. The endothermic dehydrogenation of the alkane to its corresponding alkene requires more energy than the subsequent alkylation of benzene yields. This makes the reaction as a whole endothermic. Temperatures of at least 573 K are required

to alkylate benzene with propane [83]. In Table 7, it can be seen that at temperatures of 600 K, which is quite close to the operating temperatures used in this work, the dehydroalkylation of benzene has equilibrium conversions between 3.2 and 4.4 % [62]. For the dehydroalkylation with ethane and propane the overall conversion of benzene depends on many different reactions. It can also be seen that many different reactions occur simultaneously, and that the equilibria of the reactions are interconnected. The primary reactions and their products are shown in Fig. 16, together with some secondary reactions that also produce alkylaromatic components. J. van Bokhoven and coworkers report, that the use of either alkanes or alkenes produces different alkylaromatics. The dehydroalkylation with alkanes produces terminal and branched alkylaromatics, while the alkylation with alkenes produces only branched alkylaromatics [84,85]. The formation of secondary alkylation products, that are also alkylaromatics such as the primary products, is not problematic for the application as fuel components (see chapter 4.6 Octane Number). For the production of a specific primary product, e.g. *i*-propylbenzene, these secondary reactions do lower the selectivity and needs to be minimized as far as possible.

Table 7: Equilibrium conversions of some relevant reactions calculated for temperatures of 600 and 1000 K, modified from [62].

Reaction	X_{600K} / %	X_{1000K} / %
$CH_4 \rightleftharpoons C + 2\ H_2$	9.4	91.6
$6\ CH_4 \rightleftharpoons$ benzene $+ 9\ H_2$	0.5	15.7
$CH_4 + C_2H_4 \rightleftharpoons C_3H_6 + H_2$	0.9	6.5
$CH_4 + C_2H_4 \rightleftharpoons C_3H_8$	36.9	0.1
Benzene $+ C_3H_8 \rightleftharpoons$ cumene $+ H_2$	3.2	11.6
Benzene $+ C_3H_8 \rightleftharpoons$ *n*-propylbenzene $+ H_2$	4.4	17.4
Benzene $+ C_2H_6 \rightleftharpoons$ ethylbenzene $+ H_2$	3.4	15.0
$C_3H_8 + CH_4 \rightleftharpoons 2\ C_2H_6$	30.8	37.9
$5\ C_3H_8 \rightleftharpoons CH_4 + C_2H_6 + 2\ n\text{-}C_4H_{10} + i\text{-}C_4H_{10}$	66.3	56.8
$4\ C_2H_6 \rightleftharpoons C_2H_4 + 2\ CH_4 + n\text{-}C_4H_{10} + H_2$	15.5	61.1

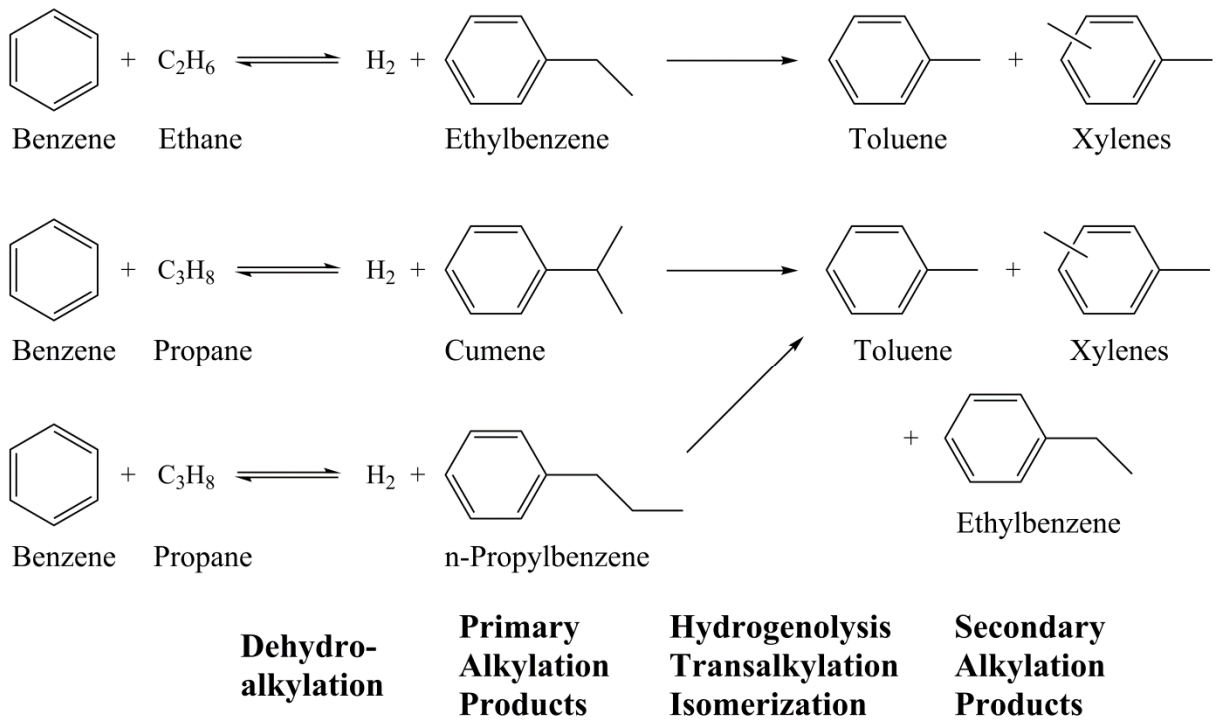

Fig. 16: Schematic of primary reactions during the dehydroalkylation of benzene and occurring secondary products [2].

The thermodynamic limit of the dehydroalkylation can be shifted towards alkylbenzenes by selectively removing hydrogen. This can be achieved by several means. One is the addition of a hydrogen scavenger to the bifunctional catalysts, which predominantly with Pt as noble metal, such as Zr_2Fe [86,87]. Here the H_2 produced by the dehydroalkylation is removed from the reaction zone via absorption as hydride into the intermetallic additive as hydride, which has to be either regenerated or replaced when its hydrogen capacity is reached. Another method is the use of a membrane reactor with a membrane selective to hydrogen instead of a conventional fixed-bed reactor [88,89].

Shifting the equilibrium of the primary reactions towards the alkylaromatics, by either means is not exclusively beneficial, however. The removal of H_2 also enforces side reactions that produce unwanted methane or even solid carbon, which manifests as coke depositions on the catalyst. This reduces the activity of the catalyst by blocking off reactants not only from the external surface, but also from entrance through the pore mouths into the pore system of a zeolite catalyst, thus greatly reducing its active surface.

Other parameters that influence the production of alkylaromatics, such as the reaction temperature, have to be considered discriminately. A higher temperature is beneficial to the dehydrogenation of the alkane [89]. Although more alkene is formed at higher temperatures,

this does not necessarily result in a higher production of alkylaromatics according to Wong *et al.* [90]. Here, the increased temperature leads to higher olefin concentrations with no significant increase in ethylbenzene production. The higher amount of ethene results in more oligomerization and cracking which ultimately promotes the formation of coke.

Most studies are carried out at atmospheric pressure. Rezai *et al.* have calculated the behavior of the dehydrogenation and dehydroalkylation reactions in conventional fixed-bed and membrane reactors selective to hydrogen at different reaction pressures [88]. For the dehydrogenation a low pressure is obviously best, since volume is increased by hydrogen production. At pressures as high as 1 MPa and 400 °C the ethane dehydrogenation is reported to drop to zero. The effect of increased pressure on the dehydroalkylation is not so pronounced, because the overall reaction has a constant number of gaseous molecules. This is true only for fixed-bed reactors, however. In hydrogen-selective membrane reactors a higher pressure increases the alkane conversion significantly. This increase depends on how well hydrogen can be removed from the reaction zone. This in turn, depends on the ratio between sweep gas and reaction stream flow rates. The higher the sweep gas flow rate the higher the conversion [88]. Rezai *et al.* further report, that the $n_{\mathrm{Alkane}}/n_{\mathrm{Aromatic}}$ ratio has little influence on the dehydroalkylation in a fixed-bed reactor [88]. In a membrane reactor the equilibrium conversion is influenced by the composition of the reactants, and it is shown that an $n_{\mathrm{Alkane}}/n_{\mathrm{Aromatic}}$ ratio of 1 or slightly below yields the highest conversion. A low $n_{\mathrm{Alkane}}/n_{\mathrm{Aromatic}}$ ratio is however more economically favorable. The risk of increased polyalkylation can be coped with, by secondary reactions to products where the side chains have been cracked, such as toluene and xylenes.

When comparing the dehydroalkylation of benzene (Bz) with either ethane (Et) or propane (Pr) (cf. Table 8), it can be seen that the selectivity to primary products is significantly higher for the reaction with ethane than for propane. Ethylbenzene is produced as major component. At high $n_{\mathrm{Ethane}}/n_{\mathrm{Benzene}}$ ratios ethene from the dehydrogenation is found, which not reacted further with aromatics, as well as methane from cracking processes. Higher alkanes such as butanes and pentanes from the oligomerization of ethene and various subsequent side reactions are only found in small amounts. The dehydroalkylation of benzene with ethane exhibits lower conversions than with propane. The dehydroalkylation of benzene with propane on the other hand is not as selective as with ethane. The higher conversion rate comes with a low selectivity to IPB and NPB. Disproportionation and cracking products such as ethane and methane along with oligomerization products (C_4-C_5) occur as major products.

The alkylaromatic mixture comprises mainly toluene and higher alkylated products, while propylbenzenes are observed only in small amounts. This is attributed to the propylbenzenes undergoing further reactions via cracking or further alkylation.

The removal of hydrogen by using Zr_2Fe as hydrogen scavenger greatly increases the conversion, as the results from Smirnov *et al.* show in Table 8. The product distribution is not significantly changed by this addition. The many side products from the dehydroalkylation of benzene with propane, which are mostly unwanted, need to be recycled or separated. Economically, it is reasonable to minimize their formation. The ethane formed from the disproportionation of propane presents no important difficulties for this work, since a mixture

Table 8: Product distribution during dehydroalkylation benzene with ethane or propane.

	[93]	**[90]**	**[86]**	**[86]**
Reactants	Et + Bz	Et + Bz	Pr + Bz	Pr + Bz
Catalyst	1.0Pt-H-MFI(15)	1.0Pt-H-MFI(36)	0.3Pt-H-MFI(25)[a]	0.3Pt-H-MFI(25)[b]
Temperature / °C	370	370	350	350
Time on stream / min	60	1200	60	60
Pressure	atmospheric	atmospheric	atmospheric	atmospheric
$\dot{n}_{Alkane}/\dot{n}_{Benzene}$	9	9	~1	~1
WHSV / h^{-1}	13	~3	1.3	1.3
Benzene conversion / %	14.2	11.1	N/A	N/A
Alkane conversion / %	2.58	1.57	44.6	76.2
Product distribution / Mol-%				
Methane	37.4	0.39	4.39	5.72
Ethene	4.67	14.27	[c]	[c]
Ethane	[d]	[d]	27.83	29.08
Propene	0.09	0.11	0.35	0.77
Propane	7.88	2.47	[d]	[d]
Butanes	0.53	0.18	10.26[e]	9.67[e]
Pentanes	[c]	[c]		
Toluene	11	0.82	19.58	11.66
Ethylbenzene	34.1	75.33	1.37	4.74
Xylenes	0.19	0.09	[c]	[c]
i-Propylbenzene	0.6[f]	2.05[f]	1.58	1.89
n-Propylbenzene			3.24	3.75
Higher alkylated products[g]	3.54	4.29	31.40	32.72

[a] without Zr_2Fe, [b] with Zr_2Fe, [c] not detected, [d] reactant, [e] sum of C_4-C_5, [f] sum of IPB and NPB, [g] polyalkylbenzenes and naphthalene

of ethane and propane is used in excess anyway. The formed butanes are four times more reactive than propane and 100 times than ethane [68]. The butane can further react to BTX aromatics [68] or crack into methane, propylene and H_2 via monomolecular cracking (cf.

Haag-Dessau-cracking [91]). Alkylation products from butane (e.g. butylbenzenes) are not expected, due to sterically constrained sites in the MFI catalyst [65].

Alotaibi *et al.* [92] report a dehydroalkylation of benzene with propane with different bifunctional catalysts. Among these were zeolite ZSM-5 catalysts functionalized with Pt, which converted ~20 % benzene after 8 h on stream at 300 °C under atmospheric pressure, with high selectivities to NPB and toluene amongst the aromatics. However, under similar conditions a dehydroalkylation separated into two catalystic steps with two catalysts beds in sequence produce IPB with 92.6 % selectivity among aromatics at 6.2 % benzene conversion. The first catalytic bed consists of 7%Pt/C to dehydrogenate the propane to propene. Then a second catalytic bed 25%HSiW/SiO_2 is used to alkylate the benzene with the produced propene. The two beds are separated by a 1mm SiO_2 layer. The HSiW catalyst does not seem to catalyze propane cracking or aromatization.

The product distribution during dehydroalkylation can change over time with increasing time on stream (TOS) as reported by Vazhnova *et al.* [93] with the results from Table 8. This change is caused by deactivation of the applied catalyst. The process of deactivation and its impact on the product distribution is covered in the following chapter.

4.4.1 Catalyst Deactivation during Benzene Alkylation

Most catalysts suffer with increasing time effects that reduce their initial activity and selectivity. This loss in activity can occur from within a matter of seconds, as for the FCC process, to up to many years [94]. The nature of catalyst deactivation can be categorized into chemical (such as poisoning, metal volatilization), mechanical (attrition/crushing, fouling/coking) and thermal (sintering) [95]. Poisoning refers to the strong, irreversible chemisorption of a compound to an active site of a catalyst, blocking the site permanently for reactants. Noble metal leaching is the formation of a volatile metallic compound, which leads to an often permanent loss of valuable active species. The thermally induced aggregation of active component, for example the clustering of small active metal particles into larger ones, is called sintering. This greatly reduces the active surface area of the metal particles irreversibly, which results in a lower activity of the catalyst. Fouling or coking is the

deposition of carbonaceous materials on the catalyst. This leads to the blocking of active sites on the outer surface and the pore system of the catalyst, because reactants can no longer diffuse to active sites within the catalyst particle.

All of the above deactivation methods can - in principle - be used deliberately to tailor the activity of a catalyst. W. O. Haag and D. H. Olson from Mobil Oil Corp. precoked a ZSM-5 catalyst in 1977 to enhance its shape-selective properties during the disproportionation of toluene to benzene and *p*-xylene [96]. The selective poisoning of nickel to nickel sulfide for example is used to enhance selectivity during dehydrogenation reactions [94]. This is called "coke selectivation". Bauer *et al*. showed that by selectively coking only the outer surface of a zeolite catalyst, the shape selectivity of the catalyst could be increased during the isomerization of EB to *p*-xylene [97]. Having the sterically unselective sites on the outer surface of the catalyst deactivated, the EB has to diffuse inside the pores and preferably reacts to the *para* isomer of xylene instead of the *meta* or *ortho* isomer. The selective coking was achieved by Bauer *et al.* by adsorbing methanol onto the H-ZSM-5 zeolite and subsequently heating to 450 °C under static conditions. While polyaromatic, "hard" coke is formed on the outer surface of the ZSM-5 crystals, "soft" coke (polyolefinic or alkylaromatic in nature) is formed inside. This intracrystalline soft coke can be removed via treatment with propane, while the sites blocked by hard coke are not regenerated by this treatment [97].

Vazhnova *et al.* report that in platinum-containing MFI catalysts two different types of Pt sites exist. It is shown that these two types of Pt sites deactivate differently during the dehydroalkylation of benzene with ethane to EB [93]. One type of Pt sites is mainly responsible for the dehydrogenation of ethane, the other mainly for hydrogenolysis. The "dehydrogenation" sites deactivate slowly, keeping an almost constant level of H_2 production during 70 h on stream. The "hydrogenolysis" sites, however, deactivate fast. During the first 4 h of the reaction, these sites deactivate significantly, which results in a change in selectivity of the catalysts. During the beginning of the reaction, polyaromatic coke forms on the outer surface of the catalyst which reduces the selectivity to the primary product ethylbenzene. It is reported that the initially high selectivity to toluene, methane and polyalkylated products drops significantly during the first few hours on stream. This behavior is attributed to the fact that these products are formed on the "hydrogenolysis" sites, which deactivate rapidly. The sites inside the pore system are only little affected by coke contents below 5 wt.-%. It is claimed that the pore system is only blocked by coke contents higher than that amount.

4.5 Automotive fuels

Fuels of hydrocarbon origin, or fossil fuels, are with very few exceptions the dominant power source for aerial, marine or ground vehicles. If not powered nuclear (e.g. ships) or electrically (e.g. trains, some cars) a vehicle is usually powered by combustion engines using fossil fuels, either natural gas or far more commonly oil-based. For the sake of simplicity, when referring to "fuels" in this chapter, liquid fossil fuels are meant. Liquid fossil fuels are composed of many different chemical substances, which can be categorized in three major groups, namely aromatics, paraffins and olefins [98].

The composition of oil-based fuels determines the application for which the fuel is used. Heavy oil is used for ships and powerplants (often mixed with diesel), while kerosine is used for airplanes and diesel or gasoline for automobiles. These types of fuels are usually distinguished by their respective boiling point range (see Table 9), which depends on the composing hydrocarbons. In Fig. 17, an overview of the processes in oil refining is given, including information on the application of zeolites in these processes. As already mentioned in chapter 4.2 Zeolites, the introduction of zeolites greatly improved the processes in the oil industry since the 1960s. An example that has greatly improved the yield of fuel from crude oil is the fluid catalytic cracking (FCC), where heavy, mainly saturated hydrocarbons are converted to lighter olefins and aromatics. To increase the yield of quality gasoline per barrel of crude oil is of course a major incentive for the industry, since the yield of straight-run products obtained from the crude oil distillation does not meet the high demand of gasoline, neither qualitatively nor quantitatively [98].

Table 9: Fuels from oil refining fractions [99].

Fuel	Boiling point range	Carbon atoms	Application
Gasoline	40-200 °C	5-11	Automobiles
Kerosine	150-250 °C	8-13	Aviation fuels
Gas Oil	200-350 °C	9-22	Diesel motors / heating
Heavy Oil	>300 °C	20-50	Marine fuel

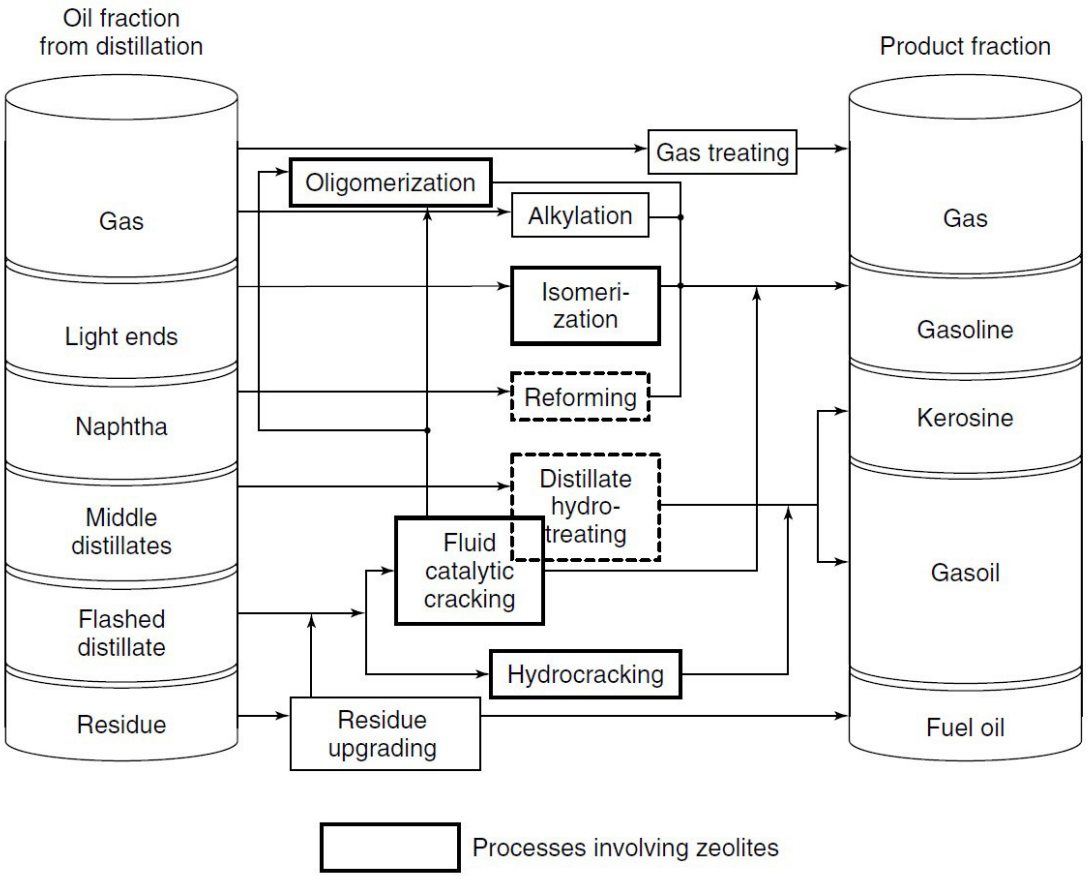

Fig. 17: Schematic of oil refining processes [100].

Since the quality of a fuel determines its application, it is attractive to produce fuel with a high market value. The low-quality fuels fetch lower prices per volume, yet these can still be utilized as fuels, since different types of engines also require different quality fuels. Diesel engines and Otto engines for example require different volatilities since for Otto engines (or ignition spark engines) the fuel has to be mixed with air prior to injection into the engines' cylinder, where it is ignited by a spark plug after compression. Diesel engines are self-igniting, due to their nature of compressing the air in the cylinder first, under nigh adiabatic conditions, and then injecting the fuel as liquid into the hot gas, where it is partially evaporated and mixed with air and then ignites [98].

The power of an Otto engine highly depends on its compression ratio at which the gasoline air mixture is ignited. The increase of the compression ratio is limited by the properties of the gasoline, since at increasing pressures in a hot cylinder the mixture may ignite prematurely. This behavior is called "engine knock" and needs to be avoided. Therefore one of the most important criteria for the quality of a gasoline is its resistance to engine knock. The knock resistance of gasoline is measured in the form of octane number. There are two commonly

referred to values in use, the motor octane number (MON) and the research octane number (RON) [98]. The difference between these two octane numbers is merely the operating conditions in a standardized test engine with a single cylinder, the so-called cooperative fuel research engine (CFR engine). The RON is measured at 600 rounds per minute (rpm) and the MON at higher engine speeds of 900 rpm. The performance of a fuel in this CFR engine is compared to the performance of a binary mixture of *n*-heptane (RON = 0, by definition) and 2,2,4- trimethylpentane (RON = 100, by definition) [98].

Knock resistance can be improved by several means. Kerosine for example consists of a particularly narrow fraction cut of hydrocarbons with 8 to 13 carbon atoms. This prevents the early ignition due to the absence of very light and volatile molecules with high vapor pressures, and since no heavy compounds are combusted the formation of residues and soot is minimized. Particle formation needs to be avoided not only for environmental reasons, but also in order to prevent engine wear and filter blocking. The vapor pressure of gasoline can be tailored by blending in butane. The blended amount is determined by climatic conditions, since in winter more butane is required to achieve a constant volatility. Another method to improve engine knock resistance is to blend additives to fuels such as $Pb(Et)_4$ [99].

To date tetraethyllead is banned from automotive fuel in the EU, and only used in aviation gasoline [101]. This “Avgas” is only used for planes with Otto engines. Since most commercial aircrafts have jet engines using kerosine, such as Jet A-1, the lead pollution is quite low. The need for increased octane numbers in fuel without lead as an additive increased the use of zeolites in reforming processes, since alkanes with higher octane rating had to be blended into the fuels at the refineries [36]. Likewise, there are attempts to forego the use of lead in aviation fuels by tailoring the composition with a mixture of alkylaromatics such as toluene, ethylbenzene and xylenes [102].

In the European Union, the legislation for automotive fuels is covered by EN 228 for gasoline [103] and EN 590 for diesel [104]. The requirements for fuels have been increased over time, mainly due to environmental and health-related reasons. The sulfur content for example is limited to 10 $mg \cdot kg^{-1}$. Currently the aromatic content in gasoline is limited to 35 vol.-%, while the concentration of benzene must not exceed 1 vol.-% [103]. This presents the opportunity to blend quite an amount of aromatics - save benzene - to gasoline. Therefore, the blending of alkylaromatics, which have higher blending octane numbers than benzene anyway, is an obvious solution to improve the RON.

4.6 Octane Number

The octane number of a mixture can be measured in many ways. The international standard method is the CFR method described in chapter 4.5 Automotive fuels. This method is, however, for some laboratory analytics impractical, since CFR operation is costly and requires frequent maintenance, as well as relatively large amounts of sample mixture [105]. Hence, many alternative methods have been developed to determine the octane number of a given mixture, such as IR [106], Raman [107] and NMR spectroscopy [108]. All these methods aim to determine the composition of the mixture and subsequently calculate the octane number of the blend from the octane numbers of its components. The composition of the mixture can also be analyzed by gas chromatography [105]. The disadvantage of these methods compared to CFR testing is that the different components do not contribute linearly to the final RON. To account for this non-linear behavior instead of the RONs of the pure components "blending RONs" have been established for calculation.

Blending RONs have been determined by measuring a mixture of 20 vol.-% of the respective substance and 80 vol.-% of a 60/40 vol.-% mixture of *i*-octane and *n*-heptane in a CFR test engine. The RONs of the components relevant for this work are listed in Table 10 [109,110]. With these blending RON values the final RON of the mixture can be calculated volumetrically according to Eq. 2 [111].

Table 10: Blending RON values of the liquid components [109, 110].

Component	Pure RON	Pure MON	Blending RON	Blending MON
i-Pentane	92	90	99	104
n-Pentane	62	62	62	67
Benzene	>100	>100	99	91
Toluene	>100	>100	124	112
Ethylbenzene	>100	98	124	107
Xylenes	>100	>100	~145[a]	
i-Propylbenzene	>100	99	132	
n-Propylbenzene	>100	98	127	

[a] 120 for *o*-, 145 for *m*- and 146 for *p*-xylene

Eq. 2:
$$V_t \cdot RON_t = \sum_i V_i \cdot r_i$$

With: V_t total Volume, RON_t total RON of the blend, V_i Volume of component i, r_i blending RON of component i.

The densities of the liquid components are nigh identical, ranging from 0.86 g · cm^{-3} for *i*-Propylbenzene to 0.88 g · cm^{-3} for benzene. The densities of *iso*-/*n*-pentane (0.62 and 0.63 g · cm^{-3} respectively) differ from those of the aromatics, however since the amount of detected pentane is consistently low the resulting error can still be neglected. In exemplary calculations the molarly weighted calculations (Eq. 3) of the final RON of the mixture differ from the volumetrically weighted calculations (Eq. 2) at the 2nd digit after the decimal point. Therefore the more convenient molarly weighted calculation method was used.

The RON of the liquid phase $RON_{(l)}$ was calculated on a molar basis according to Eq. 3.

Eq. 3:
$$RON_{(l)} = \sum_i x_i r_i$$

With x_i being the molar fraction of component i and r_i the blending RON of component i.

Compared to the initially pure benzene all products from Table 10 improve RON, except *n*-pentane, which has a lower blending RON. This is essential for the aim of the production of fuel components, since selectivity to specific alkylaromatics is of significantly lower importance. As mentioned in Table 10 the three different xylene isomers have different blending RONs. Since during this work mostly *p*- and *m*-xylene is observed, and little or no *o*-xylene, all xylene isomers will be added up and calculated with a blending RON of 145.

5 Motivation and Objectives

For the utilization of natural gas large facilities with high investment costs are required. These facilities have to be built near the natural gas site, if transportation over long distances is to be avoided. The high investment costs make only large facilities economically reasonable. Therefore, it is often not economic to utilize the natural gas in a small deposit.

In the frame of the NEXT-GTL project by the EU, this work was part of an attempt to devise a method to utilize small natural gas fields in remote locations. To transport the natural gas more easily it is supposed to be converted into a liquid form, preferably with one with a higher value. One approach is the aromatization of methane to benzene, followed by the alkylation of the produced benzene with ethane and propane. The produced alkyaromatics have a higher blending RON than pure benzene, also benzene can only be added as fuel component to an extent of 1 vol.-% in the EU. Alkylaromatics can be used as fuel components to 35 vol.-%. Therefore a conversion from natural gas to alkylaromatics would increase the value and make it more easily transportable. The aromatization of the methane to benzene was investigated by other members of the project. The aim of this work is to investigate the dehydroalkylation of benzene with mixtures of ethane and propane to maximize the RON of the liquid phase received.

A direct dehydroalkylation of the benzene with a mixture of ethane and propane requires no further separation of the alkanes and produces valuable H_2 as byproduct. Since the equilibrium reactions to alkylaromatics produce H_2 the removal of H_2 drives the equilibrium towards the alkylaromatic products. To selectively remove the H_2 from the reaction mixture a membrane reactor is utilized. The metal membrane of this reactor can only be diffused through by H_2, but no other compounds in the product stream.

To catalyze the dehydroalkylation of benzene alkanes a bifunctional catalyst is required. As catalyst an acidic zeolite support functionalized with Pd or Pt as noble metal is used. The metal sites dehydrogenate the alkane to the respective alkene, and the acidic sites then alkylate the benzene with the in situ produced alkene.

6 Experimental Section

6.1 Chemicals

The chemicals employed in this work are listed in *Table 11* and were used without further purification.

Table 11: List of the used chemicals.

Chemical Substance	**Producer, Purity / Composition**
Azepane	Fluka, >97 %
Aluminum nitrate	Riedel-de Haen, 98 %
Aluminum hydroxide	Merck, 99 %
Aluminum sulfate	Riedel-de Haen, chemically pure
Ammonia solution	Riedel-de Haen, 25 wt.-% in water
Ammonium nitrate	Merck, 99 %
Benzene	Fluka, >99.5 %
Cab-O-sil-M5	Fluka, 99 %
Ethane	Westfalen AG, 99.95 % (3.5)
Hydrochloric acid	Normapur, 32 %
Hydrogen	Westfalen AG, 99.999 % (5.0)
Levasil VPAC 4038	Bayer, 30 % SiO_2
Ludox AS 40	Du Pont, 40 wt.-% SiO_2 in water
Ludox HS 40	Sigma Aldrich, 40 wt.-% in water
Nitric acid	Merck, 65 %
Nitrogen	Westfalen AG, 99.999 % (5.0)
$[Pd(NH_3)_4]Cl_2$	Chem Pur
$[Pt(NH_3)_4]Cl_2$	Chem Pur
Propane	Westfalen AG, 99.95 % (3.5)
Pural SB	Condea, 75 % Al_2O_3
Sodium aluminate $NaAlO_2$	Riedel-de Haen, 54 wt.-% Al_2O_3, 41 wt.-% Na_2O
Sodium hydrogen carbonate	Aldrich, 99 %
Sodium hydroxide	Merck, >99 %
Sulfuric acid	Fluka, 98 wt.-%
Tetraethylammonium hydroxide solution	Sigma Aldrich, 35 wt.-% in water
Tetrapropylammonium bromide	Acros, 98 %

6.2 Preparation of the Catalysts

6.2.1 Synthesis of Zeolite ZSM-5

The parent zeolite ZSM-5(19) was prepared by M. Fritz [112]:

In a stirable autoclave, 4077 g of Levasil VPAC 4038 (Bayer, 30 % SiO_2) and 1632 g of H_2O were stirred while adding a solution of 64.18 g $NaAlO_2$ (Riedel-de Haen) in 2191 g H_2O. After the addition is complete another solution of 239.45 NaOH (Riedel-de Haen) in 8000 g H_2O were added while stirring. Crystallization of the zeolite was carried out over 5 days at 160 °C while stirring. The material was subsequently filtered, washed with water and dried at 100 °C.

The parent zeolite ZSM-5(20) was prepared by B. Gehring:

A polypropylene beaker with a solution of 2.00 g of NaOH in 80.00 g of deionized water was stirred while adding 5.93 g of TPABr and 181 mg of Pural SB (Condea, 75 % Al_2O_3). After stirring the mixture for 20 min 12.0 g Ludox AS-40 were added and stirred for additional 30 min. To the resulting gel 31.0 g of cold ammonia solution (25 wt.-%) were added and filled into Teflon-lined autoclaves (300 ml). Crystallization was carried out under static conditions at 180 °C over 6 days. Subsequently the material was filtered and washed with deionized water, dried at room temperature and calcined as described in 6.2.4 Calcination.

The parent zeolite ZSM-5(22) was prepared according to [113] by M. Paolillo:

In a glass beaker 35.4 g of TPABr (Acros, 98 %), 29.5 g of $NaHCO_3$ (Aldrich, 99 %) and 3.0 g of $Al(OH)_3$ (Merck, 99 %) were dissolved in 250 ml of deionized water and stirred for 30 min. Then 200.0 g of Ludox HS 40 (Sigma Aldrich, 40 wt.-% in water) were added while stirring, the mixture was stirred until homogeneous and then evenly filled into 4 Teflon-lined stainless-steel autoclaves (120 ml). Crystallization was carried out under static conditions and autogenous pressure at 180 °C for 5 days. Subsequently the sample was washed with deionized water, dried overnight at 80 °C and calcined as described in 6.2.4 Calcination.

The parent zeolite ZSM-5(35) was prepared according to [114] by D. Geiß:

In a glass beaker 4.6 g TPABr (Acros, 98 %) and 2.0 g $Al(NO_3)_3 \cdot 9\ H_2O$ (98%, Riedel-de Haen) were dissolved in 32 cm³ deionized water. Then, 32.0 g Ludox AS 40 (40 wt.% SiO_2 in H_2O, Du Pont) was added. To the well dispersed mixture, 43.6 cm^3 ammonia solution (25 wt.-% in water, Riedel-de Haen) was added. Crystallization occurred under rotation in stainless-steel autoclaves (V = 300 ml). Subsequently the sample was washed with deionized water, dried overnight at 80 °C and calcined as described in 6.2.4 Calcination.

The parent zeolite ZSM-5(90) was prepared by B. Gehring:

A polypropylene beaker with a solution of 2.00 g of NaOH in 80.00 g of deionized water was stirred while adding 5.93 g of TPABr and 40 mg of Pural SB (Condea, 75 % Al_2O_3). After stirring the mixture for 20 min 12.0 g Ludox AS-40 were added and stirred for additional 30 min. To the resulting gel 31.0 g of cold ammonia solution (25 wt.-%) were added and filled into Teflon-lined autoclaves (300 ml). Crystallization was carried out under static conditions at 180 °C over 6 days. Subsequently the material was filtered and washed with deionized water, dried at room temperature and calcined as described in 6.2.4 Calcination.

6.2.2 Synthesis of Zeolite Beta

The parent zeolite BEA(24) was synthesized by the "dry gel" method according to [115]:

4.43 g of $Al_2(SO_4)_3 \cdot 18\ H_2O$ were dissolved in 5.00 g of demin. water and stirred at 353 K in a beaker for 30 min. Meanwhile 49.14 g of Ludox-HS-40, 51.10 g of tetraethylammonium hydroxide solution (Sigma Aldrich, 35 wt.-% in water) and 8.78 g of a 4 M NaOH solution were homogenized and stirred at ambient temperature for 30 min. Subsequently the solution was added to the suspension and stirred for another 2 h at ambient temperature. After these 2 h the resulting gel was heated to 353 K while continuing stirring until dry. The dry gel was pulverized with mortar and pestle. Crystallization of the zeolite was conducted under static conditions in an autoclave (inner volume 120 cm³) at 448 K for 48 h. The dry gel (1.50 – 2.00

g per autoclave) was placed in a Teflon-lined inlet (inner volume 15 cm^3) and the bottom of the autoclave was covered with 2.00 g of water.

6.2.3 Synthesis of Zeolite MCM-22

The precursor MCM-22(21) material was synthesized according to [116] by M. Fritz:

In 3059.00 g of deionized water 315.30 g of Cab-O-Sil M5 (Fluka, 99%) were dissolved. While stirring, a solution of 30.81 g sodium aluminate and 19.23 g NaOH in 748.00 g water was added. After 30 min of homogenization a solution of 3.44 g concentrated H_2SO_4 in 152.00 g of water and subsequently 172.60 g of azepane were added dropwise. Crystallization was carried out by heating the mixture to 150 °C with a rate of 1 $K \cdot min^{-1}$ and keeping that temperature for 10 days under agitation. The used material of MCM-22 precursor was provided by M. Fritz. The final zeolite MCM-22 was obtained by calcination of the washed and filtered precursor material according to 6.2.4 Calcination.

6.2.4 Calcination

To remove the template from the zeolite, the sample was calcined in synth. air by heating it from room temperature to a final temperature of 540 °C at a rate of 1 $K \cdot min^{-1}$. The sample was kept at a temperature of 540 °C for 24 hours and then cooled to ambient temperature.

6.2.5 Ion Exchange

After the calcination the zeolite samples were ion exchanged twice with a fiftyfold mass excess of aqueous 1 M NH_4NO_3 solution for 4 h at 80 °C. The sample was washed with deionized water and dried at 80 °C over night.

After this treatment the ammonia cations were partly exchanged by the respective noble metal by stirring the ammonia form of the zeolite (2.00 g dry mass) in water at room temperature and adding dropwise as solution of 47 mg $[Pd(NH_3)_4]Cl_2$ or 72 mg $[Pt(NH_3)_4]Cl_2$ in 5.00 g deionized water respectively. After the addition of the noble metal salt the mixture was heated from room temperature to 80 °C and kept at that temperature for 4 hours. After cooling to ambient temperature again the mixture was filtered, thoroughly washed with deionized water and dried at 80 °C.

6.2.6 Pelletizing of the Catalyst

To minimize the pressure drop in the reactor caused by the catalyst bed the catalyst was pelletized with a PW20 press from P/O/Weber, applying ~ 120 MPa for 30 min to compress the catalyst into a tablet without binder. The tablet was crushed with mortar and pestle and particles with a size of 200 – 315 µm were sieved and used as catalyst while avoiding repulverization of the particles through mechanical stress.

6.3 Catalyst Characterization

6.3.1 Magic Angle Spinning Nuclear Magnetic Resonance Spectroscopy

The investigations of the catalyst with MAS-NMR were conducted by Apl. Prof. M. Hunger with a Bruker Avance III 400 WB. The details on the spectrometry parameters are listed in *Table 12*. During the measurements the respective sample was rotated in the "magic" angle of 54.74° to the direction of the magnetic field, which represents the half of the tetrahedral angle.

The samples for the ^{27}Al measurements were hydrated over saturated $Ca(NO_3)_2$ solution for 12 h prior to the measurements. Before the ^{1}H measurements the samples were dried for 12 h at 450 °C in vacuum.

Table 12: List of MAS-NMR spectroscopy parameters.

Parameter	**^{1}H**	**^{27}Al**	**^{29}Si**
Resonance Frequency / MHz	400.13	104.26	79,49
Rotor Diameter / mm	4	4	7
Rotation Frequency / kHz	8	8	3.5
Number of Scans	80	4800	200 - 250
Pulse	single	single	hpdec
Pulse Duration / µs	2.5	1	2
Repetition Time / s	20	0.25	20

6.3.2 Scanning Electron Microscopy (SEM)

The SEM images were collected with a Cambridge Cam Scan 44 scanning electron microscope. The images of the catalyst samples were used to determine the crystal size and crystal morphology of the parent zeolite. To make the samples electrically conductive, a ca. 200 nm thick coating of Au (from Canadian Maple Leaf coin 99.99 % Au) was applied via sputtering with an Emitech K550. The used excitation voltage was 5 - 20 kV (normally 5 kV,

if not noted otherwise). The SEM images were collected by either C. Lieder, M. Dyballa or myself.

6.3.3 Thermogravimetric Analysis (TGA)

The thermogravimetric analysis were conducted with a Setaram Setsys TG-16/18 by either B. Gehring or myself. To calculate the dry mass of the respective sample, the content of water was measured by heating the sample from 20 °C to a final temperature of 600 °C at a rate of 20 $K \cdot min^{-1}$ in a stream of nitrogen.

6.3.4 X-Ray Powder Diffractometry (XRD)

The X-ray powder diffractograms were taken with a Bruker D8 Advance diffractometer. The Cu-K_α radiation ($\lambda = 0.154$ nm) was produced from a Cu-anode (U = 35 kV, I = 40 mA). The diffractograms were collected between angles of $5° < 2\,\Theta < 50°$ with a step width of 0.0165° and a step time of 0.2 s. The collected diffractograms were compared to simulated and already measured diffractograms to ensure the purity of the zeolite phase.

6.3.5 Inductively Coupled Plasma Optical Emission Spectrometry (ICP-OES)

A Varian optical emission spectrometer with an inductively coupled plasma (ICP-OES) Vista MPX CCD was used to determine the amount of Si, Al, Na, Pd and Pt of the catalysts. Therefore 50 - 100 mg of the respective sample was dissolved in 3 ml of hydrofluoric acid (10 wt.-%) and 6 ml of aqua regia, which was prepared from 1.5 ml HNO_3 (65 %) and 4.5 ml concentrated hydrochloric acid. The resulting solution was diluted to a volume of 250 ml with

twice distilled water and then analyzed. The results of the ICP-OES were obtained by H. Fingerle.

6.3.6 Elemental Analysis (CHN)

In a Vario EL from Elementar Analysensyteme ~ 20 mg of the respective samples were decomposed at 950 °C in an oxygen stream. The resulting products of the combustion CO_2, H_2O and N_2 were analyzed via TCD. The CHN analysis was conducted by B. Gehring.

6.3.7 Gas Chromatography coupled with Mass Spectrometry (GC/MS)

The received products were identified by GC/MS with parameters presented in Table 13. Therefore the product stream was collected in a cooling trap and analyzed offline. Positive identification was ensured by co-injection of the product mixture with the respective pure compound.

Table 13: Conditions of the CG/MS analysis.

Column	Petrocol DH 150
Stationary Phase	Dimethyl polysiloxane
Length	150 m
Internal Diameter	0.25 mm
Film Thickness	1 µm
Temperature Program	10 min at 35 °C; heating to 100 °C with 1 K · min^{-1}; heating to 110 °C with 0.5 K · min^{-1}
Carrier gas	H_2
Pressure at Column Entrance	198.4 kPa
Flow through Column	1.6 ml · min^{-1}
Injection	Agilent 7683 B Injector (liquid, via syringe)
Injected Volume	1 µl
Split Ratio	10 : 1
Injector Temperature	200 °C
Detector	Flame ionization detector (FID)
Temperature	250 °C
H_2 Flow to FID	35 ml · min^{-1}
Air Flow to FID	350 ml · min^{-1}
Mass spectrometer	Agilent 5975 B inert XL MSD
Temperature of Ion Source	230 °C
Temperature of Quadrupole Analyzer	150 °C
Acceleration Voltage	70 eV
Range of Detected Mass	20 - 250 u

6.4 Catalytic Experiments

The used laboratory plant is shown in Fig. 18 with a membrane reactor installed. In the case of the fixed-bed reactor the configuration is identical, except for the reactor. The tubing for the sweep gas is simply not in use with a fixed-bed reactor.

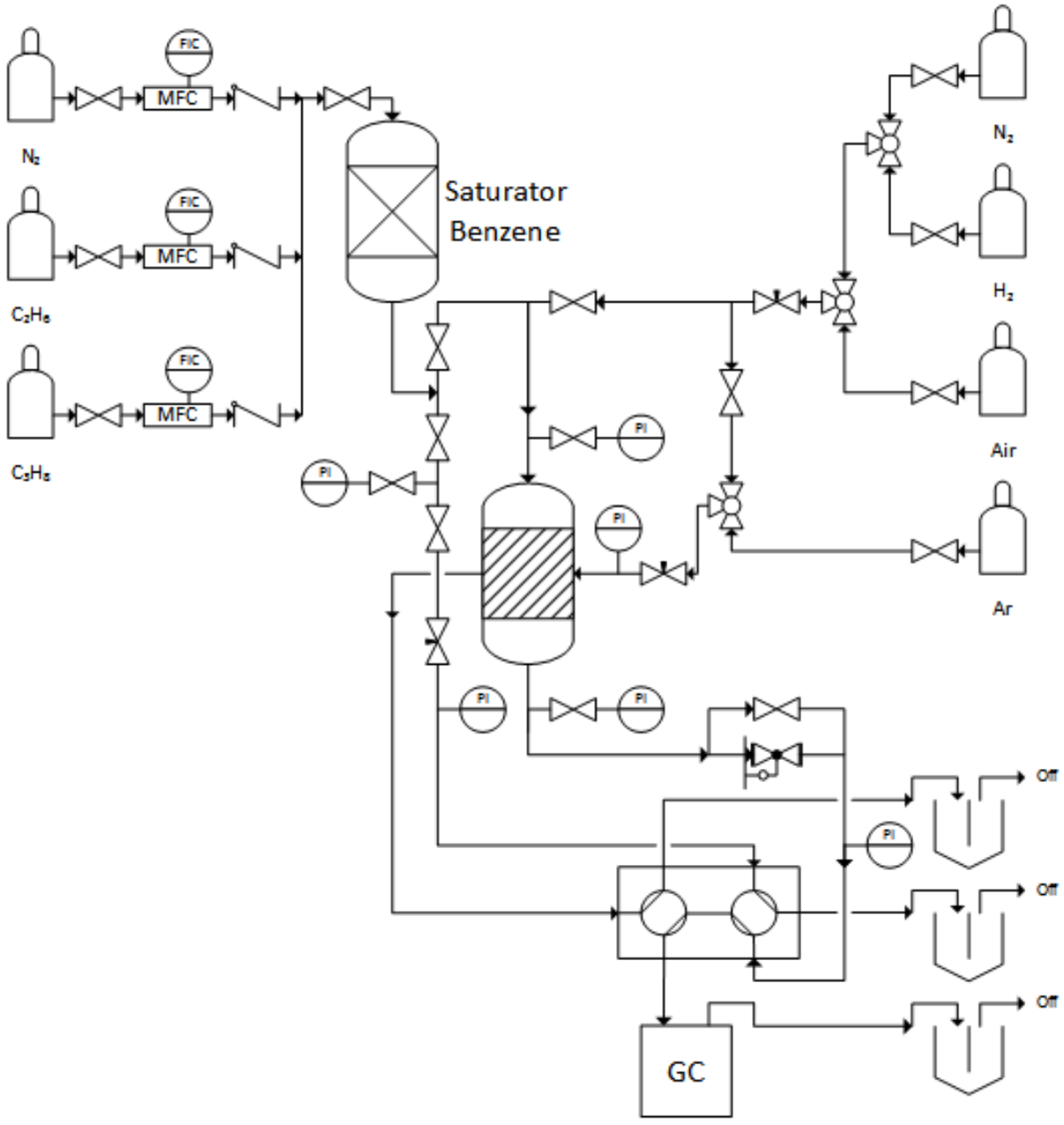

Fig. 18: Flow chart of the laboratory plant.

6.4.1 Alkylation in the Fixed-Bed Reactor

For use in the fixed-bed reactor the respective catalyst was activated in situ in the reactor by increasing the temperature with a rate of 0.25 $K \cdot min^{-1}$ from room temperature to 300 °C in a 50 $ml \cdot min^{-1}$ stream of synthetic air. The remaining air after the oxidation was flushed out of the reactor with nitrogen while increasing the temperature to 350 °C over the course of one hour. Subsequently the catalyst was treated with a stream of hydrogen with a flow rate of 50 $ml \cdot min^{-1}$ at 350 °C for 4 h. After the activation, the temperature of the reactor was lowered to 200 °C under a stream of nitrogen.

The bypass measurement was conducted at a temperature of 200 °C and a stream of reactants with a velocity of 20 $ml \cdot min^{-1}$. The reactant stream was composed of ethane, propane and benzene. The dry mass of the catalyst was 0.5 g and the pressure during the experiments was 0.58 – 0.67 MPa as noted respectively. After achieving a quasi equilibrium state the temperature of the reactor was increased with a rate of 2 $K \cdot min^{-1}$ to a final temperature of 350 °C at which the dehydroalkylation was carried out. The products were analyzed online via GC.

6.4.2 Alkylation in the Membrane Reactor

For experiments in the membrane reactor the catalyst was activated ex situ in a quartz glass reactor, by increasing the temperature from room temperature to 300 °C at a rate of 2 $K \cdot min^{-1}$ in an 50 $ml \cdot min^{-1}$ flow of air. The catalyst was kept at 300 °C for another 22 h and then flushed with nitrogen to remove the remaining air, while increasing the temperature to 350 °C over the course of one hour. Finally it was treated with a 50 $ml \cdot min^{-1}$ stream of hydrogen for 4 h, and then cooled to room temperature under nitrogen flow. The activated catalyst was then transferred to the membrane reactor and heated to 200 °C at a rate of 1 $K \cdot min^{-1}$ in a nitrogen stream before the start of the bypass measurement. The bypass measurement and dehydroalkylation in the membrane reactor was conducted similar to the procedure in the fixed-bed reactor.

After the experiments the membrane reactor with catalyst had to be flushed with nitrogen to remove all the hydrogen before cooling to ambient temperature. This was done to avoid the formation of crystalline PdH in the membrane and the resulting damage to it [117].

6.5 Evaluation of the Catalytic Experiments

6.5.1 GC Analysis

The product stream of the dehydroalkylation was analyzed online with an Agilent 6890 N gas chromatograph. The received chromatograms showed signals of the compounds listed in Table 14 with their respective retention times. The parameters of the chromatograph are shown in Table 15.

Table 14: Retention times of the detected compounds during online gas chromatography.

Compound	**t_{ret} / min**	**Compound**	**t_{ret} / min**
H_2	2.0	*n*-Pentane	19.6
Methane	2.3	Benzene	22.8
Ethane	5.3	Toluene	25.6
Propene	11.3	Ethylbenzene	27.9
Propane	11.6	*m*-, *p*-Xylene	28.0
i-Butane	15.3	*o*-Xylene	28.5
n-Butane	16.1	*i*-Propylbenzene	30.0
i-Pentane	19.1	*n*-Propylbenzene	30.9

Table 15: Conditions of the online GC analysis.

Column	HP Plot Q 19091 P-Q04
Stationary Phase	polystyrene-divinylbenzene
Length	25 m
Internal Diameter	0.32 mm
Film Thickness	20 µm
Temperature Program	5 min at 30 °C; heating to 250 °C with 10 K · min^{-1}; holding at 250 °C for 30 min
Carrier gas	Ar
Pressure at Column Entrance	1.2 bar
Flow through Column	3.0 ml · min^{-1}

Injection	sample loop
Injected Volume	5 µl
Split Ratio	20 : 1
Injector Temperature	200 °C
Front Detector	Thermal conductivity detector (TCD)
Temperature	250 °C
Reference Flow	12 ml · min^{-1}
Make Up Flow	7 ml · min^{-1}
Back Detector	Flame ionization detector (FID)
Temperature	250 °C
H_2 Flow to FID	40 ml · min^{-1}
Air Flow to FID	450 ml · min^{-1}

6.5.2 Calculations

The conversion of the reactants was calculated according to Eq. 4. In case of a concentration difference in the bypass measurements before and after the respective experiment a linear change was assumed and n_{in} was corrected by the appropriate value.

Eq. 4:
$$X = 1 - \frac{n_{out}}{n_{in}}$$

The conversion of benzene was calculated according to Eq. 5. This calculation method does not require time-dependent correction, which makes calculation more convenient. This calculation method assumes that benzene rings are neither formed nor consumed, effectively counting the benzene rings. Given the applied reaction parameters this assumption is very likely.

Eq. 5:
$$X_{benzene} = \frac{\sum n_{alkylbenzenes}}{n_{benzene,out} + \sum n_{alkylbenzenes}}$$

Both methods for conversion calculation make the assumption that no deposits on the catalyst remain. This is incorrect for longer times on stream and higher conversions, at which the

catalysts clearly show coking behavior. However, since coke amounts are limited to < 6 %, the errors are relatively small.

The yield of alkylbenzenes was calculated according to Eq. 6. The molarly yield was used for clearer assertion. When using weight yield, one has to keep in mind that an increase in molecular weight occurs from benzene to the respective alkylbenzene toluene, EB, IPB and NPB.

Eq. 6:

$$Y = \frac{\sum n_{alkylbenzenes}}{n_{benzene,in}}$$

The weight hourly space velocity (WHSV) was calculated referring to the sum of all reactants according to Eq. 7.

Eq. 7:

$$WHSV = \frac{\dot{m}_{in}}{m_{cat}}$$

7 Results and Discussion

7.1 Results of Catalyst Characterization

To ensure the used catalysts consist of pure respective phases, a combination of XRD, MAS-NMR spectrometry and SEM imaging was used. These results are compiled in chapter 9 Appendices. The results of the XRD are shown in Fig. 37 to Fig. 39 , and the results of the MAS-NMR spectrometry are shown in Fig. 40 to Fig. 44. The SEM images of the catalysts are shown in Fig. 45 to Fig. 50 and their results are compiled in Table 16.

When comparing the obtained results with exemplary characterizations from [39], it can be seen that the XRDs and MAS-NMR spectra clearly match. Also there is no or only negligible amounts of extra-framework aluminum. Therefore, the phases of the catalyst can be considered pure and structured as expected.

Table 16: Crystal morphology of the catalysts.

Zeolite	**Morphology[a]**	**Dimensions[a]**	**Size[a]**
ZSM-5(90)	Coffin-shaped	10 µm x 10 µm x 6 µm	~600 µm³
ZSM-5(20)	Coffin-shaped	7 µm x 7 µm x 7 µm	~340 µm³
ZSM-5(19)	Coffin-shaped	2 µm x 1 µm x 1 µm	~2 µm³
ZSM-5(35)	Coffin-shaped	15 µm x 8 µm x 4 µm	~480 µm³
MCM-22(21)	Platelets (agglomerated)	1 µm x 1 µm x >0.1 µm	>0.1 µm³
Beta(24)	Octahedral	1 µm x 1 µm x 1 µm	~1 µm³

[a] see chapter 9 appendices

7.2 Preliminary Experiments

The activity of the catalyst was ensured by running experiments with neutral washed sand as catalyst in the fixed-bed rector. The particle size of the sand grains was 200 to 315 µm to achieve a similar pressure drop as with catalyst particles. The length of the sand bed in the reactor was equal to the catalyst bed in other experiments. During experiments with sand less than 1 % blind conversion was observed, therefore it can be concluded that the detected conversion during experiments with catalytically active material results from the use of the respective catalyst employed.

Further, the reproducibility of the experiments was validated with fresh samples of the same batch of 1.0Pd-H-ZSM-5(35) catalyst. The compared results of the conversions of the three reactants during the two measurements are shown in Fig. 19.

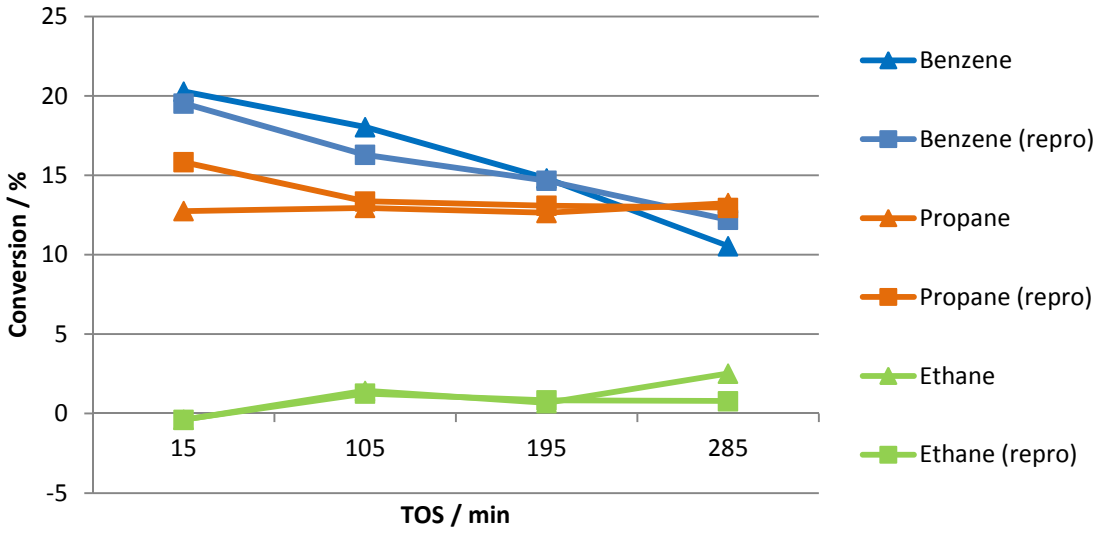

Fig. 19: Reproducibility of the conversion in fixed-bed reactor over 1.0Pd-H-ZSM-5(35) at T = 350 °C and p = 6.0 bar, $\dot{n}_{Et}$ / $\dot{n}_{Pr}$ / $\dot{n}_{Bz}$ 7.8 / 3.5 / 1.

The reproducibility of the experiments was found acceptable. The initial conversion of propane shows not an ideal match. Further experiments showed that at low TOS the results can deviate slightly, maybe because of initial adsorption and desorption effects of the fresh catalyst, but over time the results are reliable. Since the GC sampling occurs in 90 min intervals the initial fluctuations of the reaction results pose no problem from the second sample onward. After switching to a membrane reactor the reproducibility was not tested again.

7.2.1 Influence of the Reactants

As pointed out in chapter 4.4 Alkylation of Aromatics, the $n_{Olefin}/n_{Aromatic}$ ratio influences the product distribution during the alkylation with ethene or propene. A high ratio leads to polyalkylation, which is unwanted for the use as fuel component. The polyalkylation is kinetically favored, since after alkylating benzene the following alkylation of an alkylaromatic occurs at a faster rate [75]. Very low $n_{Olefin}/n_{Aromatic}$ ratios avoid polyalkylation, but require large amounts of unreacted benzene to be recycled, which is expensive. This is different for the dehydroalkylation with alkanes over bifunctional catalysts. The problem of alkylating benzene several times does not occur, since the olefin concentration is low throughout the reaction. As already shown in Fig. 16 on page 40, the main dehydroalkylation reactions of benzene with either ethane or propane are followed by several secondary reactions, which produce a wide variety of alkylaromatics and other products.

For a better understanding of the interaction between the two main alkylation reactions, the dehydroalkylation was conducted separately and combined as shown in Fig. 20. It can be seen, that the dehydroalkylation with ethane over 1.0Pd-H-ZSM-5(35) produces hardly any byproducts and secondary alkylation products. Almost exclusively EB is produced, with toluene as the only detectable byproduct from hydrogenolysis [93].

The dehydroalkylation with propane produces a wide variety of alkylaromatics (toluene, xylenes, EB, IPB & NPB), albeit only in small quantities. Toluene is the most prominent among these. The main products received are higher alkanes, namely butanes, ethane and some pentanes. The large amount of butanes and ethane derives from the disproportionation of propane into butane and ethane [74]. The disproportionation is thermodynamically favored [62]. This becomes evident, when ethane and propane are reacted together without benzene. Here the product distribution almost exclusively consists of butanes, along with methane and some pentanes. Also the butanes from the propane disproportionation may form xylenes via aromatization at the employed temperatures [68].Yet, only toluene and EB are detected as alkylaromatics. These could be formed by de-/transalkylation of xylene or by aromatization of higher alkanes. A direct aromatization of ethane or propane is unlikely, due to the required temperature of 575 °C and 450 °C, respectively.

It can be seen, that the product distribution obtained by dehydroalkylating with a mixture of ethane and propane is a combination of the two alkanes' reactions, with the reaction of

propane being far more dominant, since propane is much easier to dehydrogenate than ethane and propene is far more reactive than ethene.

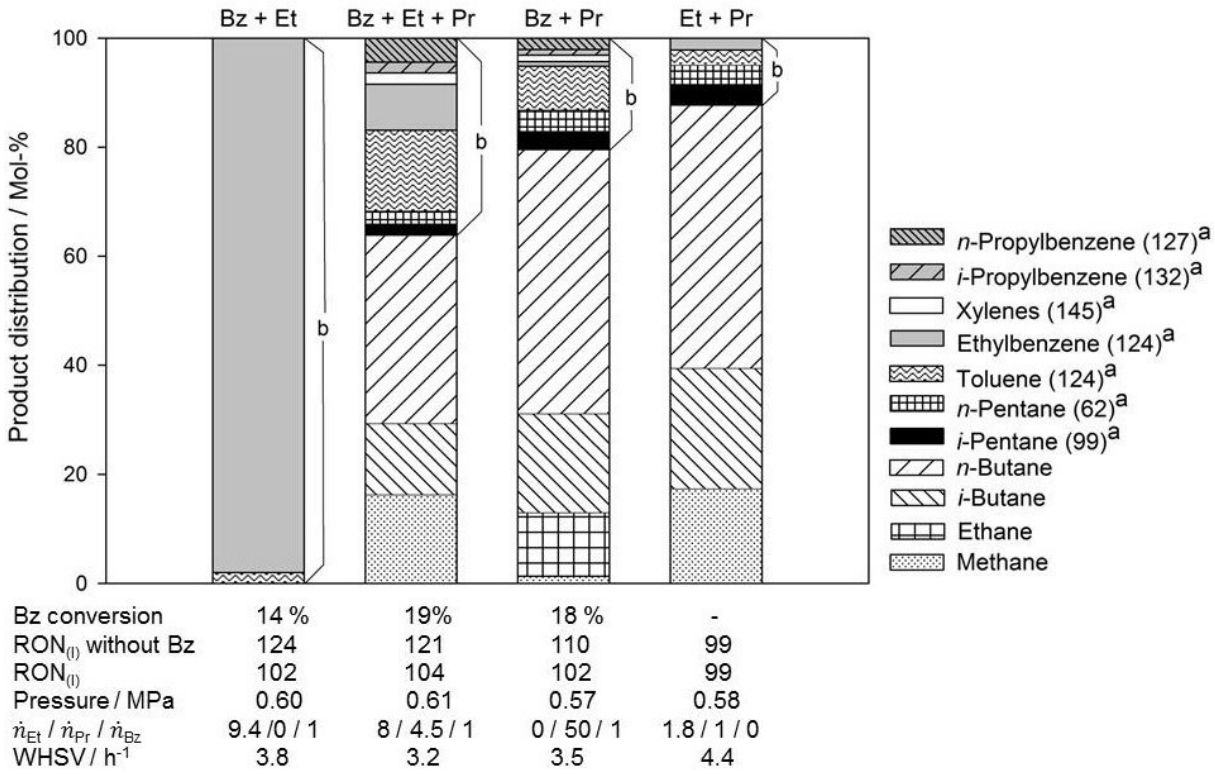

Fig. 20: Comparison of product distributions without H_2 on 1.0Pd-H-ZSM-5(35) after TOS = 105 min at T = 350 °C in fixed-bed reactor with different reactants. [a] blending RON, [b] liquid phase for RON calculation [1].

In the reactions with separated alkanes (Bz + Et and Bz + Pr) the RON of the liquid phase is influenced by the products from Table 10 on page 48 and increases from initially 99 (pure benzene) to 102 for both reactions, although their product compositions are very different, as described above. The higher reactivity of propane and the resulting higher benzene conversion is somewhat counteracted by the increased formation of side products. The RON is still only 102 at 18 % benzene conversion compared to the 14 % in the case of ethane. The $RON_{(l)}$ without benzene in Fig. 20 makes this obvious. When calculating the RON without benzene the impact of the pentane amounts, which are formed in the reaction with propane, lower the $RON_{(l)}$ significantly. The $RON_{(l)}$ with benzene mainly depends on the benzene conversion, and therefore the amount of unconverted benzene in the liquid phase. The combined reactions show the highest RON of the liquid phase (104) together with the highest benzene conversion. Since almost all observed products have a higher blending RON than benzene, the selectivity to a specific alkylaromatic is not of high importance regarding the production of fuel components.

It can be concluded, that since during the dehydroalkylation the concentration of the alkylating agent ethene and/or propene is low at any given time - dehydrogenation is presumed to be the rate-limiting step [72] - the problem of polyalkylation does not occur although an excess of ethane/propane is used. The only products pointing towards occurring polyalkylation are the xylenes. This can also result from the higher temperatures employed during the dehydroalkylation with alkanes compared to alkylation with olefins, since higher temperatures shift the equilibrium towards the monoalkylated products. An excess of benzene is therefore not required to avoid polyalkylation. Another explanation for the presence of xylenes could be disproportionation of toluene or transalkylation thereof. The dehydroalkylation with a mixture of ethane and propane yields a wide variety of products, which is a combination of the separated dehydroalkylation reactions. The reaction with ethane yields almost exclusively EB under the applied reaction parameters. The reaction with propane produces both propylbenzenes IPB and NPB, as well as toluene – most likely from cracking propylbenzene or EB – and some xylenes by further reacting with toluene. The non-alkylaromatic products also derive from the reaction with propane. The alkylation with olefins and the dehydroalkylation with alkanes can also lead to different product distributions [84] (see 7.6 Investigations of the *n*-/*iso*-Ratio of Propylbenzene during Dehydroalkylation). The most common side reaction is the propane disproportionation. The formation of methane, which is presumed to be a byproduct from cracking [74] is also observed in large amounts. Although the use as fuel component in this work only focuses on the liquid components, it has to be noted that the unwanted formation of large amounts of butane is not useless. Butanes are used as additive in gasoline during winter and also have quite good blending RON values of 113 and 122 [110].

From the comparison of the dehydroalkylation to the alkylation with olefins it can be concluded, that the dehydrogenation of the alkane is a key step, which has a major effect on product distribution. The reaction rates of the dehydrogenation of ethane and propane determine the olefin concentrations during dehydroalkylation. Increasing the dehydrogenation rate increases the benzene conversion and thus the RON of the liquid phase. The dehydrogenation rate can be influenced by the nature and content of noble metal on the catalyst, which leads to another important parameter: the design of the catalyst.

7.2.2 Influence of the n_{Si}/n_{Al} Ratio

The design of the catalyst is of great importance to the dehydroalkylation of benzene. Several parameters of the catalyst affect the benzene conversion, product distribution and therefore the RON of the liquid phase.

One major parameter of the zeolite based catalysts that has to be considered is the n_{Si}/n_{Al} ratio. The n_{Si}/n_{Al} ratio affects the concentration and strength of acidic sites. This means, that the strength of adsorption between the catalyst and aromatics or olefins is also influenced, since the π-electrons interact with the acid sites. The acid sites catalyze not only the alkylation reaction, unfortunately. They are also responsible for the formation of side products such as methane from the cracking of propane or other cracking products and also for the oligomerization of olefinic intermediates to higher alkanes such as pentanes [73]. Therefore the n_{Si}/n_{Al} ratio was varied and the compared results are shown in Table 17. It can be seen, that the influence of the n_{Si}/n_{Al} ratio is substantial. The benzene conversion is highest over a medium n_{Si}/n_{Al} ratio of 35. At the high n_{Si}/n_{Al} ratio of 90, the benzene conversion is low with only 12 %, resulting in an appropriately low $RON_{(l)}$. However, no secondary products such as xylenes are formed, and toluene occurs only in comparatively small amounts. The drawback of low conversion cancels out the high selectivity to primary alkylaromatic products, unfortunately. With a low n_{Si}/n_{Al} ratio of 20 conversion and $RON_{(l)}$ are also lower than with the medium n_{Si}/n_{Al} ratio, although not as low as with the high n_{Si}/n_{Al} ratio. Much more EB than with an n_{Si}/n_{Al} ratio of 35 is produced, while no methane is observed.10 This means, when considering the benzene conversion and the $RON_{(l)}$, catalysts with too high or too low n_{Si}/n_{Al} ratios perform poorly. The highest $RON_{(l)}$ of 104 is achieved over 1.0Pd-H-ZSM-5(35), because this catalyst provides the highest conversion. These maximum conversions at intermediate n_{Si}/n_{Al} ratios have been observed before [121,118]. During the dehydroalkylation over the low n_{Si}/n_{Al} ratio of 20 an interesting phenomenon could be observed. Unlike over other catalysts, no formation of methane was observed. As the formation of methane is unwanted, since in principle in the NEXT-GTL project it is used previously to produce the benzene for further dehydroalkylation, a catalyst that completely avoids methane production would be highly coveted. This phenomenon is connected to the next parameter of the catalyst design, and will be discussed in the next chapter.

Table 17: Comparison of product distributions over Pd-H-ZSM-5 catalysts in the fixed-bed reactor with different n_{Si}/n_{Al} ratios.

Catalyst	0.9Pd-H-ZSM-5 (20)	1.0Pd-H-ZSM-5 (35)	0.9Pd-H-ZSM-5 (90)
Temperature / °C	350	350	350
Pressure / MPa	0.62	0.61	0.60
$\dot{n}_{Et}$ / $\dot{n}_{Pr}$ / $\dot{n}_{Benzene}$	7.7 / 4.3 / 1	8 / 4.5 / 1	7.3 / 4.1 / 1
WHSV / h^{-1}	4.1	3.2	4.1
Time on stream / min	105	105	105
Benzene conversion / %	14.6	19.2	11.6
$RON_{(l)}$	102.4	103.6	101.9
Product distribution[a] / Mol-%			
Methane	[b]	16.3	10.8
i-Butane	14.9	13.1	3.7
n-Butane	32.3	34.5	18.4
i-Pentane	2.6	2.1	[b]
n-Pentane	3.2	2.4	1.5
Toluene	14.3	14.7	3.4
Ethylbenzene	23.2	8.5	9.8
Xylenes	1.4	2.1	[b]
i-Propylbenzene	2.6	2.0	4.3
n-Propylbenzene	5.6	4.4	8.0

[a] without H_2, [b] not detected

7.2.3 Influence of the Noble Metal

To further optimize the $RON_{(l)}$, a catalyst was sought-after which was more active in the important dehydrogenation of ethane/propane to the respective olefin. Therefore, the noble metal was changed to Pt to compare the obtained results. Since the zeolite with the intermediate n_{Si}/n_{Al} ratio of 35 performed best, this zeolite was used for further investigations as support for the catalysts. To ensure the comparability, an equal molar amount of noble metal was ion exchanged into the parent zeolite. This means that an amount of ~1.8 wt.-% Pt corresponds to 1.0 wt.-% Pd on the catalyst.

In Fig. 21 and Fig. 22 it is shown, that the benzene conversion and also the $RON_{(l)}$ are much higher on the platinum-containing catalyst ($X_{benzene}$ = 32%, $RON_{(l)}$ = 107) than on the palladium-containing one ($X_{benzene}$ = 18 %, $RON_{(l)}$ = 103). The missing percentage to 100 in Fig. 22 is benzene. The selectivity to secondary alkylation products such as toluene and

xylenes is significantly higher when Pt is used as noble metal. Since these products result from various side reactions, it can be deducted that these side reactions are catalyzed better by Pt than by Pd. The overall better conversion of benzene on Pt catalysts causes the $RON_{(l)}$ to increase due to the lower benzene content in the liquid phase, since benzene has the lowest blending RON (99) of all the compounds in the liquid phase, save *n*-pentane (62) which occurs only in very low amounts of 0.9 Mol-% for Pd and 1.7 Mol-% for Pt, and thus hardly affects the final $RON_{(l)}$. The Pt catalyst shows high conversion of benzene and propane. Some of the propane is converted to ethane (see chapter 4.3.2 Disproportionation of Propane), which explains the "negative conversion" of ethane due to more ethane being produced than being consumed by the dehydroalkylation.

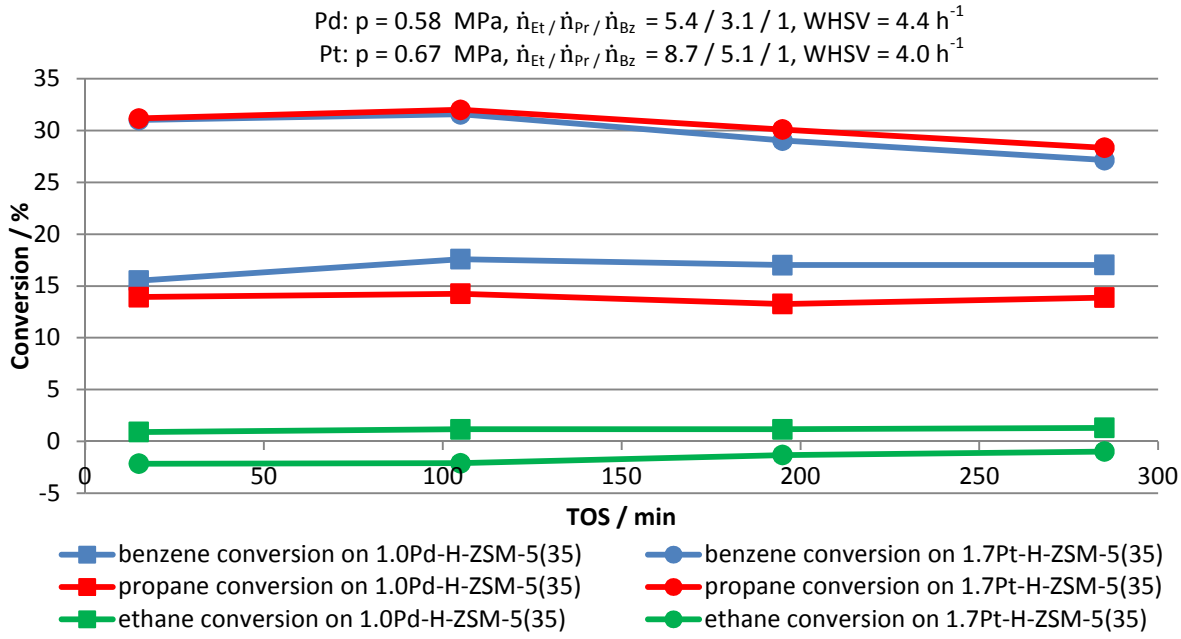

Fig. 21: Comparison of conversions during dehydroalkylation at T = 350 °C over H-ZSM-5(35) catalysts loaded with different noble metals in fixed-bed reactor.

The higher activity of Pt compared to Pd during the dehydrogenation of cyclohexane to benzene and hydrogen has been shown previously by Wang *et al.* [119]. It is reported that a 1 wt.-% Pt catalyst delivers a conversion of ~90 % at 315 °C, while a 1 wt.-% Pd catalyst converts between 30 % and 20 % of the alkane. One has to keep in mind that 1 wt.-% Pt and 1 wt.-% Pd are not equimolar amounts. In fact, the Pt catalyst performs far better during dehydrogenation while having a lower molar amount of metal [119]. The superior performance of Pt is in agreement with own results - although not to the same extent –

received during dehydroalkylation. Therefore, the following experiments were carried out with 1.7Pt-H-ZSM-5(35) as catalyst instead of 1.0Pd-H-ZSM-5(35).

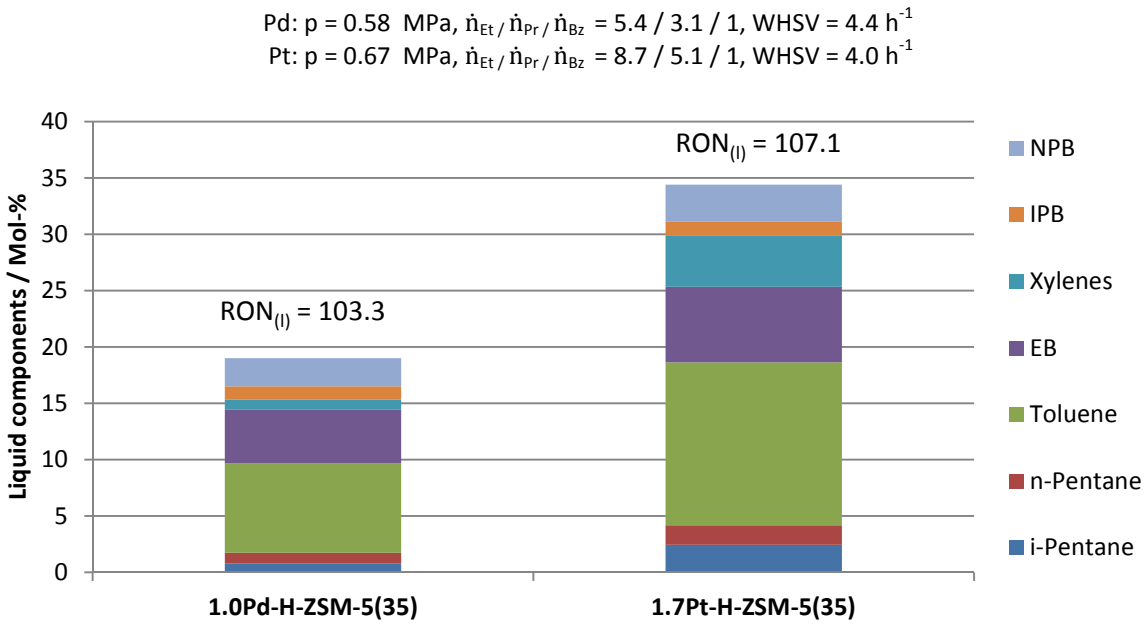

Fig. 22: Comparison of the liquid phases from the dehydroalkylation at t = 350 °C over H-ZSM-5(35) catalysts loaded with different noble metals in fixed-bed reactor at TOS = 105 min.

An interesting phenomenon was noticed during the comparison of the catalysts with different n_{Si}/n_{Al} ratios and different noble metals. During some dehydroalkylation reactions, no methane was produced. This peculiar behavior was noteworthy, since methane is a thermodynamically favored and stable hydrocarbon. The absence of methane in the product distribution is beneficial, since produced methane is essentially wasted carbon and hydrogen during the dehydroalkylation, especially when the employed benzene is supposed to be previously produced by the aromatization of methane (cf. Fig. 7 on page 22).

During the dehydroalkylation of benzene with mixtures of ethane and propane, some catalysts show absolutely no production of unwanted methane. This behavior was observed during dehydroalkylation over 0.9Pd-H-ZSM-5(20). In an attempt to maintain this characteristic, while using a more active catalyst, a catalyst with intermediate n_{Si}/n_{Al} ratio of 35 and Pt as noble metal was used. This showed a great amount of methane being produced. Therefore, the parameter, which governs this behavior was investigated. In Table 18 it can be seen, that when increasing the n_{Si}/n_{Al} ratio from 20 to 35 methane is produced. Also, when using a 1.9Pt-H-ZSM-5(23) catalyst methane is produced, but not on the same zeolite loaded

with an equimolar amount of Pd. It can therefore be concluded, that the inability of a given catalyst to produce methane is governed by two parameters. The n_{Si}/n_{Al} ratio must be below ~30 *and* the noble metal must be Pd not Pt. If the n_{Si}/n_{Al} ratio is higher than 30, the catalyst produces methane even if Pd is the noble metal. When Pt is used as noble metal the catalyst does produce methane even if the n_{Si}/n_{Al} ratio is low. However, it has been reported that an initial production of methane decreases to zero over a 0.4Pt-H-ZSM-5(28) catalyst after 60 h on stream [120]. This means the deactivation also plays a major role in methane production, and that formed coke can suppress the active sites responsible for the formation of methane while maintaining the ability to produce alkylaromatics. The amount of noble metal can also be responsible for methane production. Amounts as low as 0.02Pt-H-ZSM-5(150) show no production of light alkanes, albeit at 0.5 % conversion.

Table 18: Comparison of catalysts in respect of their methane producing abilities.

Catalyst	**0.9Pd-H-ZSM-5(20)[a]**	**1.1Pd-H-ZSM-5(23)[b]**	**1.9Pt-H-ZSM-5(23)[b]**	**1.0Pd-H-ZSM-5(35)[a]**	**1.7Pt-HZSM-5(35)[a]**
Temperature / °C	350	350	350	349	350
TOS / min	105	105	105	105	105
Pressure / MPa	0.62	0.64	0.58	0.61	0.61
$\dot{n}_{Et}$ / $\dot{n}_{Pr}$ / $\dot{n}_{Benzene}$	7.7/4.3/1	8.3/4.4/1	8.0/4.3/1	8.0/4.5/1	7.2/4.0/1
WHSV / h^{-1}	4.1	4.0	4.0	3.2	3.9
Benzene conversion / %	14.6	10.6	10.3	19.2	26.3
$RON_{(l)}$	102.4	102.0	101.6	103.6	105.7
Product distribution[c] / Mol-%					
Methane	[d]	[d]	19.9	16.3	38.3
i-Butane	14.9	[d]	[d]	13.1	12.4
n-Butane	32.3	21.9	28.9	34.5	19.2
i-Pentane	2.6	[d]	[d]	2.1	2.0
n-Pentane	3.2	[d]	3.3	2.4	1,4
Toluene	14.3	3.5	3.1	14.7	11.5
Ethylbenzene	23.2	23.0	10.4	8.5	7.0
Xylenes	1.4	[d]	[d]	2.1	3.0
i-Propylbenzene	2.6	20.1	12.9	2.0	1.6
n-Propylbenzene	5.6	31.5	21.6	4.5	3.7

[a] in fixed-bed reactor, [b] in membrane reactor,[c] without H2,[d] not detected

The results presented in Table 18 are in agreement with results from the literature. Bressel *et al.* [121] showed that during the quite similar dehydroalkylation of toluene with ethane no methane production is observed over catalysts loaded with 0.8 - 0.9 wt.-% Pd, as long as the n_{Si}/n_{Al} ratio is below 30 (see Table 19).

Sealy *et al.* [118] also reported a H-ZSM-5(20) catalyst loaded with 0.9 wt.-% Pd does not produce methane, while the same zeolite loaded with 1.8 wt.-% Pt does. It is most likely, that the production of methane requires catalytic sites active in hydrogenolysis. These seem to be more active when Pt is employed instead of Pd. The observed decrease in methane production over time on stream due to coking (see 7.4 Time on Stream Behavior and Regeneration of the Catalyst) suggest this. However, Pd shows hydrogenolysis activity for other reactions, since secondary alkylations products are regularly observed.

Table 19: Selectivity to methane depending on n_{Si}/n_{Al} ratio [121].

Catalyst	$Y_{methane}$ **/ wt.-%**	$X_{toluene}$ **/ %**
0.9Pd-H-ZSM-5(11)	0	2.85
0.9Pd-H-ZSM-5(26)	0	3.20
0.9Pd-H-ZSM-5(27)*	0	2.20
0.9Pd-H-ZSM-5(41)	0.11	5.02
0.8Pd-H-ZSM-5(59)	0.21	4.39
0.8Pd-H-ZSM-5(61)nano	0.02	1.57
0.9Pd-H-ZSM-5(122)	0.01	1.94

7.3 Influence of the Reactor Type

After concluding that a Pt-H-ZSM-5(35) catalyst was the best catalyst used for further experiments, the equilibrium of the dehydroalkylation reaction should be shifted towards the alkylaromatic products by employing a membrane reactor instead of a conventional fixed-bed reactor. If the produced hydrogen can be removed selectively from the reaction zone via permeation through a membrane, the equilibrium is shifted towards the alkylaromatic side (cf. Fig. 16). The membrane reactor shown in Fig. 23 features such a hydrogen-selective membrane.

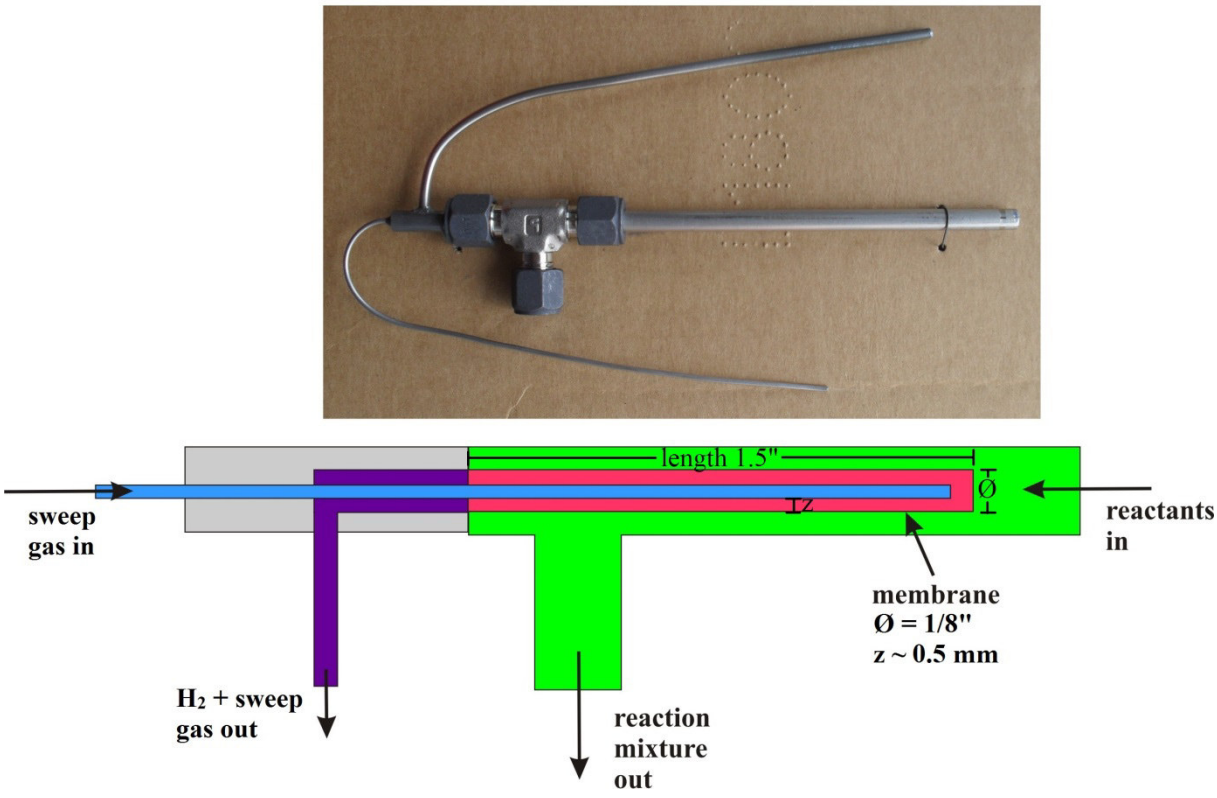

Fig. 23: Picture and schematic of the membrane reactor provided by REB Research & Consulting.

To fully utilize the membrane, the catalyst bed was at least as long as the membrane during the experiments. The entire surface of the membrane was covered with the respective catalyst. This means, for the comparison with a fixed-bed reactor, that the catalyst bed in the membrane reactor was ~25 % longer than in the fixed-bed reactor, since the same amount of catalyst was used. The displacement caused by the volume of the membrane increases the length of the bed, while the same amount and particle size is applied. Since the shape of the

catalyst bed has no influence on the WHSV, the different shape of the beds between fixed-bed and membrane reactor was ignored.

Rezai and Traa [88] describe the theoretical effects that the use of a hydrogen-selective membrane has on the dehydroalkylation reaction, and which parameters influence the equilibrium conversion. It is reported that the increase of the reaction pressure increases the conversion during the dehydroalkylation in a membrane reactor. As expected, the pressure increase has no effect in a fixed-bed reactor because the number of molecules remains constant during dehydroalkylation if no H_2 is removed [88]. When considering only the dehydrogenation reaction of ethane/propane to the respective olefin, a higher pressure is detrimental, because the increase in gas molecules from the generated H_2 is shifted towards the reactant side by the increased pressure. Therefore, H_2 removal is necessary (cf. also 7.3.2 Effects of the Membrane Reactor and H_2 Scavengers for Hydrogen Removal). The effect of the reaction temperature on the dehydroalkylation reaction is very low, when comparing the two reactor types. The dehydroalkylation reaction is endothermic, and thus the conversion increases with higher temperature. A significant difference between membrane and fixed-bed reactor is described at temperatures higher than 500 °C [88], which is not important for the temperatures used in this work.

The effect of the membrane is also determined by the sweep gas and reactant flow rates. A high $\dot{n}_{\text{Sweep gas}}/\dot{n}_{\text{Reactant}}$ ratio is beneficial for the conversion of the dehydroalkylation and the dehydrogenation reactions. This effect is more pronounced with propane than with ethane. At higher $\dot{n}_{\text{Sweep gas}}/\dot{n}_{\text{Reactant}}$ ratios the selectivity to alkylated products is reported to increase [88]. Another reaction parameter that is influenced by the membrane is reported to be the $\dot{n}_{\text{Alkane}}/\dot{n}_{\text{Benzene}}$ ratio. The maximum conversion during dehydroalkylation in a membrane reactor is calculated to occur at an $\dot{n}_{\text{Alkane}}/\dot{n}_{\text{Benzene}}$ ratio slightly below one [88].

The $\dot{n}_{\text{Alkane}}/\dot{n}_{\text{Benzene}}$ ratios used in this work are well above this value. The reasons for these chosen operating conditions are technical. The reactor cannot be streamed through much slower than 20 ml · min^{-1}. The $\dot{n}_{\text{Alkane}}/\dot{n}_{\text{Benzene}}$ ratio can be lowered by increasing the saturator temperature and thus the benzene concentration. This results in lower benzene conversion and lower $\text{RON}_{(\text{l})}$ (see later in 7.6 Investigations of the *n*-/*iso*-Ratio of Propylbenzene during Dehydroalkylation) because the WHSV is increased, since the amount of catalyst cannot be increased accordingly. More catalyst would result in a longer bed, where most of the catalyst is no longer in contact with the membrane.

Before going into detail with comparing the performance of the fixed-bed reactor and the membrane reactor, it has to be decided whether to use a fresh or a deactivated catalyst in the membrane reactor.

7.3.1 Pre-coking of the Catalyst

After the optimization of the catalyst, the shape selectivity of the catalyst should be improved. Therefore, the outer surface of the catalyst was coked selectively prior to use during dehydroalkylation. Also Rezai reported [117], that the use of uncoked catalyst could damage the membrane of the reactor, and that the outer surface should therefore be deactivated prior to use. Since far less coke is produced over pre-coked catalysts (also cf. Table 20) the membrane is less likely to coke [117]. To achieve a selective coking of the outer surface, while maintaining the active sites within the crystal particles, the activated catalyst was treated according to a procedure reported by Bauer *et al.* [122] (see Fig. 24). Hereby, the catalysts' surface was to be adsorbed with methanol at room temperature for 24 h in a stream of nitrogen with low flow rate, and heated to 500 °C without gas flow at a rate of 2 $K \cdot min^{-1}$ to form coke at that temperature for two hours. On the outer surface "hard" coke (consisting of many polyaromatic rings) was formed, while within the catalysts' pores only "soft" coke (alkylaromatic or polyolefinic in nature) could form, due to limited space. The catalyst was then treated with a stream of hydrogen (50 $ml \cdot min^{-1}$) at 500 °C for 24 h, and subsequently cooled to ambient temperature in a stream of nitrogen. This procedure is unable to remove the "hard" coke from the outer surface, but can remove the "soft" coke inside the crystals [122].

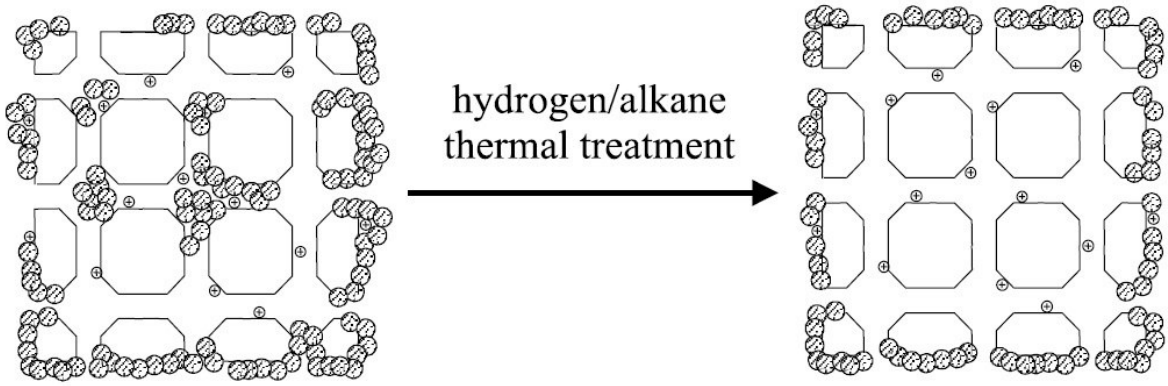

Fig. 24: Schematic of the selective coking of the outer surface [97].

The performance of the pre-coked 1.7Pt-H-ZSM-5(35) catalyst during dehydroalkylation was investigated and compared to an uncoked sample of the same catalyst. The results are shown in Fig. 25 and Table 20

Here it can be seen, that pre-coking procedure severely hampers the dehydroalkylation activity of the catalyst. The 1.7Pt-H-ZSM-5(35) catalyst loses almost half of its benzene conversion, while the selectivity to alkylation products does not improve significantly. Therefore the procedure of precoking is not beneficial to the catalysts' performance. A decreased benzene conversion is observed, which leads consecutively to a lower $RON_{(l)}$. The selectivity to methane is considerably reduced by the pre-coking procedure, the selectivity to butanes is increased, though. The selectivity to the other side products - namely pentanes - is similar, since methane is the most unwanted side product this effect of the pre-coking procedure would be welcomed. The effect on selectivity to primary and secondary products is that higher amounts of EB and IPB/NPB, and lower amounts of xylenes are formed. The high selectivity to toluene is unchanged by the pre-coking procedure.

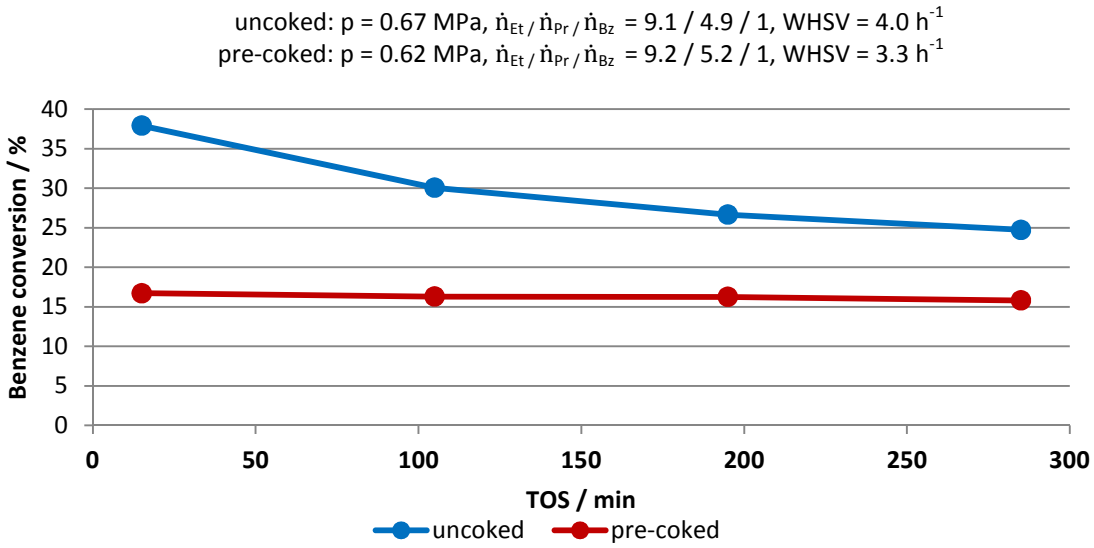

Fig. 25: Benzene conversion over pre-coked and fresh 1.7 Pt-H-ZSM-5(35) at T = 350 °C in membrane reactor [2].

However, the uncoked catalyst shows deactivation over time, while the pre-coked catalyst does not. It maintains its initially low benzene conversion while the uncoked catalysts' conversion drops to a final value, which is still considerably higher than that of the pre-coked catalyst (see Fig. 25). The carbon content of the pre-coked catalyst measured before the experiment matches that reported by Bauer *et al.* of ~ 0.3 wt.-% [97]. After the experiments much more carbon is accumulated on the uncoked catalyst, due to its higher activity. The pre-coked catalyst accumulates less carbon, despite starting with 0.36 wt.-% carbon, only 0.7 wt.-% are found after the experiment compared to the 2.2 wt.-% on the previously uncoked sample. The pre-coking procedure stabilizes the catalyst. This explains the low weight accumulation of coke and stable conversion performance. The change in selectivity by pre-coking imitates the time on stream behavior reported by Rezai *et al.* [120] (see also 7.4 Time on Stream Behavior and Regeneration of the Catalyst). Since the performance of the pre-coked catalyst was worse than the uncoked catalyst's, and after finding that the membrane is not damaged by uncoked catalyst, the pre-coking procedure was discontinued with further experiments.

Table 20: Comparison of pre-coked and fresh 1.7Pt-H-ZSM-5(35) during dehydroalkylation in the membrane reactor at T = 350 °C.

Catalyst	**pre-coked**	**uncoked**
Pressure / MPa	0.62	0.67
$\dot{n}_{Et}$ / $\dot{n}_{Pr}$ / $\dot{n}_{Benzene}$	9.2 / 5.2 / 1	9.1 / 4.9 / 1
Carbon / wt.-%[a]	0.36[b], 0.70[c]	2.23[c]
TOS / min	105	105
Benzene conversion / %	16	30
$RON_{(l)}$	103	107
Product distribution[d] / Mol-%		
Methane	18.8	39.6
i-Butane	17.2	13.1
n-Butane	34.1	18.7
i-Pentane	2.5	2.1
n-Pentane	1.6	1.4
Toluene	9.6	9.5
Ethylbenzene	7.8	6.7
Xylenes	1.0	3.0
i-Propylbenzene	2.6	1.9
n-Propylbenzene	4.7	3.8

[a] from CHN analysis, [b] before reaction, [c] after reaction, [d] without H_2,

7.3.2 Effects of the Membrane Reactor and H_2 Scavengers for Hydrogen Removal

Different methods can be employed to remove the hydrogen formed during dehydroalkylation, such as the use of a membrane reactor or mixing the catalyst with a H_2 scavenging agent like Zr_2Fe as reported by Smirnov *et al.* [86]. The results shown in Table 21 compare the results obtained in the fixed-bed reactor and the membrane reactor. The two reactor types show only little difference in conversion, $RON_{(l)}$ and product distribution. The formation of methane is lower in the membrane reactor, as can be expected due to less H_2 being available. Also a slight increase in primary alkylaromatics and a decrease in secondary alkylaromatics are observed. The effect of the membrane reactor is also evident when using only ethane and benzene as reactants. The benzene conversion decreases to 25 % with good selectivities to EB and toluene as secondary product (compare Fig. 20 in 7.2.1 Influence of the Reactants).

Table 21: Comparison of the dehydroalkylation conducted in fixed-bed and membrane reactor.

Reactor	**fixed bed**	**membrane**	**membrane**	**fixed-bed[ab]**	**fixed-bed[ac]**
Catalyst	1.7Pt-H-ZSM-5(35)	1.9Pt-H-ZSM-5(35)	1.9Pt-H-ZSM-5(35)	0.3Pt-H-MFI(25)	0.3Pt-H-MFI(25)
Pressure / MPa	6.1	6.5	6.0	atmospheric	atmospheric
Temperature / °C	350	350	350	350	350
$\dot{n}_{Et}/\dot{n}_{Pr}/\dot{n}_{Benzene}$	7.2/4.0/1	9.2/5.2/1	14/0/1	~0/1/1	~0/1/1
WHSV / h^{-1}	3.9	4.2	3.2	1.3	1.3
TOS / min	105	105	195	60	60
Benzene conversion / %	26	26	25	N/A	N/A
Propane conversion / %	26	25	N/A	44.6	76.2
$RON_{(l)}$	105.7	105.5	105.2	105.7[d]	104.8[d]
Product distribution[e] / Mol-%					
Methane	38.3	33.6	47.3	4.39	5.72
Ethane	N/A	N/A	N/A	27.83	29.08
Propene	[f]	[f]	[f]	0.35	0.77
Propane	N/A	N/A	10.0	N/A	N/A
i-Butane	12.4	13.4	[f]		
n-Butane	19.2	24.1	[f]	10.26[g]	9.67[g]
i-Pentane	2.0	2.4	[f]		
n-Pentane	1.4	1.8	[f]		
Toluene	11.5	9.0	8.7	19.58	11.66
Ethylbenzene	7.0	7.2	34.1	1.37	4.74
Xylenes	3.0	2.5	[f]	N/A	N/A
i-Propylbenzene	1.6	2.0	[f]	1.58	1.89
n-Propylbenzene	3.7	4.1	[f]	3.24	3.75
others	[f]	[f]	[f]	31.40	32.72

[a] from [86], [b] without Zr_2Fe, [c] with Zr_2Fe, [d] calculated without C_4-C_5 and others, [e] without H_2, [f] not detected, [g] sum of C_4-C_5

Adding a H_2 scavenger to the catalyst results is another method to remove the H_2 from the reaction zone used by Smirnov *et al.* [86]. Only propane and no ethane are used to dehydroalkylate benzene in these examples (Table 21). Smirnov *et al.* used Zr_2Fe as hydrogen scavenger. This was mixed together with the bifunctional catalyst to form the catalytic bed. A disadvantage of this method is, that when the scavenger material has reached its maximum H_2 uptake capacity, the catalyst must be separated from the scavenger for reuse or be discarded. New scavenger material can then be added to the catalyst in order to adsorb H_2 again.

Smirnov *et al.* conducted the experiments under atmospheric pressure and an $n_{Propane}/n_{Benzene}$ ratio of 1. Only the propane conversion is provided in [86], but the results can be compared since, at the $n_{Propane}/n_{Benzene}$ ratio of 1 and at 350 °C the benzene and propane conversion reported by Smirnov *et al.* are assumed to be similar.

Due to the $n_{Propane}/n_{Benzene}$ ratio of 1, Smirnov *et al.* is able to reduce the conversion of propane to butanes and pentanes. Yet, disproportionation of propane is avoided for the price of increased production of higher alkylated products (reported as "others"). In all experiments from Table 21, employing propane as reactant, the major alkylaromatic product is toluene rather than propylbenzenes. This means the formation of the primary products of the reaction of benzene with propane is slower than the further reaction of said products to toluene and e.g. ethane. The high amounts of butanes observed in own experiments are likely a result of the high propane concentration and the resulting disproportionation [74]. Since the Pt loading is lower in the experiments of Smirnov *et al.*, a lower methane production is observed. The reported absence of xylenes in [86] is attributed to the possible misinterpretation as ethylbenzene, since these are easily confused during GC analysis, and the presence of toluene is expected to go in hand with the presence of (small amounts of) xylenes.

The addition of Zr_2Fe as hydrogen scavenger significantly increases the propane conversion, while affecting selectivity only to a small extent. However, the amount of toluene decreases. The low pressure and WHSV contribute to this. This is very favorable behavior. The focus of Smirnov's work does not lie with the optimization of the $RON_{(l)}$. The use of Zr_2Fe actually worsens the $RON_{(l)}$, although the pentanes and higher alkylated products are not taken into account. This decrease of the $RON_{(l)}$ is attributed to the decrease of toluene. The increase in conversion is acknowledgeable, but the high selectivity to side products and the separation of spent scavenger from highly costing catalyst speak against the application of Zr_2Fe. The use of a membrane is therefore more favorable. Although the membrane effect is not as prominent as that of the Zr_2Fe, the handling of the neat catalyst is much more practical. If the hydrogen removing effect of the membrane could be increased to an extent such as that of the H_2 scavenger, the $RON_{(l)}$ would most likely increase significantly.

It was believed, that the removal of H_2 through the membrane was insufficient, since H_2 is detected in the product stream. A slower reaction flow would give the H_2 more time to diffuse through the membrane. To find out whether the removal of hydrogen through the membrane is sufficient, the maximum permeation rate of H_2 through the membrane was calculated.

7.3.3 Calculation of the H_2 Permeation Rate through the Membrane

To find out whether the membrane is limiting the H_2 permeation, and thus the removal of H_2 from the reaction zone being insufficient, the maximum permeation flow rate Q of H_2 through the membrane of the reactor was calculated.

According to [123], the general permeation through the membrane can be described as

Eq. 8:
$$Q_i = (\rho_i/z)A(p_{i,feed} - p_{i,permeate})$$

Q_i: permeation flow rate of the component i through the membrane [mol s^{-1}]

ρ_i: permeability of component i through the membrane [mol m^{-1} s^{-1} Pa^{-1}]

z: effective thickness of the membrane [m]

A: surface of the membrane [m^2]

p_i: partial pressure of the component i [Pa]

Since the only component which is permeating through the membrane is hydrogen the equation can be simplified. The fact that hydrogen diffuses through a metal membrane atomically and not molecularly as H_2 causes the power of $\Delta p^{1/2}$ in Eq. 9 for the partial pressure difference between the two membrane sides [124]. Therefore the hydrogen permeation flow rate corresponds to

Eq. 9:
$$Q_{H2} = \frac{\rho_{H2}}{z} A\sqrt{\Delta p}$$

This means for the calculation, that the hydrogen permeability ρ_{H2} at operating temperature, the thickness z, the surface A of the membrane and the difference in hydrogen partial pressure Δp between the two sides of the membrane are required parameters. These are calculated or assumed as follows:

1. The permeability ρ_{H2} is unknown, because the material of the membrane is unknown and must not be analyzed. Fig. 26 [125] shows the permeability of hydrogen through various metals. The supplier of the membrane states in [126] that the permeability is 3.5 times higher than that of a palladium silver membrane (for T = 300 °C, $\Delta p \sim 0.55$ MPa, $\rho_{H2} = 10^{-8}$ mol m^{-1} s^{-1} $Pa^{-1/2}$). Although in Ref. [124] the manufacturer proclaims a tenfold higher permeability for his membrane than with a Pd alloy membrane.

Whether these membranes are the same is not clear. Since the membrane used in this work could be either one, for this calculation the permeability will be considered to be at least $\rho_{H2} = 3.5 \cdot 10^{-8}$ mol m^{-1} s^{-1} $Pa^{-1/2}$(the worse one).

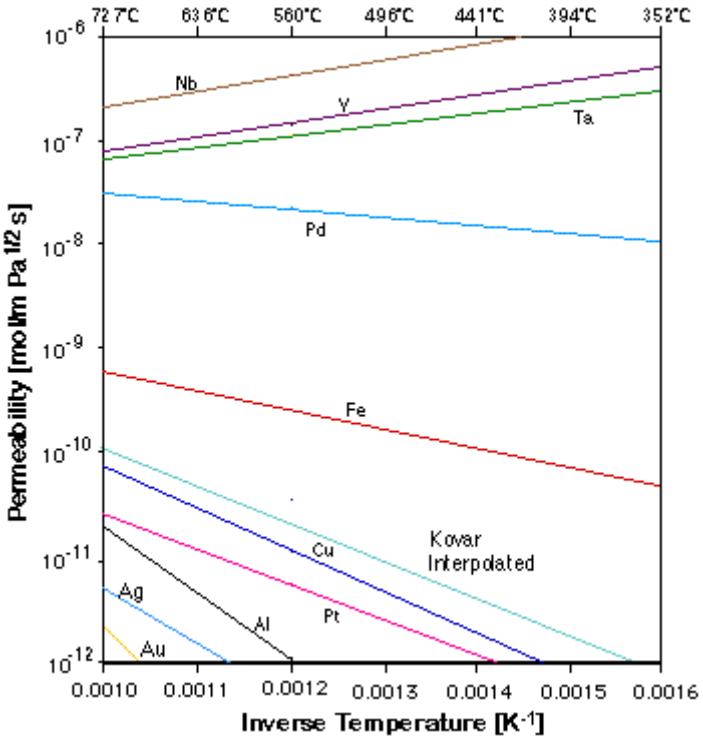

Fig. 26: Permeability of neat metals for atomic hydrogen [125].

2. The thickness z of the membrane is unknown, but will be calculated with $5 \cdot 10^{-4}$ m. This value is simply guessed, yet the order of magnitude is reasonable and that value was used as an example in Ref. [124] for the thickness of the membrane. The external surface of the membrane in contact with the reaction stream is calculated from dimensions given in a schematic of the membrane shown in Fig. 23 to be $3.8 \cdot 10^{-4}$ m² according to:

Eq. 10: $$A = \pi d \cdot l = 3.2 \cdot 10^{-3}\,\mathrm{m} \cdot \pi \cdot 38.1 \cdot 10^{-3}\,\mathrm{m} = 3.8 \cdot 10^{-4}\,\mathrm{m}^2$$

with d = diameter of membrane (1/8”) and l = length of membrane (1.5”).

3. The concentration of hydrogen on the reaction side of the membrane is about 0.5 Mol-% (from GC). The total pressure is about 0.6 MPa. This means the partial pressure of hydrogen on the reaction side is 3.0 kPa. The partial pressure on the permeate side of

the membrane will be considered zero for the calculation, due to the more than tenfold higher flow rate on the permeate side. Therefore the difference in hydrogen partial pressure would be $\Delta p = 3$ kPa. Yet, this model does not represent a gradient in H_2 partial pressure along the membrane. The assumption of a constant Δp along the entire surface of the membrane is hence incorrect. As an assumption half of the pressure difference ($\Delta p = 1.5$ kPa) will be considered constant along the entire surface of the membrane to account for the gradient. Since the Δp at the end of the membrane cannot be zero and the decline in Δp is not linear this model still is inaccurate.

With the above assumptions the permeation flow rate of hydrogen through the membrane can be calculated from Eq. 9 according to:

Eq. 11:

$$Q = \frac{\rho}{z} A\sqrt{\Delta p} = 3.5 \cdot 10^{-8} \frac{mol}{m \cdot s \cdot \sqrt{Pa}} \cdot \frac{1}{5 \cdot 10^{-4}\, m} \cdot 3.8 \cdot 10^{-4}\, m^2 \cdot \sqrt{1.5 \cdot 10^3\, Pa}$$
$$= 1.0 \cdot 10^{-6} \frac{mol}{s}$$

The actual hydrogen flow rate through the reactor, detected by GC, on the reaction side is in the order of $1 \cdot 10^{-7}$ mol $\cdot$ s^{-1}. This means the membrane is not limiting to hydrogen permeation, since ten times the amount of H_2 present in the reaction stream can permeate through the membrane.

Improving the hydrogen flow rate through the membrane would be difficult. The only parameters that can be manipulated are the permeability ρ via the reaction temperature and the partial pressure of H_2. The other parameters are determined by the membrane used. Changing the reaction temperature to increase the permeability obviously has far more impact on the equilibrium by itself than the permeation rate has, and is therefore not an option. The Δp – the driving force of the permeation – could be increased to improve the permeation. This can be achieved by either increasing the H_2 partial pressure on the reaction side, or lower the H_2 partial pressure on the permeate side. Adding H_2 on the reaction side is counterproductive, since the membrane is supposed to shift the equilibrium by removing hydrogen from the reaction side. Operating at a higher overall pressure and so enabling a higher partial pressure on the reaction side is unfeasible due to the pressure limitations posed by the use of propane as a reactant, which would liquefy at higher pressures. Hence, to increase the Δp of H_2 the permeate side has to be thoroughly flushed with sweep gas to achieve a hydrogen partial

pressure close to zero. This is already the case, since the hydrogen concentration in the sweep gas flow is barely detectable by GC during experiments.

Thickness and surface of the membrane could only be changed by using a different membrane. The design of the reactor determines whether the membrane operates at its theoretical limits [123] or not. The reactor used operates with co-current flows on both sides. The observed hydrogen permeation flow rate through the membrane is obviously only a fraction of the calculated, theoretical limit. Since the permeability can only be influenced by the reaction temperature and the H_2 partial pressure only via the overall pressure, an optimization of the permeation flow rate was not conducted. The temperature has a much larger effect on its own (see 7.5 Dehydroalkylation at Different Temperatures and Influence on Product Distribution) and the pressure cannot be elevated further when using propane as reactant.

However, to prove that the membrane does affect the equilibrium of the dehydroalkylation, the $\dot{n}_{\text{sweep gas}}/\dot{n}_{\text{reactants}}$ ratio was lowered by reducing the sweep gas flow rate during dehydroalkylation experiments (see Fig. 27 and also the following chapter 7.4 Time on Stream Behavior and Regeneration of the Catalyst). It can be seen that the benzene conversion drops, if the $\dot{n}_{\text{sweep gas}}/\dot{n}_{\text{reactants}}$ ratio is reduced from ~15 to ~ 1.5 and rises again, when the sweep gas flow rate is increased again.

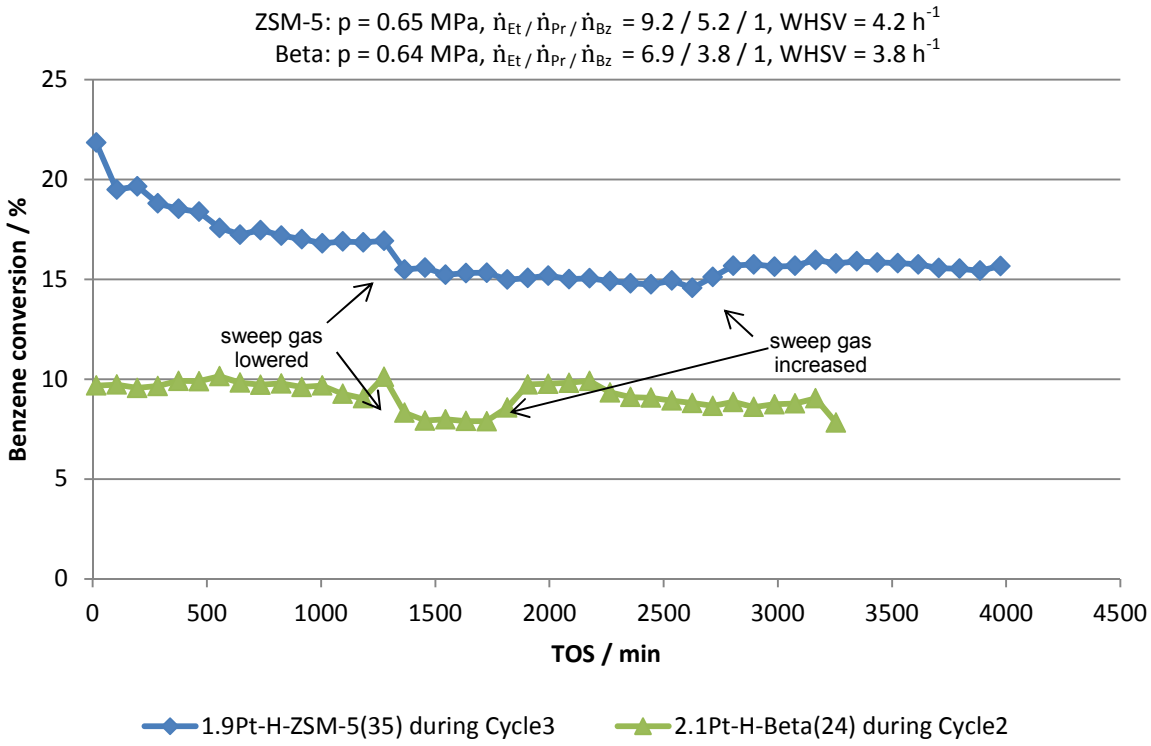

Fig. 27: Effect of reduced sweep gas flow rate from 300 ml · min^{-1} to 30 ml · min^{-1} over different catalysts at T = 350 °C.

7.4 Time on Stream Behavior and Regeneration of the Catalyst

During the experiments clear signs of catalyst deactivation over time on stream were observed. To further understand the nature of this deactivation, measurements with long times on stream were conducted. Also, attempts to regenerate the catalyst's activity were conducted to reuse the regenerated catalyst in further reaction cycles.

Since during the experiments the used catalysts showed deactivation behavior, the reason for this was investigated further. The deactivation most likely originates from carbonaceous deposits on the catalyst. Removing this coke can in principle be done oxidatively by burning the coke away forming CO_2 or reductively by hydrogenating the coke into hydrocarbons again. An oxidative approach is not a good option for this specific case of coke removal. The used catalyst may lose noble metal during the regeneration process due to conversion into PdO or PtO, which is more volatile than the respective metal. At higher temperatures, this could lead to leaching of active noble metal or sintering. More of concern is the fact that the membrane in the reactor could be damaged by such a procedure [117]. Therefore, a non-oxidative procedure was developed to remove the coke via hydrogenation. Since the catalysts already possess hydrogenation activity from their noble metal sites this approach seems advisable.

The main objective of the regeneration procedures was to restore the initially high $RON_{(l)}$ values obtained especially in the initial phase of the reactions. With increasing time on stream the conversion, and thus the $RON_{(l)}$, declines to a final value (see Fig. 28). In the 3rd cycle shown in Fig. 28 the benzene conversion "dips" for a 24 h period and returns to its former value. This is explained through the alteration of the sweep gas flow rate in the membrane reactor described in the previous chapter (cf. Fig. 27).

The regeneration was done under ca. 0.5 MPa H_2 pressure at the reaction temperature of 350 °C between the 1st and 2nd cycle, and at 400 °C between the 2nd and 3rd cycle. The catalyst was kept in the hydrogen stream of 30 ml · min^{-1} for 24 hours, then flushed with nitrogen and cooled to 200 °C (bypass temperature) again.

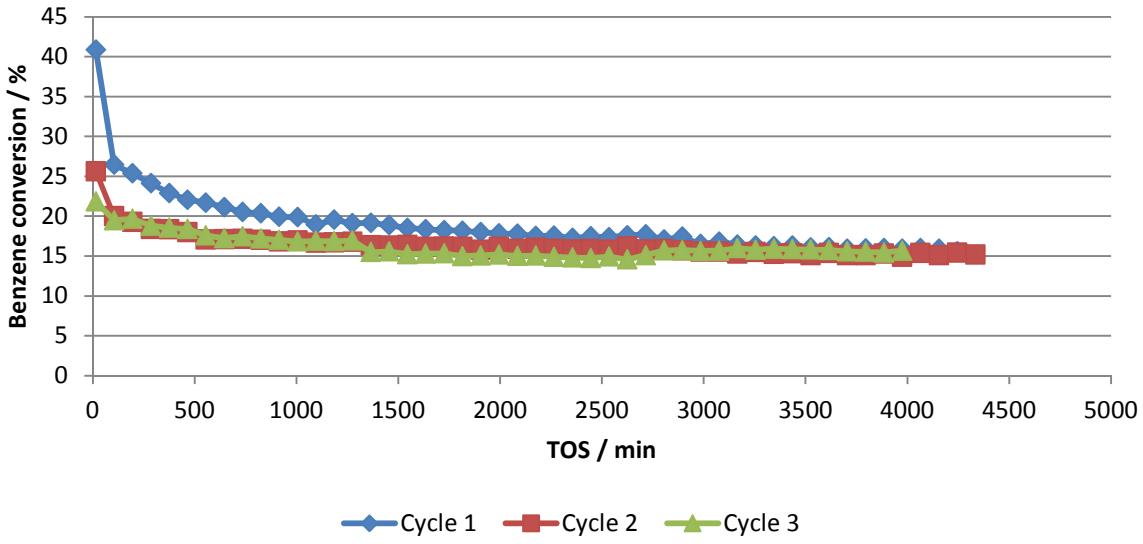

Fig. 28: Dehydroalkylation over 1.9Pt-H-ZSM-5(35) during three reaction cycles in membrane reactor, T = 350 °C p = 0.64 MPa, WHSV = 4.0 h^{-1}, $\dot{n}_{Et}/\dot{n}_{Pr}/\dot{n}_{Bz}$ = 9.5/5/1, regenerated with 0.5 MPa H_2 for 24 h at 350 °C after cycle 1 and 400 °C after cycle 2, modified from [1].

It can be seen in Fig. 28, that the initial activity is not restored by the regeneration procedure. The benzene conversion at the beginning of the reaction decreases from cycle to cycle. What can also be seen is that the final conversions of the three reaction cycles are the same. The reason for the different temperatures during regeneration with H_2 was the perception of the results from the 2nd cycle. Since regenerating at reaction temperature did not seem to restore activity, a higher regeneration temperature of 400 °C was utilized. To illustrate the effects on the product distribution, it has been listed in Table 22 for each cycle at the beginning of the reaction, after nearly one day on stream and after nearly three days on stream.

In Table 22 it is shown that, after 15 min on stream the benzene conversion amounted to 41% and the $RON_{(l)}$ amounted to 110. Initially, benzene is mainly converted to secondary alkylation products, such as toluene and xylenes. This is presumed to occur through the formation of the primary alkylation products ethylbenzene or propylbenzenes, followed by hydrogenolysis to toluene, and further disproportionation to xylenes. The Pt sites active for hydrogenolysis are proposed to deactivate within the first few hours on stream [93] leading to a quick decrease of the formation of toluene and xylenes, and within less than 1 day, the observed product distributions equilibrate, with the primary alkylation products ethylbenzene and propylbenzenes being the main constituents of the liquid phase. The $RON_{(l)}$ is then about

103 and stays the same for the rest of the cycle in all 3 cycles [1]. The Pt sites active for de-/hydrogenation deactivate slower than those active for hydrogenolysis [93]. The product distribution therefore shifts towards the primary products during a reaction cycle.

Table 22: Product distributions, RON, benzene conversion on 1.9Pt-H-MFI(35) in membrane reactor during three reaction cycles at T = 350 °C, p = 0.64 MPa, WHSV = 4.0 h^{-1}, $\dot{n}_{Et}/\dot{n}_{Pr}/\dot{n}_{Bz}$ = 9.5/5/1, regenerated with 0.5 MPa H_2 for 24 h at 350 °C after cycle 1 and 400 °C after cycle 2, modified from [1].

TOS	**15 min**			**~21.5 hours**			**69 hours**		
Cycle	**1st**	**2nd**	**3rd**	**1st**	**2nd**	**3rd**	**1st**	**2nd**	**3rd**
Benzene convers. / %	40.9	25.6	21.9	19.1	16.8	16.9	15.9	15.1	15.4
$RON_{(l)}$	110.2	105.4	104.2	103.6	103.1	103.1	102.9	102.8	102.8
Product distribution[a] / %									
Methane	52.0	35.6	22.0	20.8	12.8	9.9	14.6	9.9	7.6
i-Butane	9.3	12.1	15.0	12.2	8.3	8.1	9.5	5.6	5.5
n-Butane	12.5	22.4	31.5	33.2	35.8	39.2	36.3	33.8	36.5
i-Pentane	1.6	2.2	2.8	2.2	[b]	[b]	[b]	[b]	[b]
n-Pentane	0.9	1.7	2.4	2.6	3.7	4.3	3.2	4.0	4.7
Toluene	11.6	8.5	7.6	5.9	3.5	3.0	3.9	2.3	2.2
Ethylbenzene	4.6	7.8	7.9	9.0	10.1	8.3	10.2	9.3	8.8
Xylenes	5.1	2.6	1.9	1.5	[b]	[b]	[b]	[b]	[b]
i-Propylbenzene	0.7	2.3	3.1	4.5	10.2	11.3	8.7	14.9	14.9
n-Propylbenzene	1.9	4.7	6.0	8.1	15.6	15.9	13.5	20.2	19.7

[a] without H_2. [b] below detection limit.

The regeneration procedure seems to have little effect on the catalyst's activity. The initial conversion during the 1st cycle is not restored. Therefore, the regeneration between the 2nd and the 3rd cycle was conducted at a higher temperature, still with only little effect. However, the initial benzene conversion during the 2nd cycle is with 26 % notably higher than at the end of the 1st cycle (16 %). Assuming this is no desorption effect when starting the experiment, the regeneration does partly restore activity.

Removing the coke might not be necessary though, since the coked catalyst shows a higher selectivity to primary products. This coke selectivation is therefore not exclusively detrimental but also beneficial. The reduced conversion of benzene that goes along with a reduced $RON_{(l)}$ is somewhat balanced out by the greatly reduced formation of methane and the fact that propylbenzenes are the main constituents of the liquid phase followed by EB. The shift in selectivity towards the primary products within a cycle becomes more pronounced from cycle to cycle. In the case of xylenes the selectivity drops below the detection limit during the entire 3rd cycle. Also, the coked catalysts produced mainly butanes as side product, which can be used as fuel additive as well (especially during winter) to improve the RON of

gasoline. The reduced effort of not having to regenerate the catalyst would greatly reduce investment costs for commercial application.

The formation of the carbonaceous deposits on the catalyst is influenced by the activity of the catalyst and the time it is on stream. With longer time on stream and with higher conversions more coke is formed on the catalyst. In Table 23 it can be seen, that the amount of coke is mainly influenced by the benzene conversion, which in turn is influenced by the reaction temperature (see next chapter 7.5 Dehydroalkylation at Different Temperatures and Influence on Product Distribution). The pore system is an also important factor. Zeolite ZSM-5 offers the least space and therefore the smallest amount of coke is observed on it (only up to 6 wt.-%). In comparison, the zeolites MCM-22 and Beta have larger pores and ~16 wt.% coke is observed on these catalysts after the dehydroalkylation reaction. In the case of Beta the amount of 16 wt.-% coke is attained at < 10 % benzene conversion in contrast to the MCM-22 catalyst (see chapter 7.7 Dehydroalkylation over different Pore Systems).

Table 23: Carbon content from CHN analysis of different catalysts after dehydroalkylation.

Catalyst	wt.-% carbon	Ø $X_{Benzene}$ [a]	Temperature	total TOS
1.9Pt-H-ZSM-5(35)	1.8	12.4 %	300 °C	48 h
1.9Pt-H-ZSM-5(35)[b]	5.6	17.2 %	350 °C	220 h
1.9Pt-H-ZSM-5(35)	6.0	21.2 %	380 °C	70 h
1.9Pt-H-ZSM-5(35)	5.6	27.4 %	400 °C	26 h
2.1Pt-H-Beta(24)[c]	15.8	9.3 %	350 °C	108 h
2.2Pt-H-MCM-22(21)	16.4	21.2 %	350 °C	24 h
1.8Pt-H-ZSM-5(35)[d]	2.2	29.8 %	350 °C	4.75 h

[a] mean value of benzene conversion over entire TOS, [b] 3 reaction cycles with 2 regeneration cycles, [c] 2 reaction cycles with one regeneration cycle, [d] in fixed-bed reactor

Also it can be deducted that the formation of coke with increasing TOS is mostly completed when the benzene conversion maintains a final value. Results from the fixed-bed reactor with shorter TOS show that ZSM-5 catalyst after ~ 5 h on stream has only 2.2 wt.-% coke compared to 5.6 wt.-% after a long term measurement with the same conditions. The higher average benzene conversion in the fixed-bed reactor results from the shorter duration, otherwise the conversion would be similar. The coke content from Table 23 at 400 °C is suspiciously low, maybe because the 26 h on stream were not sufficient to reach the final conversion (cf. Fig. 30 in the following chapter). Another explanation could be that zeolite ZSM-5 cannot support more coke than ~6 %, although at 400 °C more coke would have been expected. The “more spacious” zeolites Beta and MCM-22 show significantly higher carbon contents, even at benzene conversions < 9 %.

In Fig. 29 the benzene conversion over zeolite Beta does not change significantly during two reaction cycles with three and two days on stream, respectively. The change in conversion during the 2nd cycle was due to sweep gas flow rate alteration for 8 h (cf. Fig. 27). Although after the reaction up to 16 wt.-% of carbon is found on the catalyst no change in conversion is caused by the accumulated coke. However, a change in product distribution is observed and will be discussed in chapter 7.7 Dehydroalkylation over different Pore Systems.

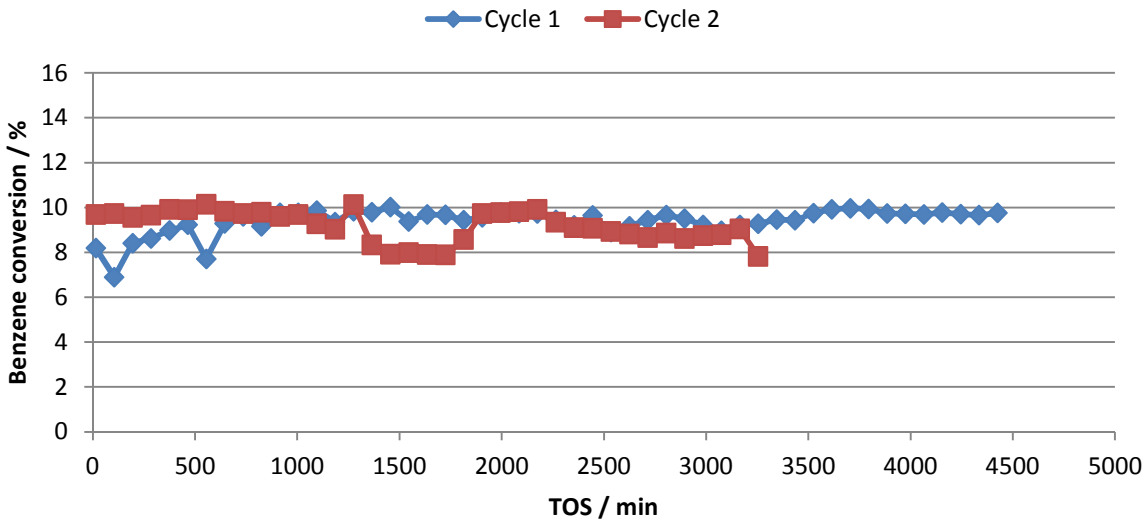

Fig. 29: Dehydroalkylation over 2.1Pt-H-BEA(24) during two reaction cycles in membrane reactor, T = 350 °C, p = 0.64 MPa, WHSV = 3.8 h^{-1}, $\dot{n}_{Et}/\dot{n}_{Pr}/\dot{n}_{Bz}$ = 6.9/3.8/1, regenerated at T = 350 °C in 150 ml · min^{-1} H_2 for 24 h between cycle1 and cycle 2, sweep gas flow rate lowered from 300 ml · min^{-1} to 30 ml · min^{-1} during cycle 2 for ca. 10 h.

7.5 Dehydroalkylation at Different Temperatures and Influence on Product Distribution

Since the benzene conversion has a major impact on the $RON_{(l)}$ and the conversion is determined by the reaction temperature, dehydroalkylation experiments were conducted at different temperatures. For commercial application, changing the reaction temperature would be an easy and simple method to influence the reaction. As can be seen in Fig. 30, the temperature greatly influences the initial conversion. It can also be seen, that in the temperature range of 350 - 400 °C the final conversion is very similar.

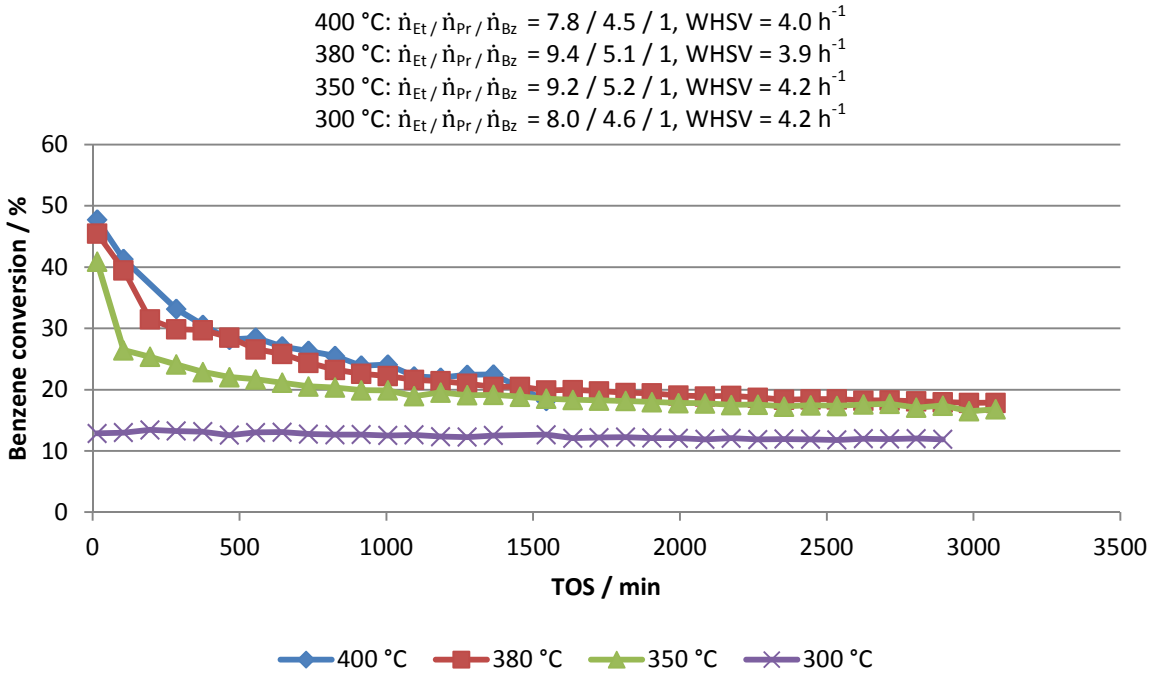

Fig. 30: Time on stream behavior of benzene conversion over 1.9Pt-H-ZSM-5(35), p = 0.63-0.65 MPa, at different reaction temperatures in membrane reactor, modified from [2].

At temperatures of 350 °C and higher, more benzene is converted; therefore, the $RON_{(l)}$ increases to very high values up to 113 at 400 °C (see Table 24). The formed alkylaromatics prove that this increase of activity results from increased formation of secondary products. The primary alkylation products ethylbenzene and propylbenzenes are to a large extent converted further to toluene and xylenes. Therefore, the hydrogenolysis reaction benefits greatly from higher temperatures. Unfortunately, the increased activity comes with a great amount of gaseous side products. However, methane can easily be separated and could be recycled to the dehydroaromatization unit in an integrated process (cf. Fig. 7 page 22) [1].

Table 24: Product distributions, $RON_{(l)}$ and benzene conversion on 1.9Pt-H-ZSM-5(35) at different reaction temperatures in membrane reactor, modified from [1].

TOS	**15 min**				**1 day**			
Temperature / °C	**300**	**350**	**380**	**400**	**300**	**350**	**380**	**400**
Pressure / MPa	0.63	0.65	0.64	0.64	0.63	0.65	0.64	0.64
$\dot{n}_{Et}$ /	8.0 /	9.2 /	9.4 /	7.8 /	8.0 /	9.2 /	9.4 /	7.8 /
$\dot{n}_{Pr}$ / $\dot{n}_{Bz}$	4.6 / 1	5.2 / 1	5.1 / 1	4.5 / 1	4.6 / 1	5.2 / 1	5.1 / 1	4.5 / 1
WHSV / h^{-1}	4.2	4.2	3.9	4.0	4.2	4.2	3.9	4.0
Benzene conversion / %	12.9	40.9	45.5	47.8	12.7	18.9	20.5	20.3
$RON_{(l)}$	102.6	110.2	112.1	113.1	102.6	103.6	103.9	104.0
Product distribution[a] / %								
Methane	19.0	51.9	58.6	66,5	12.3	19.7	30.5	37,0
i-Butane	9.0	9.3	6.7	3,3	8.0	11.9	9.2	5,9
n-Butane	27.4	12.5	8.7	3,9	27.5	33.7	29.7	25,9
i-Pentane	[b]	1.6	1.1	0,5	[b]	2.2	1.8	1,3
n-Pentane	[b]	0.9	0.6	0,2	[b]	2.7	2.8	2,9
Toluene	6.0	11.6	11.8	13,7	4.6	5.8	4.4	3,5
Ethylbenzene	10.8	4.6	4.0	3,8	9.5	9.3	7.9	7,7
Xylenes	[b]	5.1	5.8	5,9	[b]	1.5	2.1	2,0
i-Propylbenzene	11.1	0.7	0.6	0,4	15.4	4.7	4.2	5,3
n-Propylbenzene	16.7	1.9	2.1	1,8	22.7	8.5	7.3	8,5

[a] without H_2. [b] below detection limit.

The observed shift from primary to secondary products over TOS discussed in the previous chapter is also more prominent with an increasing reaction temperature. As an example, this shift is shown in Fig. 31 for T = 380 °C. Here it can be seen, that the amounts of toluene and xylene decline very fast, while those of the primary products IPB and NPB continuously increase. The amount of EB decreases slightly over time on stream, since the more reactive propane is converted more easily, but the sum of primary products increases with TOS.

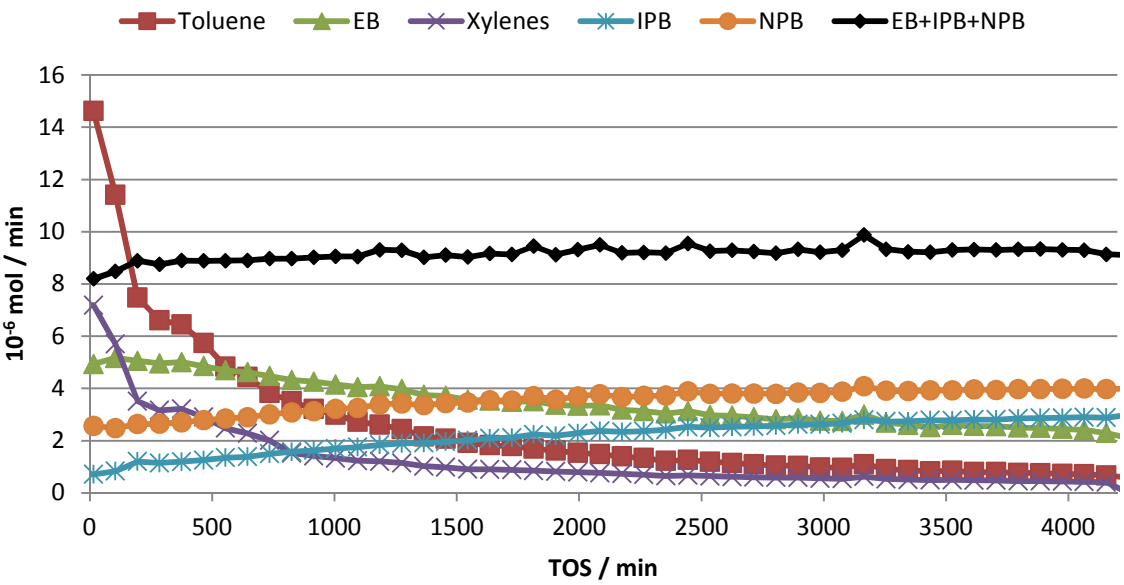

Fig. 31: Alkylaromatics during dehydroalkylation in membrane reactor over 1.9 Pt-H-ZSM-5(35) at T = 380 °C, p = 0.64 MPa, $\dot{n}_{Et}/\dot{n}_{Pr}/\dot{n}_{Bz}$ = 9.4/5.1/1, WHSV = 3.9 h^{-1}.

The decline of toluene and xylenes is faster with higher reaction temperatures and slowest at T = 300 °C. At this temperature, the initial deactivation of the catalyst is not observed. The $RON_{(l)}$ is lower than at 350 °C, because of the lower benzene conversion, while no deactivation and no significant change in product distribution with an increasing TOS is detected, as with higher reaction temperatures. The small amount of the secondary products, toluene and xylenes, at 300 °C proves that, preferably, the reaction to primary products occurs at lower temperatures, because the hydrogenolysis activity of the catalyst is low. The deactivation observed at higher temperatures between 350 and 400 °C results from the loss of hydrogenolysis activity of the catalysts, because the product distribution after 15 min of TOS includes large amounts of toluene, xylenes, and methane, whereas the amounts of these typical hydrogenolysis products are strongly reduced after 1 day of TOS [1].

Wong *et al.* showed in [90] that the direct alkylation of benzene with ethane proceeds via the two consecutive steps of dehydrogenation of ethane to ethene and further the alkylation of benzene with ethene to ethylbenzene. The focus of Wong's work lies on the influence of the reaction temperature which was varied from 290 °C to 490 °C. The used catalyst was 1.0Pt-H-MFI(36), the reaction was carried out under atmospheric pressure and the $\dot{n}_{Ethane}/\dot{n}_{Benzene}$ ratio was 9. It has been shown that the endothermic dehydrogenation of ethane increases with higher temperature, while the selectivity to ethylbenzene during the exothermic alkylation of

benzene with ethene decreases. This behavior can be expected from endothermic and exothermic reactions, respectively. At low temperatures, ethene reacts preferably with benzene and nearly no byproducts are observed.

This behavior was also observed during own experiments conducted with mixtures of ethane and propane. The benzene conversion in [90] also increases with temperature, despite the alkylation being exothermic at -113 kJ · mol^{-1} for the reaction of ethene [75]. Since the dehydrogenation is highly endothermic ranging from 137 kJ · mol^{-1} for ethane and 123 kJ · mol^{-1} for propane down to 113 for higher alkanes [64] the overall dehydroalkylation is endothermic. The high selectivity towards ethylbenzene decreases with increased temperature due to the increased formation of byproducts like toluene and propylbenzenes in [90], which is also true for primary products in Table 24. Also Wong reports that higher temperature leads to higher concentrations of ethene which are responsible for polyalkylated byproducts as well as deactivation of the catalyst through coking (cf. previous chapter). Coke forms from oligomerized alkenes which form polyaromatics and then coke [90,93]. Wong *et al.* state that the optimal temperature for the dehydroalkylation of benzene with ethane is around 370 °C for high selectivity to ethylbenzene and conversion. Yet, for optimization of the $RON_{(l)}$, selectivity is not as important as conversion. Since the in [90] "unwanted" byproducts also have high blending RONs for this work these byproducts are not unwanted, because their blending RON is equal to or higher than that of benzene. To maximize the $RON_{(l)}$ the results from Table 24 suggest employing high reaction temperatures, such as 400 °C, and short reaction times, with frequent or even continuous catalyst regeneration. This would allow operating in the initial regime of the reaction where a $RON_{(l)}$ of more than 113 is observed, or $RON_{(l)}$ = 110 at 350 °C. However, the large amounts of methane and the greater requirements to the equipment likely make the easier operation in the regime of long times on stream at a temperature of 350 °C favorable, because the $RON_{(l)}$ is still good with 103 (cf. Table 24) and the main side products are butanes instead of methane at higher temperatures, which also can be separated comfortably and are generally more useful than methane is.

7.6 Investigations of the *n*-/*iso*-Ratio of Propylbenzene during Dehydroalkylation

The NPB/IPB ratio during the dehydroalkylation of benzene with ethane and propane was of particular interest for a participating project partner. The NPB/IPB ratio is not of great importance for the use as fuel components, since the blending RONs are so similar (127 & 132) and conversion into either from benzene (blending RON = 99) is highly beneficial to the $RON_{(l)}$. For the application in the chemical industry, the selectivity to IPB is of more interest, since IPB is a more coveted bulk chemical than NPB.

In the last chapter the influence of the reaction temperature during dehydroalkylation was discussed. In Fig. 32 it can be seen that the reaction temperature also greatly influences the initial NPB/IPB ratio. With increasing temperature more NPB is produced at the beginning of the reaction. The NPB/IPB ratio is linked to the benzene conversion which can be seen when comparing Fig. 32 with Fig. 30 from the last chapter. The higher the benzene conversion is, the higher the initial NPB/IPB ratio in the product distribution. With increasing time on stream - after ~1 day - the ZSM-5-based catalyst produces a mixture with similar NPB/IPB ratios of ~1.5 throughout the temperature range of 300 - 400 °C. The great difference in the initial NPB/IPB ratios most likely results from the further reaction of produced IPB to NPB, since the catalyst's sites active in hydrogenolysis are very active at higher temperatures and deactivate fast (cf. 7.4 Time on Stream Behavior and Regeneration of the Catalyst). These are responsible for the further reaction of formed IPB to NPB [93]. This temperature dependency of the NPB/IPB ratio is also observed during the industrial transalkylation of polyalkylated aromatics recycled back into the process of IPB production [127].

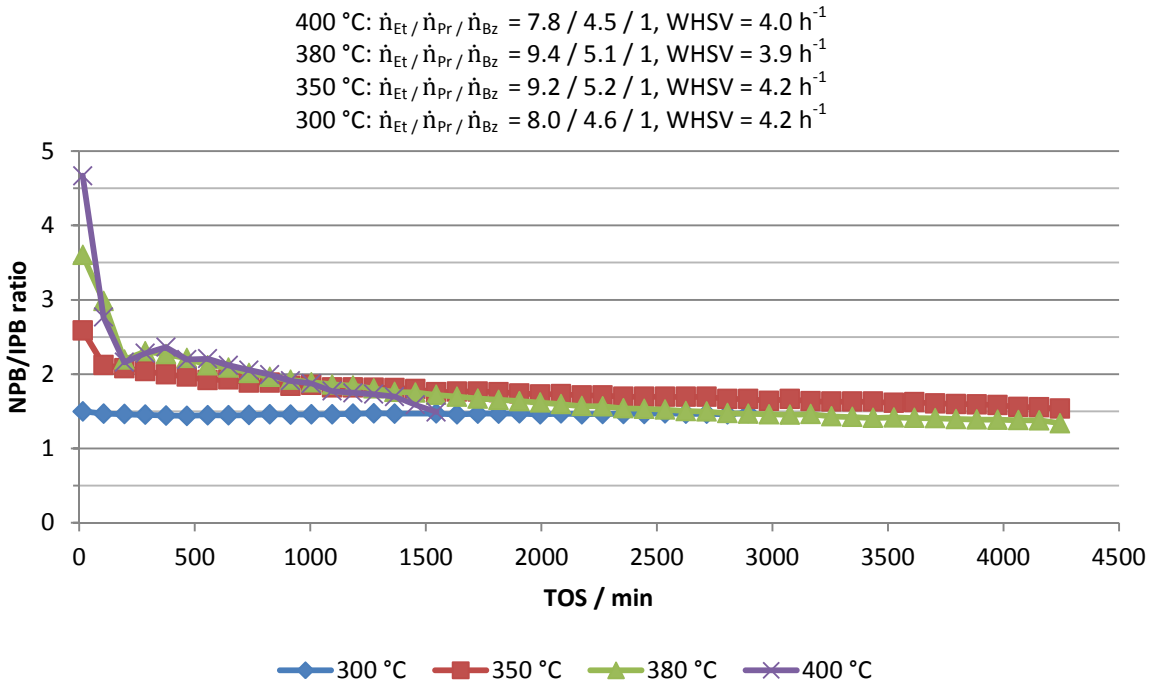

Fig. 32: NPB/IPB ratios during dehydroalkylation over 1.9Pt-H-ZSM-5(35), p = 0.63-0.65 MPa, at different reaction temperatures in membrane reactor.

The group of J. van Bokhoven presents in [84] results, which indicate the NPB/IPB ratio depends on the reactant used for the alkylation/dehydroalkylation. When alkylating benzene with an olefin instead of an alkane, only branched alkylbenzenes were observed as products and no terminal alkylbenzene. This can partly be explained by the milder reaction conditions employed during the alkylation with olefins. The reaction was carried out at 205 °C [84]. A monomolecular activation from the used alkane to the corresponding olefin was not observed at that temperature. An activation of the alkane via adsorbed aromatic carbenium ions is hypothesized [84]. The absence of terminal alkylbenzene is attributed to the instability of the primary carbenium ion required for terminal alkylation. An isomerization from branched to terminal alkylbenzene in the presence of neat benzene, as described in [82], is not observed, which speaks against the reaction shown in Fig. 15 on page 38. Transalkylation was not observed in the reaction of 2- and 3-phenylhexane together with benzene over an acidic H-ZSM-5 catalyst, since no 1-phenylhexane was formed [84]. This behavior is attributed by van Bokhoven to the small pore size of ZSM-5. With larger pore sizes, such as mordenite or zeolite Y, higher amounts of bulkier products were observed. For the dehydroalkylation of benzene with an alkane such as *n*-hexane, it is reported that 1-phenylhexane is formed in significant amounts, contrary to the alkylation with 1-, 2-, or 3-hexene [84].

These results from van Bokhoven suggest the alkylation with either alkane or olefin proceed via different mechanisms. The alkylation with an olefin is supposed to proceed via a carbenium ion. To form a carbenium ion from an alkane protonation and then dehydrogenation is required. If this was simply the case v. Bokhoven would not have detected 1-phenylhexane during dehydroalkylation and none during alkylation with an olefin. This stands in contrast to the suggestions that during the dehydroalkylation of benzene with propane NPB is formed via IPB and further isomerization/transalkylation [82] or that propylbenzenes react to methane & EB or toluene & ethane [86]. Danilina *et al.* have tested for this isomerization/transalkylation under their reaction conditions and found no products expected by these processes [84]. During own experiments with alkanes all of these products are regularly observed. Results from Wong *et al.* [90], where the dehydroalkylation of benzene with ethane to EB is discussed, also suggest that dehydroalkylation with alkanes proceed via two consecutive steps of dehydrogenation and subsequent alkylation. However, van Bokhoven also reports elsewhere [85], during the dehydroalkylation of benzene with *n*-hexane over a bifunctional ZSM-5 catalyst, a selectivity to 2-phenylhexane of up to 89 % at *n*-hexane conversion of 25 % (benzene/*n*-hexane ratio = 1, T = 210 °C, 16-27 h in batch setup). This means, that hardly any 1- or 3-phenylhexane is observed, and that the isomerization of the 2-phenylhexane main product does not seem to occur. Zeolite ZSM-5 therefore possesses pores large enough for IPB. An effect of the space offered by the pore system on the NPB/IPB ratio can however be seen when comparing zeolites with different pore sizes (cf. 7.7 Dehydroalkylation over different Pore Systems), as shown in Fig. 33.

In Fig. 33 it can be seen, that the NPB/IPB ratios are greatly influenced by the choice of the pore system of the parent zeolite. The medium-pore zeolite ZSM-5 with pores accessible through 10-MR offers the least space, while zeolite MCM-22 has large cavities, which are only accessible through 10-MR openings, though. Large-pore zeolite Beta offers the most space and its pores are accessible via 12 MR openings, therefore the highest amounts of the bulkier propylbenzene IPB can be observed over the zeolite Beta catalyst. As described above, over ZSM-5-based catalysts the initial NPB/IPB ratio can vary, but ends up at similar values ~1.5 after enough time on stream for the hydrogenolysis sites to deactivate. With a MCM-22 catalyst, the amounts of NPB and IPB equilibrate at almost the same value, leading to an NPB/IPB ratio of 1. Only over a zeolite Beta catalyst an excess of IPB over NPB is observed, yielding an NPB/IPB ratio average of 0.5 with values as low as 0.3.

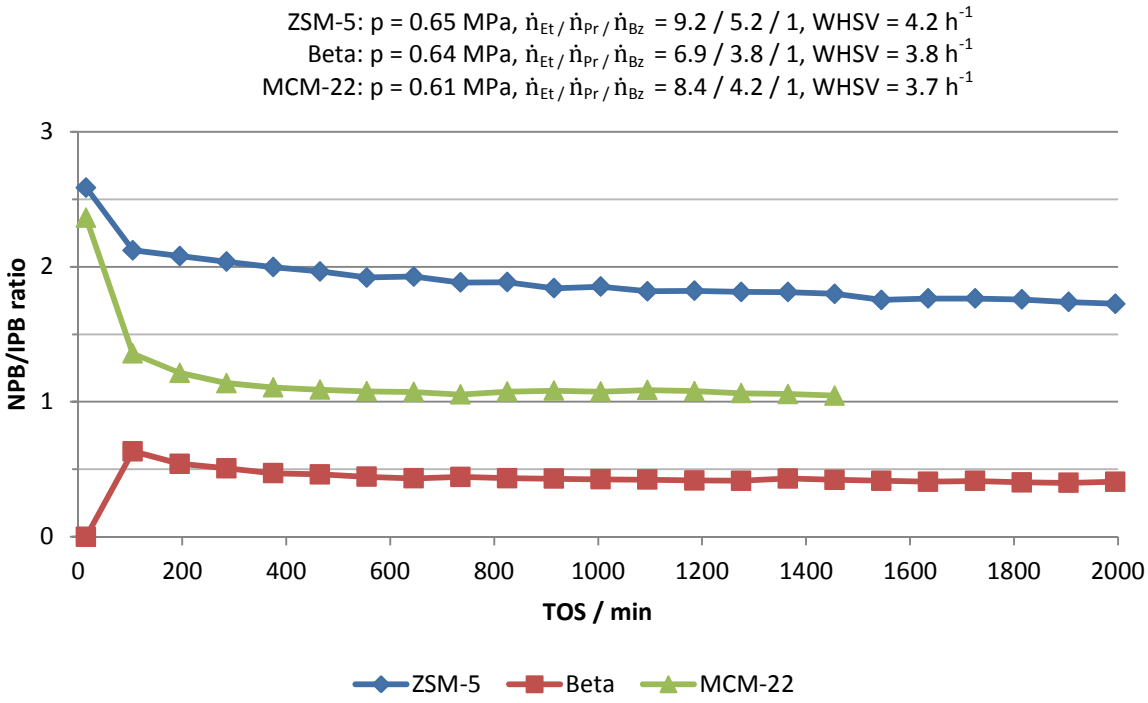

Fig. 33: NPB/IPB ratios during dehydroalkylation over catalysts with different zeolite structures at T = 350 °C in membrane reactor.

The results reported in [84] cannot be ignored. The missing terminal alkylaromatics expected from isomerization might be explained by the mild temperature used (205°C), although isomerization is reported to begin at 200°C [82]. But the reported absence of activation from *n*-hexane to hexenes also stands in contrast to own results obtained with propane at these temperatures. Also, the activation of hexane should be easier than that of propane, thus, requiring even lower temperatures for activation. This is suggested to arise from the absence of benzene in van Bokhoven's test reaction, who tests for monomolecular activation of the alkane [84]. It is suggested that the presence of benzene together with the bifunctional catalyst aids the activation of *n*-hexane. This might favor a reaction mechanism that leads directly to a terminal alkylaromatic product. If this is the case, then the own results where the even harder activation of propane is observed at 200 °C (although only in very small or negligible amounts) can be explained by the aid of the admittedly low amount of benzene. However, at temperatures of 350 °C the activation of a mixture of ethane and propane without benzene was very well observed. The influence of the reactant being an alkane or alkene on the NPB/IPB ratio is therefore indeed debatable. If the alkylation with an alkene, and the dehydroalkylation of benzene with an alkane proceed via different mechanisms, and not via the consecutive steps of dehydrogenation and alkylation, the

NPB/IPB ratio could be controlled more easily. If the latter is the case, then choosing alkane as reactant limits the entire dehydroalkylation to the reaction rate of the dehydrogenation, which in turn results in an ordinary alkylation with a constantly low olefin concentration and fast subsequent equilibrium reactions.

Alotaibi *et al.* have shown that with a two-step dehydrogenation of benzene with propane over two different catalysts in separated beds can be highly selective to IPB [92]. The selectivity is attributed to the spatial constraints e.g. a zeolite provides. Those catalysts with large pores which provide much space produce more IPB, and those with small pores produce mainly NPB, EB and toluene (cf. Table 27 in 7.7.3 Comparison of Catalysts with different Pore Systems). In conclusion it can be stated, that the direct dehydroalkylation of benzene with a mixture of ethane and propane over a bifunctional zeolite catalyst is ill-suited for the selective production of a specific compound, such as IPB. A two-step approach with a dehydrogenation and subsequently an alkylation is much more advisable. For the production of fuel components the direct dehydroalkylation is eligible, since selectivity is of less importance, and benzene conversion is what matters most for the $RON_{(l)}$. However, for the selective production of a specific compound, the alkylation of benzene with the corresponding olefin (propene for IPB) is most preferable, if an alkane is not required as reactant. The increased cost of using propene as alkylating agent compared to propane is compensated by the simpler methods required for the separation of the product mixture. The lower reaction temperature and noble metal-free catalyst is easier to handle. The lower amount of waste production, which requires recycling into the product stream, e.g. polyalkylated benzene, is a clear advantage of alkylation with olefins over dehydroalkylation with alkanes. When an extensive purification of the obtained liquid phase is not required, as for the use as fuel, dehydroalkylation is an alternative, since the cheap and abundant alkanes can be used in lieu of the more expensive olefins. The *n*-/*iso* ratio of propylbenzenes simply has too little impact on the $RON_{(l)}$ to matter.

7.7 Dehydroalkylation over different Pore Systems

7.7.1 Benzene Dehydroalkylation over MCM-22

In search of a more suitable catalyst for the dehydroalkylation of benzene, other supports than zeolite ZSM-5 have been modified in a similar fashion. The dehydroalkylation of benzene with ethane and propane was conducted with a sample of zeolite 2.2Pt-H-MCM-22(21) in the membrane reactor. The obtained results have been compared to results from Kato *et al.* (see Table 25). Kato *et al.* have studied the dehydroalkylation of benzene with ethane over a platinum-loaded catalyst [128] with zeolite H-MCM-22 as support. It should be noted that the catalyst used by Kato *et al.* has a significantly higher Pt loading of 6.8 wt.-%. Also the dehydroalkylation is conducted at a higher temperature of 500 °C. Kato reports high amounts of ethene in the product stream, which is most likely caused by the high Pt content in the catalyst together with the high temperature. Both factors, high temperature and Pt content, favor the dehydrogenation of ethane. As with Pd-H-ZSM-5 (cf. 7.2.1 Influence of the Reactants), the dehydroalkylation of benzene with only ethane is far more selective than in combination with propane. Apart from ethene, the only other products reported are ethylbenzene and a small amount of styrene, which is produced by dehydrogenation of EB.

The compared results from own investigations (Fig. 34) with additional propane are conducted at 350 °C. Here, the dehydroalkylation shows as with ZSM-5 based catalysts an initially high benzene conversion (Table 25, left column), which decreased over TOS. This is accompanied by a very high selectivity to methane of 77 % in the beginning, which decreases over 24 hours to still 54 % (Table 25, middle column). This corresponds to 17 wt.-% of the product mass being unwanted methane, which means methane is the major byproduct. Minor byproducts (butanes and pentanes) are produced from e.g. oligomerization or disproportionation, and increase with time on stream from initially 10 % to ~20%. This results in an amount of alkylaromatic compounds of ~25 % (~50 wt.-%) in the products over the MCM-22 based catalyst. The composition of these alkylaromatics is slightly different however, compared to zeolite ZSM-5 catalysts. The product distribution shows higher selectivity to propylbenzenes, and a lower selectivity to ethylbenzene. Overall, the zeolite MCM-22 catalyst at long times on stream produces mainly methane and primary products, and propylbenzenes more than EB. The large amounts of methane at long times on stream mean MCM-22 retains a large portion of its hydrogenolysis ability, although a shift of alkyl-

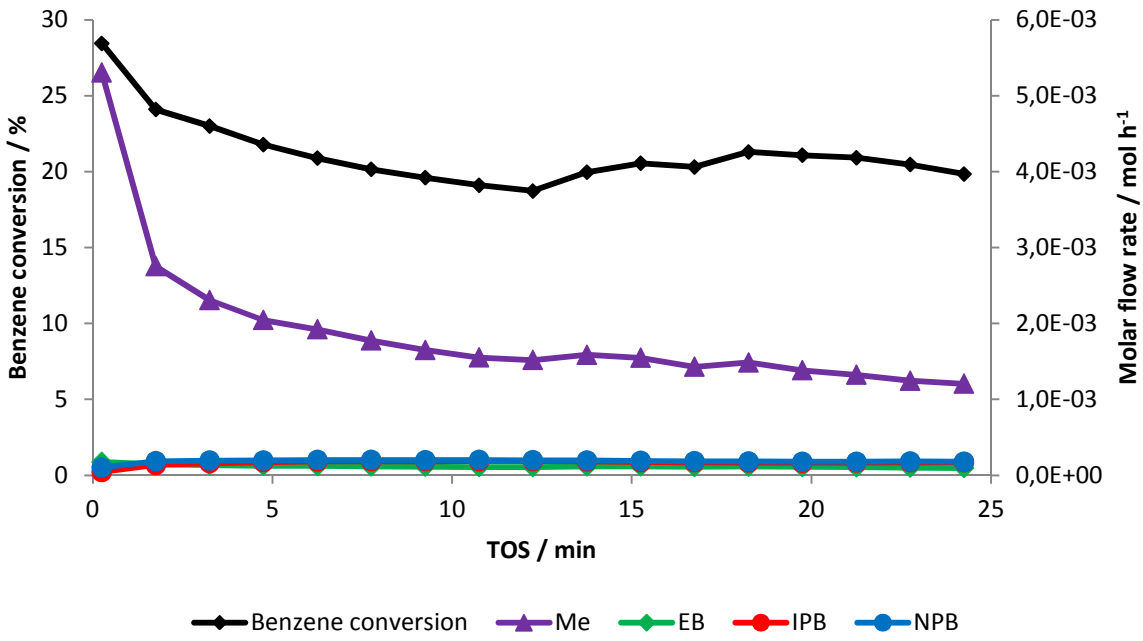

Fig. 34: Dehydroalkylation over 2.2Pt-H-MCM-22(21) at T = 350 °C, p = 0.61 MPa, $\dot{n}_{Et}$ / $\dot{n}_{Pr}$ / $\dot{n}_{Bz}$ = 8.4 / 4.2 / 1, WHSV = 3.7h^{-1} in membrane reactor.

Table 25: Dehydroalkylation of benzene over MCM-22.

Catalyst	**2.2Pt-H-MCM-22(21)**	**2.2Pt-H-MCM-22(21)**	**6.8Pt-H-MCM-22(12.5) [128]**
Reactor type	membrane	membrane	fixed-bed
Temperature / °C	350	350	500
Pressure / MPa	0.61	0.61	atmospheric
$\dot{n}_{Et}$ / $\dot{n}_{Pr}$ / $\dot{n}_{Benzene}$	8.4 / 4.2 / 1	8.4 / 4.2 / 1	5 / 0 / 1
WHSV / h^{-1}	3.7	3.7	4.6
Time on stream / min	15	1455	30
Benzene conversion / %	28.4	19.8	63
$RON_{(l)}$	107	104	124
Product distribution[a] / Mol-%			
Methane	77.0	53.8	[b]
Ethene	[d]	[d]	84.9[c]
i-Butane	3.9	3.8	[b]
n-Butane	5.0	13.7	[b]
i-Pentane	0.8	[d]	[b]
n-Pentane	0.3	2.3	[b]
Toluene	6.1	5.0	[b]
Ethylbenzene	2.5	4.3	14.1[c]
Styrene	[d]	[d]	1.0[c]
Xylenes	2.2	1.6	[b]
i-Propylbenzene	0.6	7.6	[b]
n-Propylbenzene	1.5	8.0	[b]
***n*-/*iso* ratio**	**2.36**	**1.05**	

[a] without H_2, [b] not reported, [c] calculated from reported yield, [d] not detected,

aromatics from secondary to primary products is observed, as with ZSM-5 catalysts. A possible explanation for the ongoing high methane production could be the presence of larger Pt-clusters in the half-cavities on the outer surface of zeolite MCM-22. Another explanation could be the increased space MCM-22 offers promotes methane production, since a high selectivity to methane at long times on stream is observed especially over catalysts with larger pores (see the next two chapters).

The alkylation of benzene with ethene or propene has been studied by Corma *et al.* [81]. Over acidic zeolite MCM-22, alkylation occurs already at temperatures of 180-220 °C. At these low temperatures, NPB/IPB ratios below 1 % have been reported by Corma. The thermodynamically favored NPB is hardly produced at all. The kinetically favored IPB is produced from a more stable secondary carbenium ion and benzene. According to Corma *et al.*, the alkylation follows an Eley-Rideal mechanism where benzene reacts with an adsorbed propenium ion. Benzene and propene compete over the acidic sites, but the benzene coverage is very low. Corma *et al.* also report a faster deactivation rate of the used catalysts with higher n_{Si}/n_{Al} ratio during the alkylation with propene. This behavior is attributed to the greater strength of the acidic sites. The carbenium ions are supposedly longer adsorbed and thus have more time to oligomerize. This results in more coke formation and faster deactivation.

The alkylation of benzene with the more expensive propene is much more selective and therefore superior to the dehydroalkylation with propane. This is because of the lower temperature requirement, that allows a selective reaction via a secondary carbenium ion to achieve a high selectivity to IPB. For the production of chemical commodities, the dehydroalkylation over Pt-H-MCM-22 is impractical. The products need extensive separation and purification. Also large amounts of methane are produced. The application as fuel components upgrading catalyst does not require such extensive purification of the product as with the use as bulk chemical. The produced methane can be separated relatively easy and reused or burnt to produce energy for the endothermic reaction.

7.7.2 Benzene Dehydroalkylation over Zeolite Beta

During the dehydroalkylation over platinum-loaded zeolite Beta, a stable benzene conversion (see Fig. 35) together with a high selectivity to primary products (see Table 26) was observed. Yet, the higher selectivity to propylbenzenes comes together with a lower activity. With longer times on stream of approximately one day, the product distribution changed from initially high selectivity to toluene among the alkylaromatics, along with very high selectivity to methane (>60 %) to increased formation of primary alkylation products over time. This change in the product distribution is observed during the first few hours on stream. The low benzene conversion has the benefit of producing no oligomerization products after nearly 24 hours on stream. This makes zeolite Beta based catalysts very selective for the production of primary products, with only methane as side product, no secondary alkylation products, and the primary product fraction consisting mostly of IPB. The decline in toluene concentration is exceptionally fast. This is attributed to the fast deactivation of "hydrogenolysis sites" [93] and zeolite Beta being more prone to their deactivation, due to offering more space for the formation of coke. Since these sites deactivate first, the change in the product distribution with zeolite Beta is also faster than with catalysts that coke slower. However, as with zeolite MCM-22 the production of methane continues to be very high at long times on stream compared to ZSM-5 catalysts (cf. Table 27 in 7.7.3 Comparison of Catalysts with different Pore Systems). Although these sites deactivate fast, the benzene conversion is stable in the range of 8-10 % over the course of two days. The side products that are produced via oligomerization, e.g. butanes, decline much slower and are detectable for up to 23 h on stream. Methane remains a constant byproduct, although the amount of produced methane decreases over time to 23 % (77 % propylbenzene, NPB/IPB ratio = 0.3, X_{benzene} = 8 %, $\text{RON}_{(l)}$ = 101, ~120 h on stream).

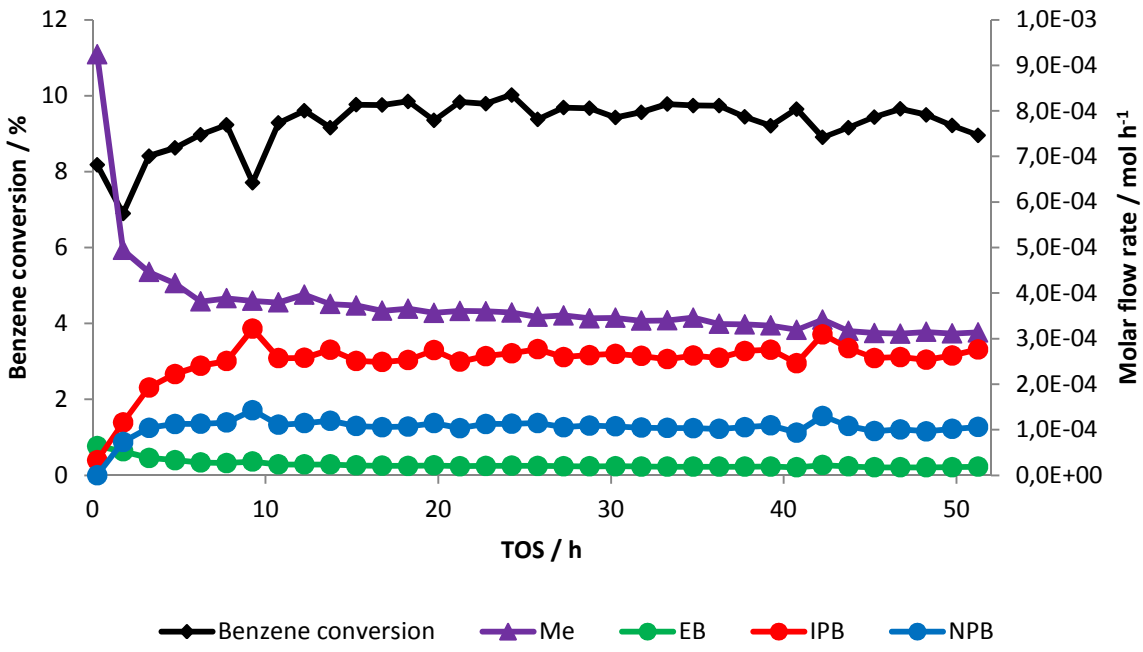

Fig. 35: Dehydroalkylation over 2.1Pt-H-Beta(24) at T = 350 °C, p = 0.64 MPa, $\dot{n}_{Et}$ / $\dot{n}_{Pr}$ / $\dot{n}_{Bz}$ = 6.9 / 3.8 / 1, WHSV = 3.8h^{-1} in membrane reactor.

Table 26: Product distribution of Dehydroalkylation over 2.1Pt-H-Beta(24) at T = 350 °C, p = 0.64 MPa, $\dot{n}_{Et}$ / $\dot{n}_{Pr}$ / $\dot{n}_{Bz}$ = 6.9 : 3.8 : 1, WHSV = 3.8h^{-1} at different times on stream in membrane reactor.

Time on stream / min	**15**	**105**	**4425**
Benzene conversion / %	8.2	6.9	9.8
$RON_{(l)}$	101	101	102
Product distribution[a] / Mol-%			
Methane	65.6	60.0	46.9
i-Butane	5.4	[b]	[b]
n-Butane	7.4	6.3	[b]
i-Pentane	[b]	[b]	[b]
n-Pentane	[b]	[b]	[b]
Toluene	14.7	4.5	[b]
Ethylbenzene	4.5	6.4	2.4
Xylenes	[b]	[b]	[b]
i-Propylbenzene	2.3	14.0	37.4
n-Propylbenzene	[b]	8.9	13.3
***n-/iso* ratio**	**0**	**0.63**	**0.36**

[a] without H_2, [b] not detected

7.7.3 Comparison of Catalysts with different Pore Systems

Since the quality of a catalyst can be determined by its activity during the dehydroalkylation of benzene together with the blending RON of the product phase, it can be concluded that the zeolites ZSM-5 and MCM-22 are on par in respect of conversion and resulting blending RON (see Fig. 36 and Table 27). Zeolite Beta shows better selectivity with regard to primary products. In fact, the only non-primary product is methane, while mainly propylbenzenes are produced, especially IPB. However, Zeolite Beta does not match the other two pore systems in terms of conversion and blending RON. Zeolites ZSM-5 and MCM-22 are comparable in conversion and $RON_{(l)}$, however, their respective product distributions show significant differences. Over the MCM-22 catalyst, less butane is produced than over ZSM-5. This advantage is offset by an increased formation of methane. This indicates that MCM-22 is more active in the side reactions that lead to cracking products than ZSM-5, which in turn favors more the oligomerization of alkenes. Therefore, higher amounts of methane can be observed over MCM-22, while higher alkanes are formed in larger quantities over ZSM-5.

The comparison of different pore systems shows that larger pore systems, which offer more space for the reacting components, produce a lower NPB/IPB ratio than more confined ones after one day on stream. The dehydroalkylation over zeolite Beta shows much lower benzene conversion and thus, also lower blending RON than over ZSM-5 or MCM-22. Yet, the selectivity to primary products is far higher than with the zeolites ZSM-5 and MCM-22. This selectivity to primary products continues to improve for 9 hours on stream. Furthermore, with the exception of methane, only primary products are produced.

The confined 10-MR zeolite ZSM-5 (total surface area S_{Tot} = 366 m²/g, $\Sigma n_{SiOHAl}+n_{SiOH}$ = 0.42 mmol/g [129]) produces the highest *n*-/*iso* ratio, while the spacious zeolite Beta (12-MR pores, S_{Tot} = 668 m²/g, $\Sigma n_{SiOHAl}+n_{SiOH}$ = 1.12 mmol/g [129]) produces the lowest. Zeolite MCM-22 (S_{Tot} = 441 m²/g, $\Sigma n_{SiOHAl}+n_{SiOH}$ = 0.79 mmol/g [129]) with its large cavities lies in between the former two, since the large cavities, which in principle offer the most space of these three pore systems, are accessible only via 10-MR windows. In the case of ZSM-5, more NPB than IPB is observed, while with MCM-22 both isomers are produced in approximately equal amounts.

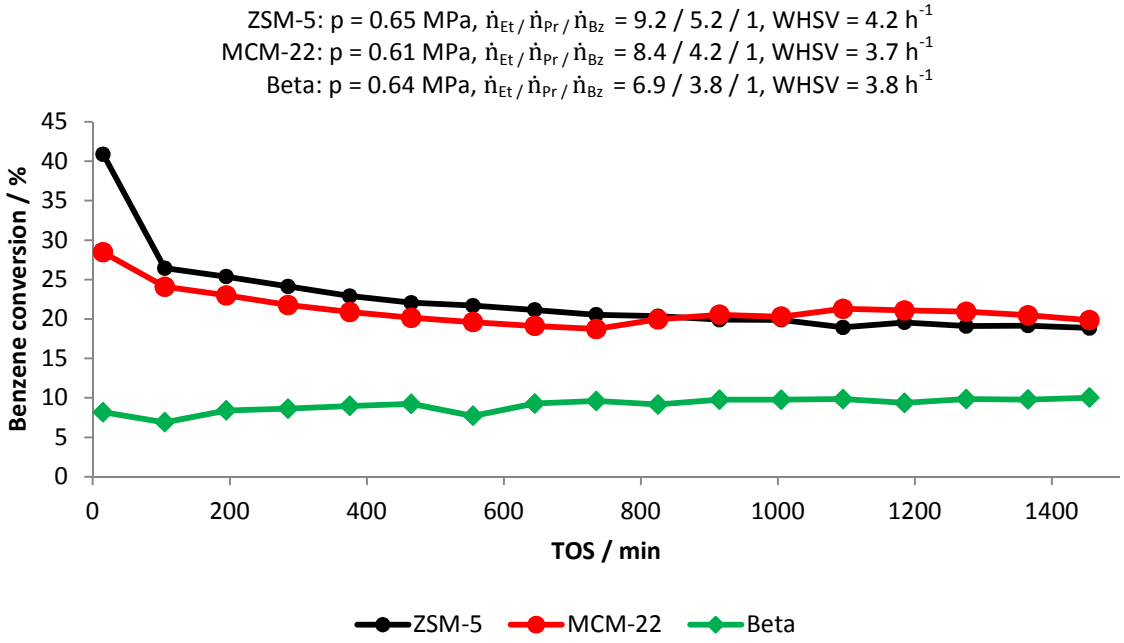

Fig. 36: Benzene conversions of the dehydroalkylation over catalysts with different pore systems at T = 350 °C for one day on stream in membrane reactor.

Table 27: Comparison of the dehydroalkylation over zeolites ZSM-5, MCM-22 and Beta.

Catalyst	**1.9Pt-H-ZSM-5(35)**	**2.2Pt-H-MCM-22(21)**	**2.1Pt-H-Beta(24)**
S_{Tot} / $m^2 \cdot g^{-1}$	366	441	668
Reactor type	membrane	membrane	membrane
Temperature / °C	350	350	350
Pressure / MPa	0.65	0.61	0.64
$\dot{n}_{Et}$ / $\dot{n}_{Pr}$ / $\dot{n}_{Benzene}$	9.2 / 5.2 / 1	8.4 / 4.2 / 1	6.9 / 3.8 / 1
WHSV / h^{-1}	4.2	3.7	3.8
Time on stream / min	1455	1455	1455
Benzene conversion / %	18.9	19.8	10.0
$RON_{(l)}$	104	104	102
Product distribution[a] / Mol-%			
Methane	19.7	53.8	47.1
i-Butane	11.9	3.8	[b]
n-Butane	33.7	13.7	[b]
i-Pentane	2.2	[b]	[b]
n-Pentane	2.7	2.3	[b]
Toluene	5.8	5.0	[b]
Ethylbenzene	9.3	4.3	2.7
Xylenes	1.5	1.6	[b]
i-Propylbenzene	4.7	7.6	35.3
n-Propylbenzene	8.5	8.0	14.9
***n-/iso* ratio**	**1.81**	**1.05**	**0.42**

[a] without H_2, [b] not detected

Zeolite Beta favors IPB over NPB. This trend following pore size and surface area is consistent considering the higher sterical requirement IPB has. More constraint catalyst produce more NPB [92]. The selectivity to primary alkylation products also follows this trend, while the benzene conversion decreases. The formation of methane does not follow this trend in pore size. The formation of methane is most prominent over MCM-22, and lowest over ZSM-5. The activity for hydrogenolysis is therefore higher over zeolite MCM-22 and zeolite Beta than over zeolite ZSM-5.

The zeolites MCM-22 and ZSM-5 clearly show deactivation behavior, while the conversion over zeolite Beta is stable. When analyzing the coke content over these catalysts, ZSM-5 shows the lowest carbon content (5.6 wt.-%), while MCM-22 (16.4 wt.-%) and Beta (15.8 wt.-%) show similar and significantly higher amounts of carbonaceous deposits after their respective experiments. It is therefore clear that zeolite Beta indeed deactivates in a way, that changes the product distribution over time, while maintaining a stable benzene conversion. (cf. Table 23 in chapter 7.4 Time on Stream Behavior and Regeneration of the Catalyst)

Since the ZSM-5 catalyst and the MCM-22 catalyst are on par considering benzene conversion and $RON_{(l)}$ but the ZSM-5 catalyst produces less methane, the ZSM-5 catalyst's performance during the dehydroalkylation can be considered best among the three catalysts used. The main side product butane is more welcome than the other non-liquid side products. The NPB/IPB ratio, however, is worst among the used zeolite types, but for use as fuel component the NPB/IPB ratio is of little importance (cf. 7.6 Investigations of the *n*-/*iso*-Ratio of Propylbenzene during Dehydroalkylation). It remains to be investigated, if the NPB/IPB ratio during the dehydroalkylation over zeolite MCM-22 increases with higher temperatures as over zeolite ZSM-5 [127].

If the use as fuel component with a high $RON_{(l)}$ is not intended, but the production of IPB via dehydroalkylation, then the use of zeolite Beta might be practical. The amount of methane is considerable, but can be separated easily from the product stream along with ethane/propane, and recycled to an aromatization unit. The NPB/IPB ratio over zeolite Beta is the lowest achieved in this work.

8 References

[1] D. Wan Hussin, Y. Traa, *Energy & Fuels*, **2014**, 28, 3352-3356, DOI: 10.1021/ef500333b.

[2] D. Wan Hussin, Y. Traa in "Small-Scale Gas to Liquid Fuel Synthesis", chapter 13 "Production of High-Octane Fuel Components by Dehydroalkylation of Benzene with Mixtures of Ethane and Propane", CRC Press, Boca Raton, **2015**, ISBN 1466599383.

[3] Y. Traa and D. Wan Hussin: "Production of High-Octane Fuel Components by Alkylation of Benzene with Mixtures of Ethane and Propane", 21st World Petroleum Congress Pre-print Proceedings, World Petroleum Council, **2014**, Forum 13.

[4] Y. Liu, W. B. Whitman, *Ann. N.Y. Acad. Sci.*, **2008**, 1125, p. 180, DOI: 10.1196/annals.1419.019.

[5] G. Hammer, T. Lübcke, R. Kettner, M. R. Pillarella, H. Recknagel, A. Commichau, H.-J. Neumann, B. Paczynska-Lahme in: Ullmann's Encyclopedia of Industrial Chemistry, vol. 23, chapter "Natural Gas", Wiley-VCH, Weinheim, **2012**, p. 739, DOI: 10.1002/14356007.a17_073.pub2.

[6] H. Andruleit, A. Bahr, H. G. Babies, M. Blumenberg, G. Mayer, J. Meßner, M. Pein, D. Rebscher, M. Schauer, S. Schmidt. P. Schulz, G. von Goeme, M. Winchenbach in: „*Energy Study 2015: Reserves, Resources and Availability of Energy Resources*", BGR, Hannover, **2015**.

[7] R. K. Flad, „Salt Production and Social Hierarchy in Ancient China", Cambridge University Press, New York, 2011, p. 39, ISBN 978-1-107-00941-7.

[8] R. D. Vidic, S. L. Brantley, J. M. Vandenbossche, D. Yoxtheimer, J. D. Abad, *Science*, **2013**, 340, 6134, DOI: 10.1126/science.1235009.

[9] R. A. Field, J. Soltis, S. Murphy, *Environ. Sci: Processes Impacts*, **2014**, 16, 954-969, DOI: 10.1039/c4em00081a.

[10] P. Budzik, K. Teller in: „Annual Energy Outlook 2014", U.S. Energy Information Administration, **2014** (http://www.eia.gov/forecasts/aeo/pdf/0383(2014).pdf).

[11] F.-Y. Liang, M. Ryvak, S. Sayeed, N. Zhao, *Chemistry Central Journal*, **2012**, 6(Suppl 1):S4, DOI: 10.1186/1752-153X-6-S1-S4.

[12] S. Thomas, R. A. Dawe, *Energy*, **2003**, 28, 1461-1477, DOI: 10.1016/S0360-5442(03)00124-5.

[13] R. Ghofrani, C. Marx in: "Landolt-Börnstein Group VIII Advanced Materials and Technologies Fossil Energy", vol. 3A, chapter "Natural gas exploitation technologies", Springer, **2002**, 40-88, DOI: 10.1007/b71804.

[14] B. Cramer, H. Andruleit, H. Rempel, H.-G. Babies in: *„Energy Resources 2009: Reserves, Resources, Availability"*, BGR, Hannover, **2009**, p. 49, ISBN 978-3-9813373-9-6.

[15] H.-G. Behrendt, *Erdöl Erdgas Kohle*, **2000**, 116, 58-62.

[16] M. Uken, *Spiegel Online*, 04 Jan. 2010, Press article 668826.

[17] M.-F. Chabrelie in „2007 Survey of Energy Resources", chapter „Natural Gas", World Energy Council, **2007**, 145-169, ISBN: 0 946121 26 5.

[18] BP Statistical Review of World Energy, June 2016, accessed via www.bp.com (14.03.2017).

[19] *Spiegel Online*, 12 Mar. 2013, Press Article 888348.

[20] Y. F. Makogon, *Journal of Natural Gas Science and Engineering*, **2010**, 2, 49-59, DOI: 10.1016/j.jngse.2009.12.004.

[21] N.-J. Kim, J. H. Lee, Y. S. Cho, W. Chun, *Energy*, **2010**, 35, 2717-2722, DOI: 10.1016/j.energy.2009.07.020.

[22] J. Javanmardi, Kh. Nasrifar, S. H. Najibi, M. Moshfeghian, *Applied Thermal Engineering*, 2005, 25, 1708-1723, DOI: 10.1016/j.applthermaleng.2004.10.009

[23] http://www.ngvjournal.com/worldwide-ngv-statistics/ (30.06.2014).

[24] C. Hammond, M. M. Forde, M. H. Ab Rahim, A. Thetford, Q. He, R. L. Jenkins, N. Dimitratos, J. A. Lopez-Sanchez, N. F. Dummer, D. M. Murphy, A. F. Carley, S. H. Taylor, D. J. Willock, E. E. Stangland, J. Kang, H. Hagen, C. J. Kiely, G. J.

Hutchings, *Angew. Chem. Int. Ed.*, **2012**, 51, 5129 –5133, DOI: 10.1002/anie.201108706.

[25] B. G. Hashiguchi, M. M. Konnick, S.M. Bischof, S. J. Gustafson, D. Devarajan, N. Gunsalus, D. H. Ess, R. A. Periana, *Science*, **2014**, 343, 1232-1237, DOI: 10.1126/science.1249357.

[26] A. P. E. York, T.-C. Xiao, M. L. H. Green, J. B. Claridge, *Catal. Rev.: Sci. Eng.*, **2007**, 49, 511-560, DOI: 10.1080/01614940701583315.

[27] C. Perego, R. Bortolo, R. Zennaro, *Catalysis Today*, **2009**, 142, 9-16, DOI: 10.1016/j.cattod.2009.01.006.

[28] F. Fischer, H. Tropsch, *Ber. deutsch. Chem. Ges. A/B*, **1926**, 59, 830-831, DOI: 10.1002/cber.19260590442.

[29] M. E. Dry in: „Handbook of Heterogeneous Catalysis“, chapter „The Fischer-Tropsch (FT) Synthesis Processes“, 2nd Ed., G. Ertl, H. Knözinger, F. Schüth, J. Weitkamp (Eds.), Vol. 6, Wiley-VCH, Weinheim, **2008**, p. 2965.

[30] D. J. Wilhelm, D. R. Simbeck, A. D. Karp, R. L. Dickenson, *Fuel Process. Technol.*, **2001**, 71, 139-148, DOI: 10.1016/S0378-3820(01)00140-0.

[31] K. Aasberg-Petersen, T. S. Christensen, C. S. Nielsen, I. Dybkjær, *Fuel Process. Technol.*, **2003**, 83, 253-261, DOI: 10.1016/S0378-3820(03)00073-0.

[32] T. J. Remans, G. Jenzer, A. Hoek in: „Handbook of Heterogeneous Catalysis“, chapter „Gas-to-Liquids“, 2nd Ed., G. Ertl, H. Knözinger, F. Schüth, J. Weitkamp (Eds.), Vol. 6, Wiley-VCH, Weinheim, **2008**, p. 2994.

[33] H. O. Hobbs Jr., L. S. Adair, *Oil & Gas Journal*, 06.08.2012, 110(8), 68-75.

[34] „Innovative Catalytic Technologies & Materials for Next Gas to Liquid Processes“, Annex 1 – Description of the Work, p. 36.

[35] A. F. Cronstedt in „An Essay Towards a System of Mineralogy, Volume 1“, **1756**, translated by G. von Engestrom, 2nd Ed.. J. H. de Magellan (Ed.), Vol. 1, London, **1788**.

[36] A. F. Masters, T. Maschmeyer, *Micropor. Mesopor. Mater.* **2011**, 142, 423‑428, DOI: 10.1016/j.micromeso.2010.12.026.

[37] J. Weitkamp, *Solid State Ionics*, **2000**, 131, 175-188, DOI: 10.1016/S0167-2738(00)00632-9.

[38] W. Loewenstein, *Am. Mineralogist*, **1954**, 39, 92-96.

[39] http://www.iza-structure.org (10.04.2017).

[40] D. S. Coombs, A. Alberti, T. Armbruster, G. Artioli, C. Colella, E. Galli, J. D. Grice, F. Liebau, J. A. Mandarino, H. Minato, E. H. Nickel, E. Passaglia, D. R. Peacor, S. Quartieri, R. Rinaldi, M. Ross, R. A. Sheppard, E. Tillmanns, G. Vezzalini, *Can. Mineral.* **1997**, 35, 1571-1606, ISSN: 00084476.

[41] L. B. McCusker, F. Liebau, G. Engelhardt, *Pure Appl. Chem.*, **2001**, 73, 381-394.

[42] H. Deuel, F. Hostettler, *Experientia*, **1950**, 6(12), 445 - 456 , DOI: 10.1007/BF02154099.

[43] O. Weigel, E. Steinhoff, *Z. Kristallogr.*, **1924**, 61, 125-154, DOI: 10.1524/zkri.1924.61.1.125.

[44] W. Vermeiren, J.-P. Gilson, *Top. Catal*., **2009**, 52, 1131-1161, DOI: 10.1007/s11244-009-9271-8.

[45] E. R. Geus, M. J. den Exter, H. van Bekkum, *J. Chem. Soc., Faraday Trans.*, **1992**, 88, 3101-3109, DOI: 10.1039/FT9928803101.

[46] J. C. Jansen, J. H. Koegler, H. van Bekkum, H. P. A. Calis, C. M. van den Bleek, F. Kapteijn, J. A. Moulijn, E. R. Geus, N. van der Puil, *Micropor. Mesopor. Mater.,* **1998**, 21, 213-226, DOI: 10.1016/S1387-1811(97)00061-9.

[47] W. J. W. Bakker, F. Kapteijn, J. Poppe, J. A. Moulijn, *J. Membr. Sci.*, **1996**, 117, 57-78, DOI: 10.1016/0376-7388(96)00035-X.

[48] U.S. Patent 3702886, 14.11.1972, Mobil Oil Corp. (Inv.: R. J. Argauer, G. R. Landolt).

[49] M. D. Foster, I. Rivin, M. M. J. Treacy, O. Delgado Friedrichs, *Micropor. Mesopor. Mater.,* **2006**, 90, 32-38, DOI: 10.1016/j.micromeso.2005.08.025.

[50] G. T. Kokotailo, S. L. Lawton, D. H. Olson, W. M. Meier, *Nature*, **1978**, 272, 437-438, DOI: 10.1038/272437a0.

[51] E. M. Flanigen, J. M. Bennett, R. W. Grose, J. P. Cohen, R. L. Patton, R. M. Kirchner, J. V. Smith, *Nature*, **1978**, 271, 512-516, DOI: 10.1038/271512a0.

[52] Y.-Q. Deng, W.-F. Zhou, H.-M. Lv, Y.-Y. Zhang, C.-T. Au, S.-F. Yin, *RSC Adv.*, **2014**, 4, 37296-37301, DOI: 10.1039/C4RA04126G.

[53] R. Roque-Malherbe, R. Wendelbo, A. Mifsud, A. Corma, *J. Phys. Chem.*, **1995**, 99, 14064-14071, DOI: 10.1021/j100038a043.

[54] U.S. Patent 3308069, 07.03.1967, Mobil Oil Corp. (Inv.: R. L. Wadlinger, G. T. Kerr, E. J. Rosinski).

[55] A. Corma, M. Moliner, Á. Cantín, M. J. Díaz-Cabañas, J. L. Jordá, D. Zhang, J. Sun, K. Jansson, S. Hovmöller, X. Zou, *Chem. Mater.*, **2008**, 20, 3218–3223, DOI: 10.1021/cm8002244.

[56] D. Santi, *Ph.D. Thesis, University of Stuttgart*, **2012**, p. 15.

[57] M. M. J. Treacy, J. M. Newsam, *Nature*, **1988**, 332, 249-251, DOI: 10.1038/332249a0.

[58] J. C. Jansen, E. J. Creyghton, S. L. Njo, H. van Koningveld, H. van Bekkum, *Catal. Today*, **1997**, 38, 205-212, DOI: 10.1016/S0920-5861(97)00070-9.

[59] M. E. Leonowicz, J. A. Lawton, S. L. Lawton, M. K. Rubin, *Science*, 264, **1994**, 1910-1913.

[60] U.S. Patent 4954325, 04.09.1990, Mobil Oil Corp. (Inv.: M. K. Rubin, P. Chu).

[61] A. Corma, V. Fornes, J. M. Guil, S. Pergher, T. L. M. Maesen, J. G. Buglass, *Micropor. Mesopor. Mater.*, 38, **2000**, 301-309, DOI: 10.1016/S1387-1811(00)00149-9.

[62] Y. Traa in: „Handbook of Heterogeneous Catalysis“, chapter „Non-Oxidative Activation of Alkanes“, 2nd Ed., G. Ertl, H. Knözinger, F. Schüth, J. Weitkamp (Eds.), Vol. 7, Wiley-VCH, Weinheim, **2008**, p. 3194.

[63] J. H. Lunsford, *Catalysis Today*, **2000**, 63, 165-174, DOI: 10.1016/S0920-5861(00)00456-9.

[64] K. J. Caspary, H. Gehrke, M. Heinritz-Adrian, M. Schwefer in: „Handbook of Heterogeneous Catalysis“, chapter „Dehydrogenation of Alkanes“, 2nd Ed., G. Ertl, H. Knözinger, F. Schüth, J. Weitkamp (Eds.), Vol. 7, Wiley-VCH, Weinheim, **2008**, p. 3206.

[65] I. Kley, *Ph.D. Thesis, University of Stuttgart*, **2013**, p. 72.

[66] R. Gounder, E. Iglesia, *Chem. Commun.*, **2013**, 49, 3491-3509, DOI: 10.1039/c3cc40731d.

[67] R. Gounder, E. Iglesia, *J. Am. Chem. Soc.*, **2009**, 131, 1958-1971, DOI: 10.1021/ja808292c.

[68] C. T. O`Connor in: „Handbook of Heterogeneous Catalysis“, chapter „Aromatization of Light Alkanes“, 2nd Ed., G. Ertl, H. Knözinger, F. Schüth, J. Weitkamp (Eds.), Vol. 7, Wiley-VCH, Weinheim, **2008**, p. 3123.

[69] Z. Cao, H. Jiang, H. Luo, S. Baumann, W. A. Meulenberg, J. Assmann, L. Mleczko, Y. Liu, J. Caro, *Angew. Chem. Int. Ed.*, **2013**, 52, 13794-13797, DOI: 10.1002/anie.201307935.

[70] K. S. Wong, J. W. Thybaut, E. Tangstad, M. W. Stöcker, G. B. Marin, *Micropor. Mesopor. Mater.*, **2012**, 164, 302-312, DOI: 10.1016/j.micromeso.2012.07.002.

[71] J. J. Spivey, G. Hutchings, *Chem. Soc. Rev.*, **2014**, 43, 792-803, DOI: 10.1039/c3cs60259a.

[72] G. Caeiro, R. H. Carvalho, X. Wang, M. A. N. D. A. Lemos, F. Lemos, M. Guisnet, F. Ramôa Ribiero, *J. Mol. Catal. A: Chem.*, **2006**, 255, 131-158, DOI: 10.1016/j.molcata.2006.03.068.

[73] Y. Ono, *Catal. Rev.-Sci. Eng.*, **1992**, 34, 179-226, DOI: 10.1080/01614949208020306.

[74] I. I. Ivanova, A. I. Rebrov, E. B. Pomakhina, E. G. Derouane, *J. Mol. Catal. A: Chem.*, **1999**, 141, 107-116, DOI: 10.1016/S1381-1169(98)00254-4.

[75] M. C. Clark, C. M. Smith, D. L. Stern, J. S. Beck in: „Handbook of Heterogeneous Catalysis“, chapter „Alkylation of Aromatics“, 2nd Ed., G. Ertl, H. Knözinger, F. Schüth, J. Weitkamp (Eds.), Vol. 7, Wiley-VCH, Weinheim, **2008**, p. 3153.

[76] L. Schmerling, J.A. Vesely, *J. Org. Chem.*, **1973**, 38, 312-315, DOI: 10.1021/jo00942a023.

[77] G. A. Olah, P. Schiiling, J. S. Staral, Y. Halpern, J. A. Olah, *J. Am. Chem. Soc.*, **1975**, 97, 6807-6810, DOI: 10.1021/ja00856a034.

[78] N. Y. Chen, W. E. Garwood, R. H. Heck, *Ind. Eng. Chem. Res.*, **1987**, 26, 706-711, DOI: 10.1021/ie00064a014.

[79] K. Griesbaum, A. Behr, D. Biedenkapp, H.-W. Voges, D. Garbe, C. Paetz, G. Collin, D. Mayer, H. Höke, R. Schmidt in Ullmann’s Encyclopedia of Industrial Chemistry, chapter „Hydrocarbons“, Wiley-VCH, Weinheim, **2012**, pp. 35, DOI: 10.1002/14356007.a13_227.pub2.

[80] J. Cejka, B. Wichterlova, *Catal. Rev.-Sci. Eng.*, **2002**, 44, 375-421, DOI: 10.1081/CR-120005741.

[81] A. Corma, V. Martínez-Soria, E. Schnoeveld, *J. Catal.*, **2000**, 192, 163-173, DOI: 10.1006/jcat.2000.2849.

[82] I. I. Ivanova, D. Brunel, J. B. Nagy, E. G. Derouane, *J. Mol. Catal. A: Chem.*, **1995**, 95, 243-258, DOI: 10.1016/1381-1169(94)00018-2.

[83] I. I. Ivanova, N. Blom, E.G. Derouane, *J. Mol. Catal. A: Chem.*, **1996**, 109, 157-168, DOI: 10.1016/1381-1169(96)00018-0.

[84] N. Danilina, E. L. Payrer, J. A. van Bokhoven, *Chem. Commun.*, **2010**, 46, 1509-1510, DOI: 10.1039/b922789j.

[85] N. Danilina, E. L. Payrer, E. Troussard, J. A. van Bokhoven, *Catal. Lett.*, **2011**, 141, 391-399, DOI: 10.1007/s10562-010-0511-0.

[86] A. V. Smirnov, E. V. Mazin, V. V. Yuschenko, E. E. Knyazeva, S. N. Nesterenko, I. I. Ivanova, L. Galperin, R. Jensen, S. Bradley, *J. Catal.*, **2000**, 194, 266-277, DOI: 10.1006/jcat.2000.2910.

[87] V. V. Ordomskiy, L. I. Rodionova, I. I. Ivanova, F. Luck, *ChemCatChem*, **2012**, 4, 681-686, DOI: 10.1002/cctc.201100445.

[88] S. A. S. Rezai, Y. Traa, *J. Membr. Sci.*, **2008**, 319, 279-285, DOI: 10.1016/j.memsci.2008.03.051.

[89] S. A. S. Rezai, Y. Traa, *Chem. Commun.*, **2008**, 2382-2384, DOI: 10.1039/b800486b.

[90] K. S. Wong, T. Vazhnova, S. P. Rigby, D. B. Lukyanov, *Appl. Catal. A*, **2013**, 454, 137-144, DOI: 10.1016/j.apcata.2013.01.012.

[91] D. S. Santilli, B. C. Gates in: „Handbook of Heterogeneous Catalysis“, chapter „Hydrocarbon Reaction Mechanisms“, 2nd Ed., G. Ertl, H. Knözinger, F. Schüth, J. Weitkamp (Eds.), Vol. 3, Wiley-VCH, Weinheim, **2008**, p. 1630.

[92] A. Alotaibi, H. Bayahia, E. F. Kozhevnikova, I. V. Kozhevnikov, *ACS Catal.*, **2015**, 5, 5512-5518, DOI: 10.1021/acscatal.5b01102.

[93] T. Vazhnova, S. P. Rigby, D. B. Lukyanov, *J. Catal.*, **2013**, 301, 125-133, DOI: 10.1016/j.cat.2013.02.002.

[94] J. A. Moulijn, A. E. van Diepen, F. Kapteijn in: „Handbook of Heterogeneous Catalysis“, chapter „Activity Loss“, 2. Ed., G. Ertl, H. Knözinger, F. Schüth, J. Weitkamp (Eds.), Vol. 4, Wiley-VCH, Weinheim, **2008**, p. 1829.

[95] C. H. Bartholomew, *Appl. Catal. A*, **2001**, 212, 17-60, DOI: 10.1016/S0926-860X(00)00843-7.

[96] U.S. Patent 4097543, 21.01.1977, Mobil Oil Corp. (Inv.: W. O. Haag, D. H. Olson).

[97] F. Bauer, W. Chen, Q. Zhao, A. Freyer, S. Liu, *Micropor. Mesopor. Mater.*, **2001**, 47, 67-77, DOI: 10.1016/S1387-1811(01)00318-3.

[98] W. Dabelstein, A. Reglitzky, A. Schütze, K. Reders in: Ullmann's Encyclopedia of Industrial Chemistry, vol. 4, chapter "Automotive Fuels", Wiley-VCH, Weinheim, **2012**, DOI: 10.1002/14356007.a16_719.pub2.

[99] G. Alfke, W. W. Irion, O. S. Neuwirth in: Ullmann's Encyclopedia of Industrial Chemistry, vol. 25, chapter "Oil Refining", Wiley-VCH, Weinheim, **2012**, DOI: 10.1002/14356007.a18_051.pub2.

[100] U. Dingerdissen, A. Martin, D. Herein, H. J. Wernicke in: „Handbook of Heterogeneous Catalysis", chapter „The Development of Industrial Heterogeneous Catalysis", 2nd Ed., G. Ertl, H. Knözinger, F. Schüth, J. Weitkamp (Eds.), Vol. 1, Wiley-VCH, Weinheim, **2008**, p. 40.

[101] B. C. Windom, T. M. Lovestead, T. J. Bruno, *Energy & Fuels*, **2010**, 24, 3275–3284, DOI: 10.1021/ef100178e.

[102] U.S. Patent 20140123548A1, 08.05.2014, G. W. Braly.

[103] DIN EN 228:2014-10 "Automotive fuels - Unleaded petrol - Requirements and test methods", German version.

[104] DIN EN 590:2012-01 "Automotive fuels – Diesel - Requirements and test methods"; German version.

[105] N. Nikolaou, C. E. Papadopoulos, I. A. Gaglias, K. G. Pitarakis, *Fuel*, **2004**, 83, 517-523, DOI: 10.1016/j.fuel.2003.09.011.

[106] B. G. Rohrback, *Trends in Analytical Chemistry*, **1991**, 10, 269-271, DOI: 10.1016/0165-9936(91)85003-A.

[107] J. B. Cooper, K. L. Wise, J. Groves, W. T. Welch, *Anal. Chem.*, **1995**, 67, 4096-4100, DOI: 10.1021/ac00118a011.

[108] W. G. Hiller, F. Abu-Dagga, B. Al-Tahou, *J. prakt. Chem.*, **1992**, 334, 691-695, DOI: 10.1002/prac.19923340809.

[109] K. Owen in: Modern Petroleum Technology, 5th Ed., G. D. Hobson (Ed.), Wiley, Chichester U.K., **1984**, Part II, p. 786.

[110] C. N. Satterfield, Heterogenous Catalysis in Practice; McGraw-Hill Book, New York, **1980**, p. 241.

[111] J. H. Gary, G. E. Handwerk, M. J. Kaiser, „Petroleum Refining Technology and Economics“, 5th Ed., CRC Press (Taylor and Francis Group), Boca Raton FL, **2007**; p. 261.

[112] M. Fritz, *Ph.D. Thesis*, *University of Stuttgart*, **1996**.

[113] J. Kornatowski, *Zeolites*, **1988**, 8, 77-78, DOI: 10.1016/S0144-2449(88)80034-4.

[114] S. Ernst, *Ph.D. Thesis, University of Karlsruhe*, **1987**, p. 23.

[115] Y. Miyamoto, N. Katada, M. Niwa, *Micropor. Mesopor. Mater.*, **2000**, 40, 271-281, DOI: 10.1016/S1387-1811(00)00264-X.

[116] S. Unverricht, M. Hunger, S. Ernst, H.G. Karge, J. Weitkamp, in: „Zeolites and Related Microporous Materials: State of the Art 1994“, J. Weitkamp, H.G. Karge, H. Pfeiffer, W. Hölderich (Eds.), *Studies in Surface Science and Catalysis*, Vol. 84, Part A, Elsevier, Amsterdam, London, New York, Tokyo, **1994**, 37-44.

[117] S. A. S. Rezai, *Ph.D. Thesis, University of Stuttgart*, **2011**.

[118] S. Sealy, D. Singer, Y. Traa in: “Oxidation and Functionalization: Classical and Alternative Routes and Sources”, S. Ernst, E. Gallei, J.A. Lercher, S. Rossini, and E. Santacesaria (Eds.); DGMK, Hamburg, Milan (2005) 245-251.

[119] Y. Wang, N. Shah, G. P. Huffman, *Energy & Fuels*, **2004**, 18, 1429-1433, DOI: 10.1021/ef049959o.

[120] S. A. S. Rezai, Y. Traa, *Catal. Lett.*, **2008**, 122, 91-97, DOI: 10.1007/s10562-007-9348-6.

[121] A. Bressel, T. Donauer, S. Sealy, Y. Traa, *Micropor. Mesopor. Mater.*, **2008**, 109, 278-286, DOI: 10.1016/j.micromeso.2007.05.002.

[122] F. Bauer, W. Chen, H. Ernst, S. Huang, S. Freyer, S. Liu, *Micropor. Mesopor. Mater.,* **2004**, 72, 81-89, DOI: 10.1016/j.micromeso.2004.04.007.0,

[123] M. E. Prudich, H. Chen, T. Gu, R. B. Gupta, K. P. Johnston, H. Lutz, G. Ma, Z. Su in: „Perry´s Chemical Engineers` Handbook“, chapter „Alternative Separation Processes“, 8th Edn., D. W. Green (Eds.), R. H. Perry, McGraw-Hill, New York, 2008, pp 20-58.

[124] R. E. Buxbaum, A. B. Kinney, *Ind. Eng. Chem. Res.*, **1996**, 35, 530-537, DOI: 10.1021/ie950105o.

[125] http://www.rebresearch.com/H2perm2.htm (10.04.2013).

[126] http://www.rebresearch.com/papers/membs/MetMems.html (10.04.2013).

[127] D. L. Stern, S. H. Brown, J. S. Beck in: „Handbook of Heterogeneous Catalysis“, chapter „Isomerization and Transalkylation of Alkylaromatics “, 2nd Ed., G. Ertl, H. Knözinger, F. Schüth, J. Weitkamp (Eds.), Vol. 7, Wiley-VCH, Weinheim, **2008**, p. 3183.

[128] S. Kato, K. Nakagawa, N. Ikenaga, T. Suzuki, *Catalysis Letters*, **2001**, 73, 175-180, DOI: 10.1023/A:1016637607166.

[129] Y. Jiang, Jm Huang, W. Dai, M. Hunger, *Solid State Nuclear Magnetic Resonance*, **2011**, 37, 116-141, DOI: 10.1016/j.ssnmr.2011.03.007.

8.1 Table of Figures

Fig. 1: Anaerobic food chain for the conversion of organic matter to methane, modified from [4]. 12
Fig. 2: Global distribution of natural gas potential, data status 2014 [6]. 13
Fig. 3: Comparison of the transportation costs for different fossil fuels [14]. 16
Fig. 4: Traded natural gas volume (worldwide) in billion cubic meters (bcm), used by permission of the World Energy Council, London, www.worldenergy.org []. 17
Fig. 5: Global trade of natural gas in 2014 [18]. 18
Fig. 6: Schematic of the Fischer-Tropsch process. 20
Fig. 7: Conceptual scheme of the Next-GTL project []. 22
Fig. 8: Schematic of the MFI structure of zeolite ZSM-5, modified from [39]. 25
Fig. 9: Illustration of the 3-dimensional channel system of the MFI structure []. 26
Fig. 10: Schematic of the *BEA structure of zeolite Beta, modified from [39], marked with arrows to indicate the directions of the two other channel systems []. 27
Fig. 11: Schematic of the structures of polymorph A (a), polymorph B (b) and polymorph C (c) of zeolite Beta viewed along [010], with their respective stacking orders ABAB…(a), ABCABC…(b) and AA…(c) [55]. 28
Fig. 12: Schematic of the BEC structure of polymorph C in zeolite Beta, modified from [39]. 28
Fig. 13: Schematic of the large cavity in the MWW structure, together with dimensions of the two channel systems, modified from [39]. 30
Fig. 14: Schematic of a crystal layer in the MWW structure []. 31
Fig. 15: Isomerization of i-propylbenzene and n-propylbenzene in the presence of benzene, after [82]. 38
Fig. 16: Schematic of primary reactions during the dehydroalkylation of benzene and occurring secondary products [2]. 40
Fig. 17: Schematic of oil refining processes []. 46
Fig. 18: Flow chart of the laboratory plant. 60
Fig. 19: Reproducibility of the conversion in fixed-bed reactor over 1.0Pd-H-ZSM-5(35) at T = 350 °C and p = 6.0 bar, n_{Et} / n_{Pr} / n_{Bz} 7.8 / 3.5 / 1. 67

Fig. 20: Comparison of product distributions without H_2 on 1.0Pd-H-ZSM-5(35) after TOS = 105 min at T = 350 °C in fixed-bed reactor with different reactants. [a] blending RON, [b] liquid phase for RON calculation [1]. 69
Fig. 21: Comparison of conversions during dehydroalkylation at T = 350 °C over H-ZSM-5(35) catalysts loaded with different noble metals in fixed-bed reactor. 73
Fig. 22: Comparison of the liquid phases from the dehydroalkylation at t = 350 °C over H-ZSM-5(35) catalysts loaded with different noble metals in fixed-bed reactor at TOS = 105 min. 74
Fig. 23: Picture and schematic of the membrane reactor provided by REB Research & Consulting. 77
Fig. 24: Schematic of the selective coking of the outer surface [97]. 80
Fig. 25: Benzene conversion over pre-coked and fresh 1.7 Pt-H-ZSM-5(35) at T = 350 °C in membrane reactor [2]. 81
Fig. 26: Permeability of neat metals for atomic hydrogen [125]. 86
Fig. 27: Effect of reduced sweep gas flow rate from 300 ml · min^{-1} to 30 ml · min^{-1} over different catalysts at T = 350 °C. 89
Fig. 28: Dehydroalkylation over 1.9Pt-H-ZSM-5(35) during three reaction cycles in membrane reactor, T = 350 °C p = 0.64 MPa, WHSV = 4.0 h^{-1}, $n_{Et}/n_{Pr}/n_{Bz}$ = 9.5/5/1, regenerated with 0.5 MPa H_2 for 24 h at 350 °C after cycle 1 and 400 °C after cycle 2, modified from [1]. 91
Fig. 29: Dehydroalkylation over 2.1Pt-H-BEA(24) during two reaction cycles in membrane reactor, T = 350 °C, p = 0.64 MPa, WHSV = 3.8 h^{-1}, $n_{Et}/n_{Pr}/n_{Bz}$ = 6.9/3.8/1, regenerated at T = 350 °C in 150 ml · min^{-1} H_2 for 24 h between cycle1 and cycle 2, sweep gas flow rate lowered from 300 ml · min^{-1} to 30 ml · min^{-1} during cycle 2 for ca. 10 h. 94
Fig. 30: Time on stream behavior of benzene conversion over 1.9Pt-H-ZSM-5(35), p = 0.63-0.65 MPa, at different reaction temperatures in membrane reactor, modified from [2]. 95
Fig. 31: Alkylaromatics during dehydroalkylation in membrane reactor over 1.9 Pt-H-ZSM-5(35) at T = 380 °C, p = 0.64 MPa, $n_{Et}/n_{Pr}/n_{Bz}$ = 9.4/5.1/1, WHSV = 3.9 h^{-1}. 97
Fig. 32: NPB/IPB ratios during dehydroalkylation over 1.9Pt-H-ZSM-5(35), p = 0.63-0.65 MPa, at different reaction temperatures in membrane reactor. 100
Fig. 33: NPB/IPB ratios during dehydroalkylation over catalysts with different zeolite structures at T = 350 °C in membrane reactor. 102
Fig. 34: Dehydroalkylation over 2.2Pt-H-MCM-22(21) at T = 350 °C, p = 0.61 MPa, n_{Et} / n_{Pr} / n_{Bz} = 8.4 / 4.2 / 1, WHSV = 3.7h^{-1} in membrane reactor. 105

Fig. 35: Dehydroalkylation over 2.1Pt-H-Beta(24) at T = 350 °C, p = 0.64 MPa, n_{Et} / n_{Pr} / n_{Bz} = 6.9 / 3.8 / 1, WHSV = 3.8h^{-1} in membrane reactor. 108
Fig. 36: Benzene conversions of the dehydroalkylation over catalysts with different pore systems at T = 350 °C for one day on stream in membrane reactor. 110
Fig. 37: XRD-patterns of ZSM-5 catalysts. 128
Fig. 38: XRD-pattern of NH_4-MCM-22(21). 129
Fig. 39: XRD-pattern of NH_4-Beta(24). 129
Fig. 40: MAS-NMR spectra of ZSM-5(19). 130
Fig. 41: MAS-NMR spectra of ZSM-5(20). 130
Fig. 42: MAS-NMR spectra of ZSM-5(35). 131
Fig. 43: MAS-NMR spectra of MCM-22(21). 131
Fig. 44: MAS-NMR spectra of Beta(24). 132
Fig. 45: SEM images of ZSM-5(19). 132
Fig. 46: SEM images of NH_4-ZSM-5(20). 133
Fig. 47: SEM images of NH_4-ZSM-5(35). 133
Fig. 48: SEM images of NH_4-ZSM-5(90). 134
Fig. 49: SEM images of MCM-22(21). 134
Fig. 50: SEM images of NH_4-Beta-5(24). 134

8.2 Table Summary

Table 1: Composition of natural gas []..... 13
Table 2: Comparison of transport conditions for ship-bound NG transport [12]..... 19
Table 3: Reactions during Fischer-Tropsch synthesis [27]..... 20
Table 4: Existing GTL plants []. 21
Table 5: Crystallographic data for the structures of zeolite Beta. 29
Table 6: Aromatization temperatures of alkanes..... 33
Table 7: Equilibrium conversions of some relevant reactions calculated for temperatures of 600 and 1000 K, modified from [62]. 39
Table 8: Product distribution during dehydroalkylation benzene with ethane or propane. 42
Table 9: Fuels from oil refining fractions []..... 45
Table 10: Blending RON values of the liquid components [109, 110]..... 48
Table 11: List of the used chemicals. 51
Table 12: List of MAS-NMR spectroscopy parameters..... 56
Table 13: Conditions of the CG/MS analysis..... 59
Table 14: Retention times of the detected compounds during online gas chromatography. ... 63
Table 15: Conditions of the online GC analysis. 63
Table 16: Crystal morphology of the catalysts..... 66
Table 17: Comparison of product distributions over Pd-H-ZSM-5 catalysts in the fixed-bed reactor with different n_{Si}/n_{Al} ratios. 72
Table 18: Comparison of catalysts in respect of their methane producing abilities..... 75
Table 19: Selectivity to methane depending on n_{Si}/n_{Al} ratio [121]. 76
Table 20: Comparison of pre-coked and fresh 1.7Pt-H-ZSM-5(35) during dehydroalkylation in the membrane reactor at T = 350 °C. 82
Table 21: Comparison of the dehydroalkylation conducted in fixed-bed and membrane reactor. 83
Table 22: Product distributions, RON, benzene conversion on 1.9Pt-H-MFI(35) in membrane reactor during three reaction cycles at T = 350 °C, p = 0.64 MPa, WHSV = 4.0 h^{-1}, $n_{Et}/n_{Pr}/n_{Bz}$ = 9.5/5/1, regenerated with 0.5 MPa H_2 for 24 h at 350 °C after cycle 1 and 400 °C after cycle 2, modified from [1]. 92
Table 23: Carbon content from CHN analysis of different catalysts after dehydroalkylation. 93
Table 24: Product distributions, $RON_{(l)}$ and benzene conversion on 1.9Pt-H-ZSM-5(35) at different reaction temperatures in membrane reactor, modified from [1]..... 96

Table 25: Dehydroalkylation of benzene over MCM-22. 105
Table 26: Product distribution of Dehydroalkylation over 2.1Pt-H-Beta(24) at T = 350 °C, p = 0.64 MPa, n_{Et} / n_{Pr} / n_{Bz} = 6.9 : 3.8 : 1, WHSV = 3.8h^{-1} at different times on stream in membrane reactor. 108
Table 27: Comparison of the dehydroalkylation over zeolites ZSM-5, MCM-22 and Beta.. 110

9 Appendices

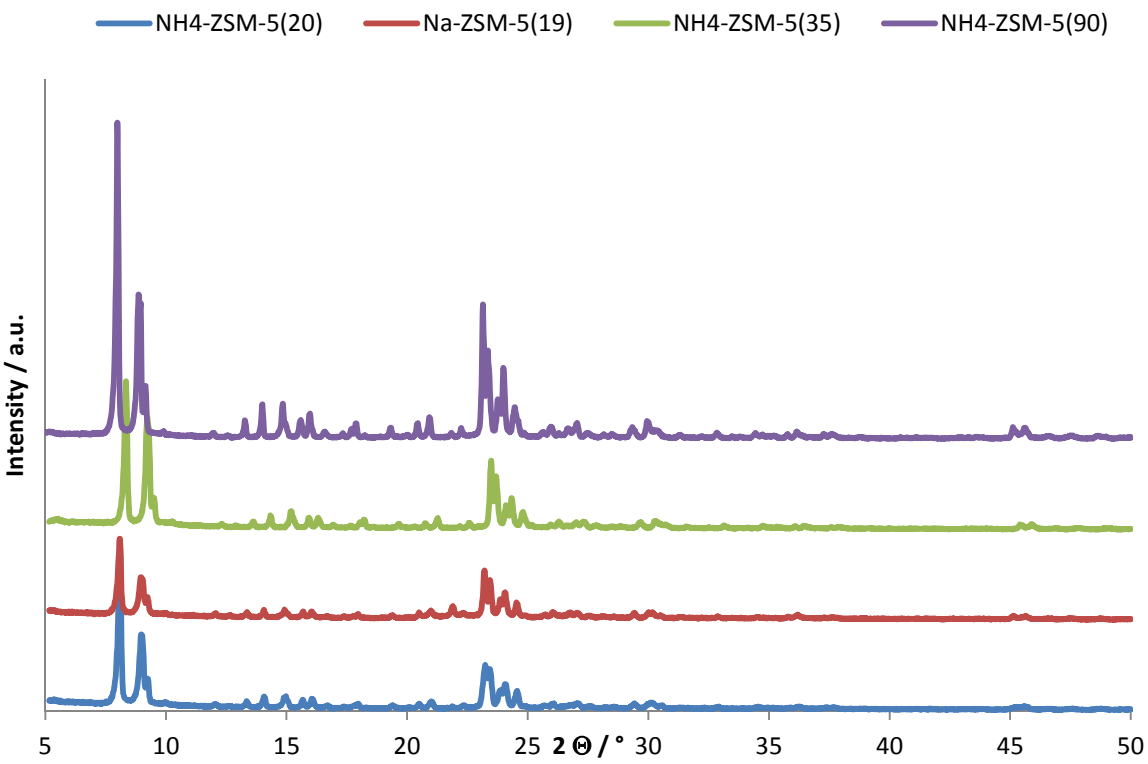

Fig. 37: XRD-patterns of ZSM-5 catalysts.

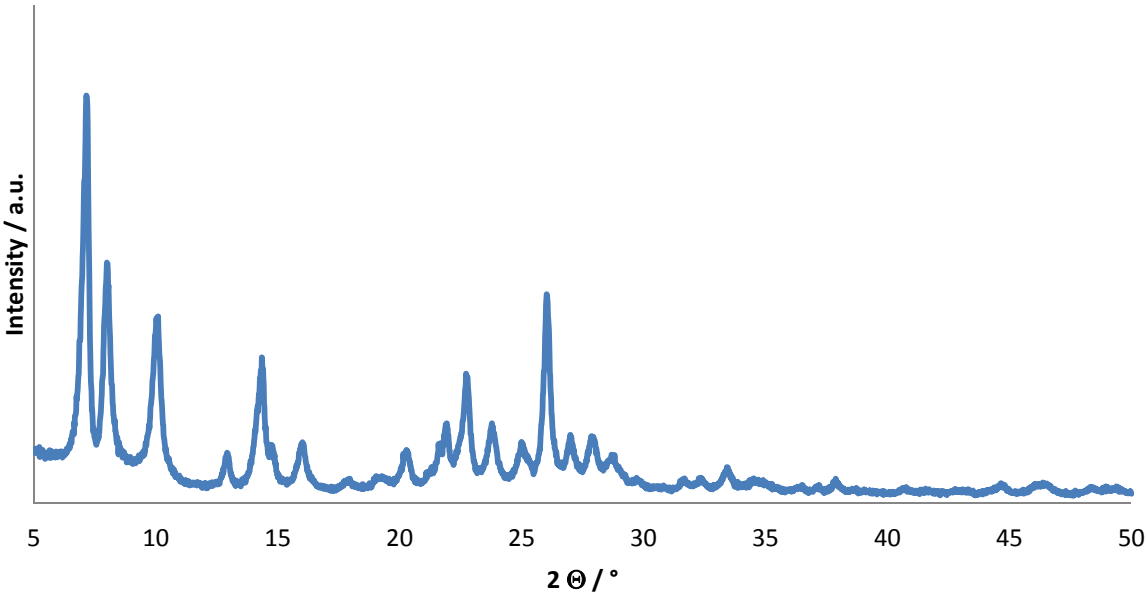

Fig. 38: XRD-pattern of NH_4-MCM-22(21).

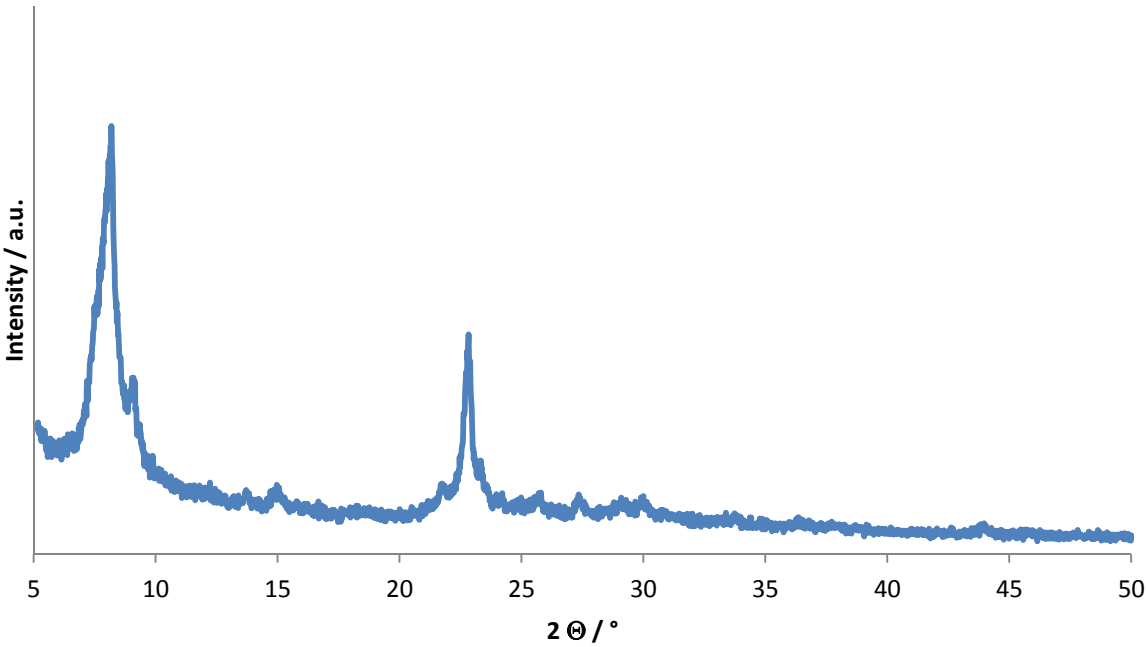

Fig. 39: XRD-pattern of NH_4-Beta(24).

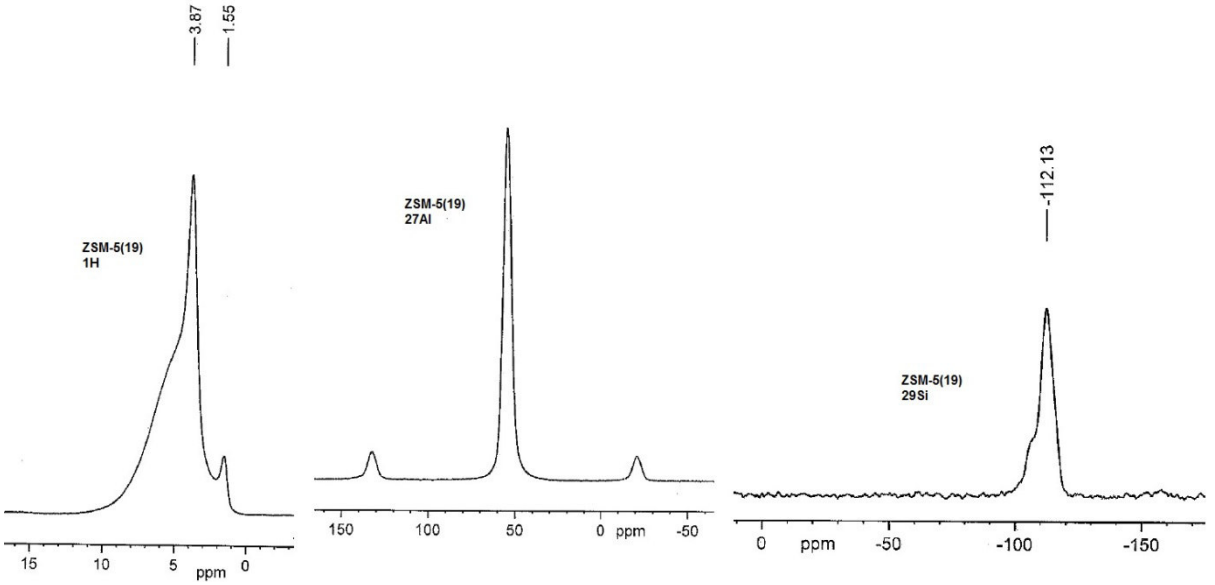

Fig. 40: MAS-NMR spectra of ZSM-5(19).

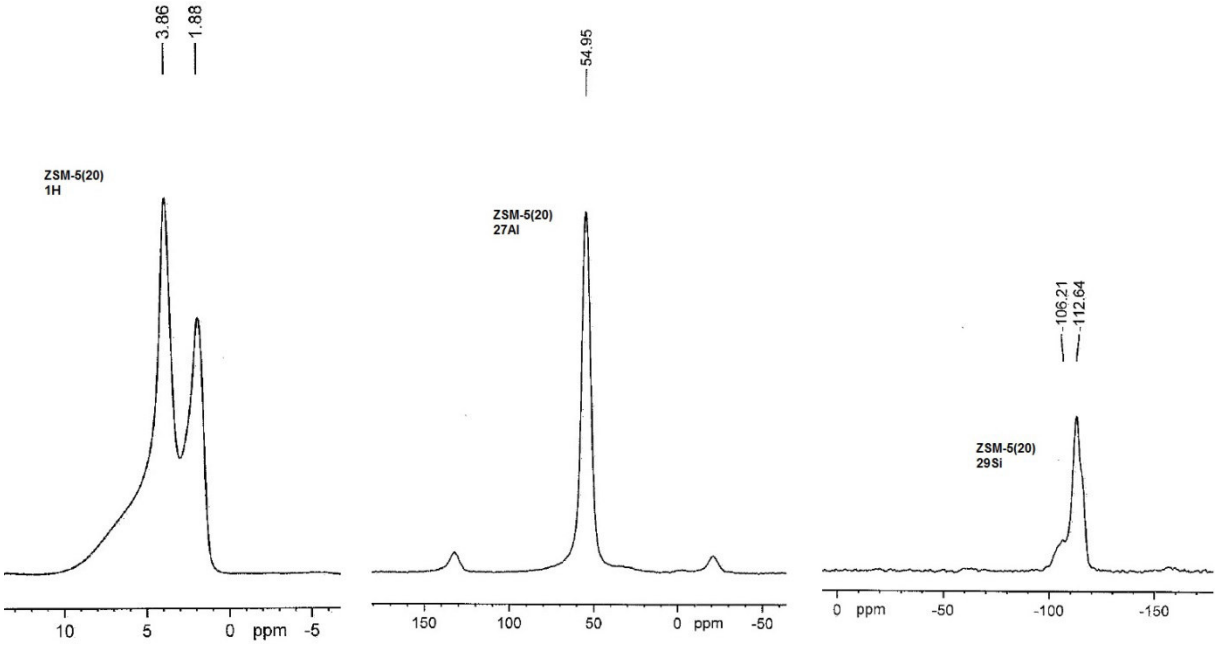

Fig. 41: MAS-NMR spectra of ZSM-5(20).

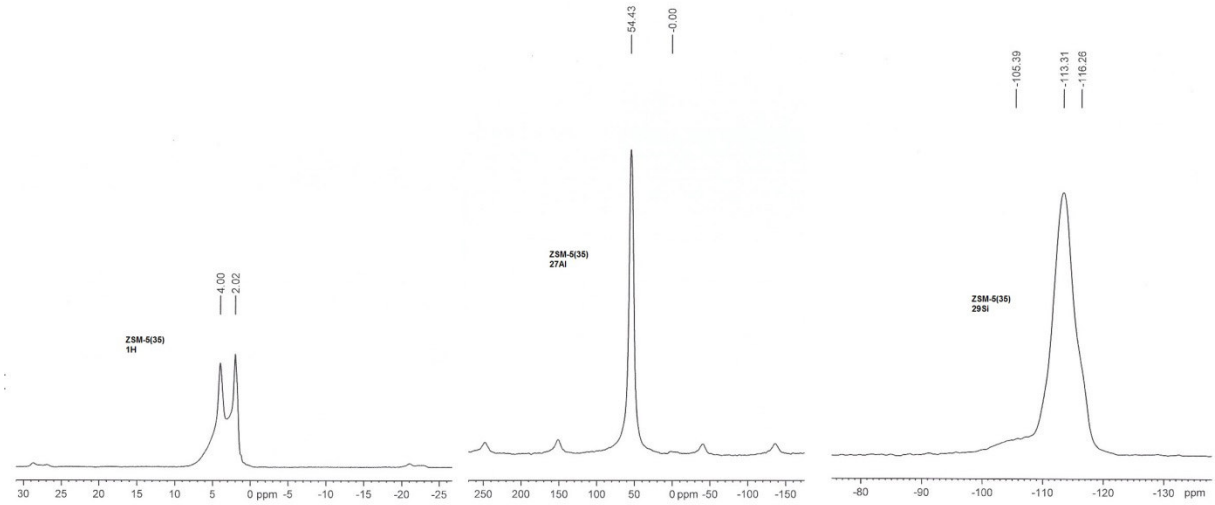

Fig. 42: MAS-NMR spectra of ZSM-5(35).

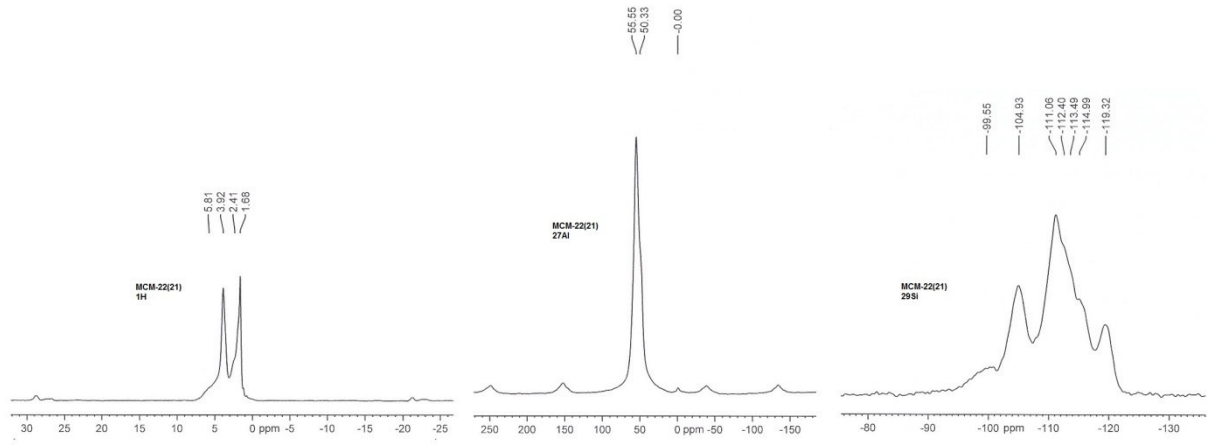

Fig. 43: MAS-NMR spectra of MCM-22(21).

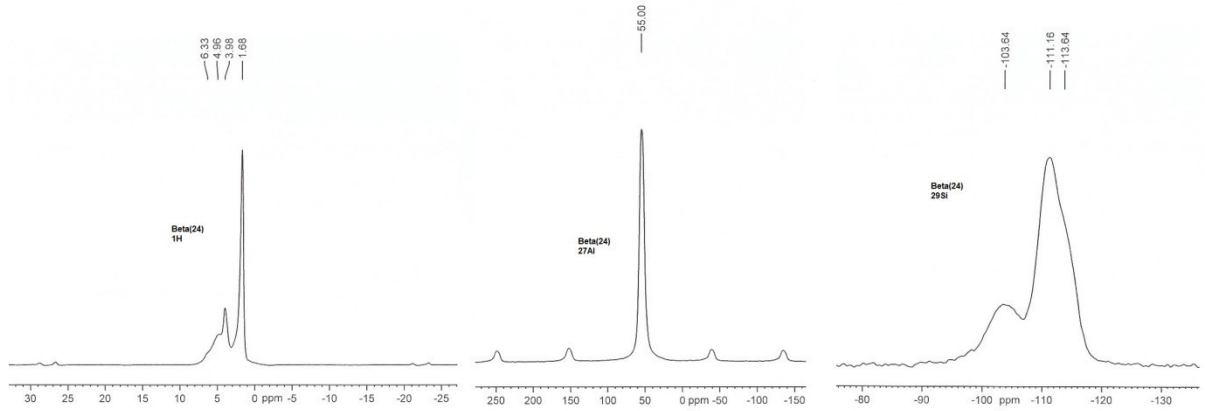

Fig. 44: MAS-NMR spectra of Beta(24).

Fig. 45: SEM images of ZSM-5(19).

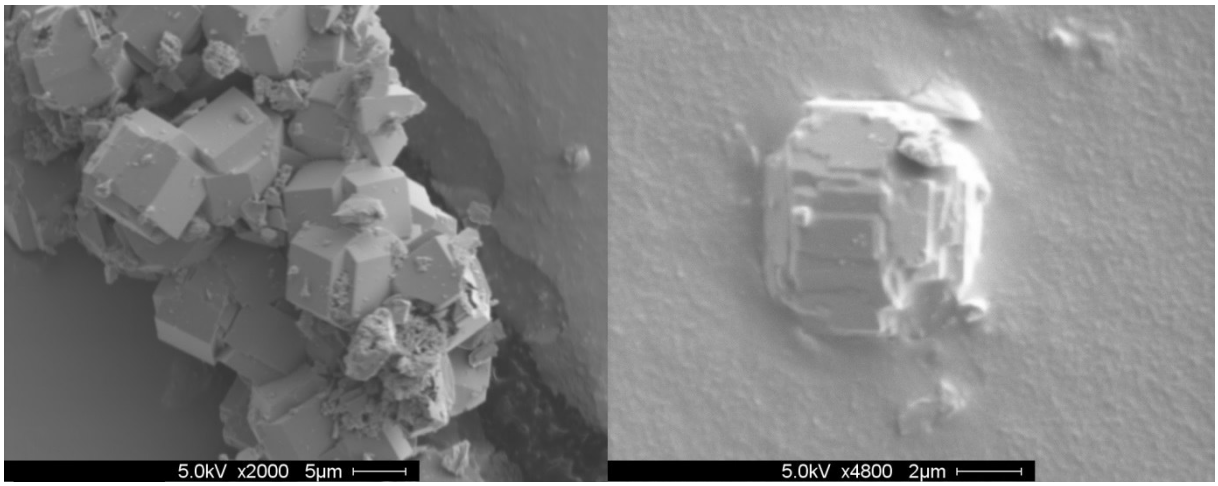

Fig. 46: SEM images of NH_4-ZSM-5(20).

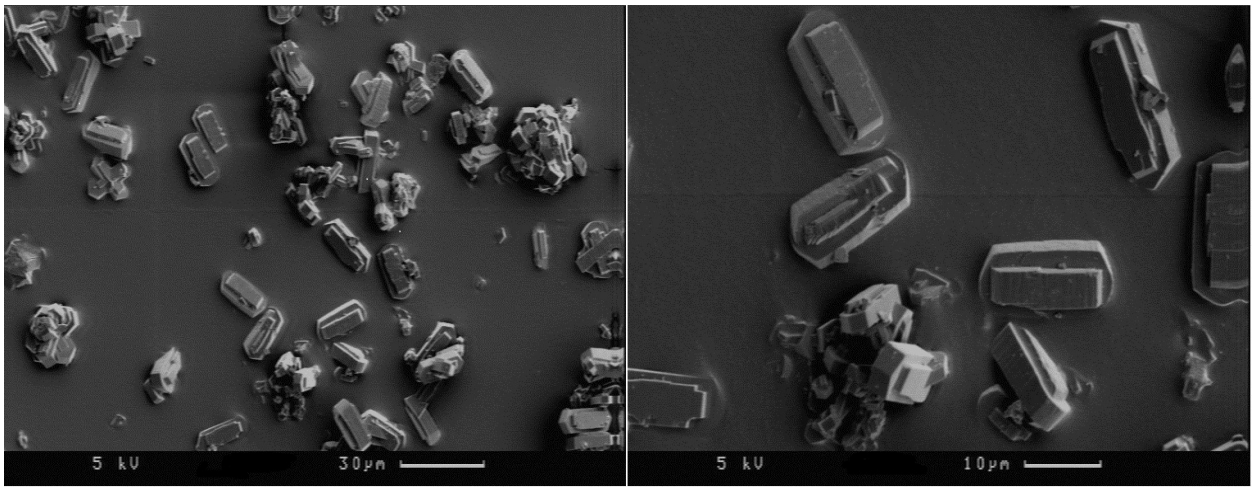

Fig. 47: SEM images of NH_4-ZSM-5(35).

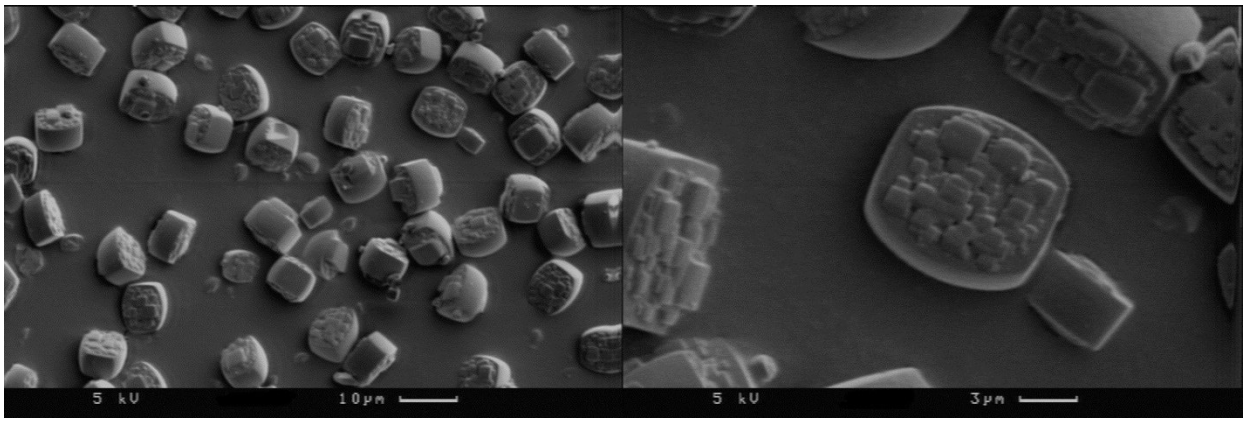

Fig. 48: SEM images of NH_4-ZSM-5(90).

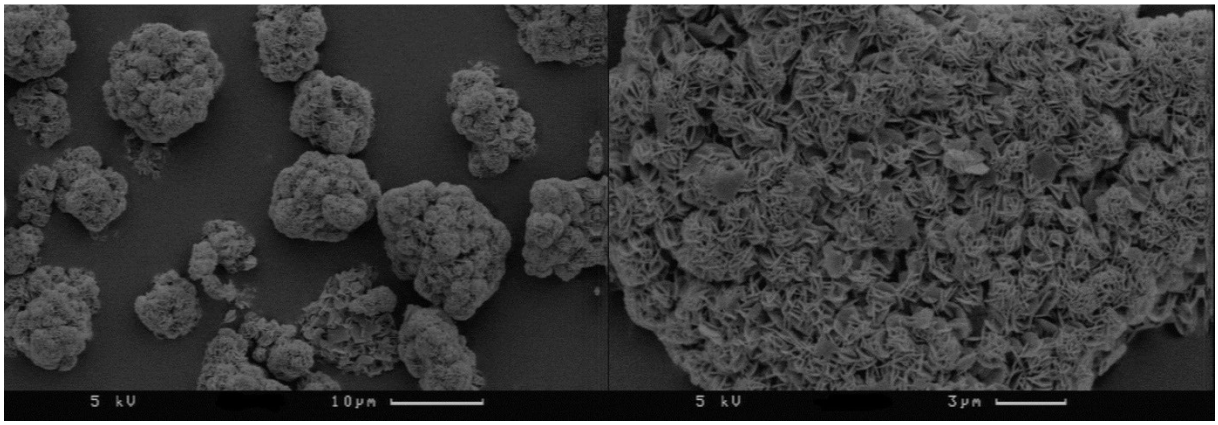

Fig. 49: SEM images of MCM-22(21).

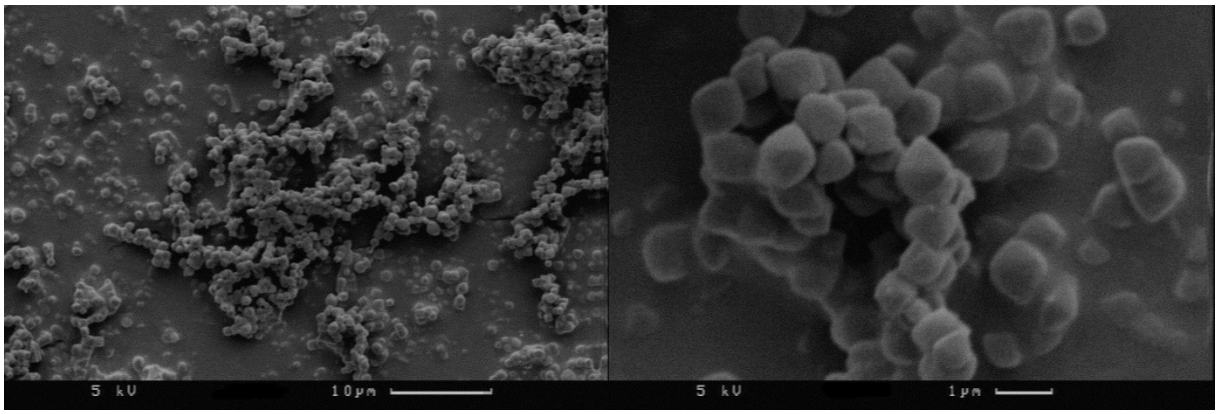

Fig. 50: SEM images of NH_4-Beta-5(24).

Ehrenwörtliche Erklärung

Hiermit versichere ich, dass die vorliegende Arbeit von mir selbstständig und ohne unerlaubte Hilfe angefertigt worden ist, insbesondere dass ich alle Stellen, die wörtlich oder annähernd wörtlich aus Veröffentlichungen entnommen sind durch Zitate als solche gekennzeichnet habe. Ich versichere auch, dass die von mir eingereichte schriftliche Version mit der digitalen Version übereinstimmt. Weiterhin erkläre ich, dass die Arbeit in gleicher ähnlicher Form noch keiner Prüfungsbehörde/Prüfungsstelle vorgelegen hat.

Stuttgart, den 02.07.18 Dennis Wan Hussin